Doctoral Thesis

Structure and Stability Studies on the Lipid Monolayers Exposed to Low-level Ozone

（低濃度オゾンに曝露した脂質単分子膜の構造と安定性に関する研究）

Lin QIAO

喬　琳

Graduate School of Environmental Science

Hokkaido University

February 2015

Contents

Chapter 5

Structure and Stability Studies of POPC Monolayer and DPPC-POPC Mixed Monolayers in Low-level Ozone

Chapter 1

Introduction

1.1 Lipids in Cell Membrane

Cell membranes, which separate the living individual from the external environment, play crucial roles in the functionality of cells such as mass transport, metabolism, information exchange, and energy conversion.[1] Although the living species show extraordinary diversity, all cells share certain common structural characters of the cell membrane.

The cell membrane (in a thickness of ca. 5nm) can be regarded as a phospholipid bilayer embedded with various membrane proteins and carbohydrates, as shown in Figure 1.1a.[2] Lipid and protein are the major components of cell membranes. Generally, 50% of the mass in most animal cell membranes are lipids.[3] The lipids are amphiphilic molecules composed of both hydrophilic and hydrophobic moieties (Figure 1.1b). The hydrophobic tails of lipids are faced each other and combined by hydrophobic force and van der Waals interaction, that result in an interior hydrophobic region between the two hydrophilic surface of the polar head group.[4-5]

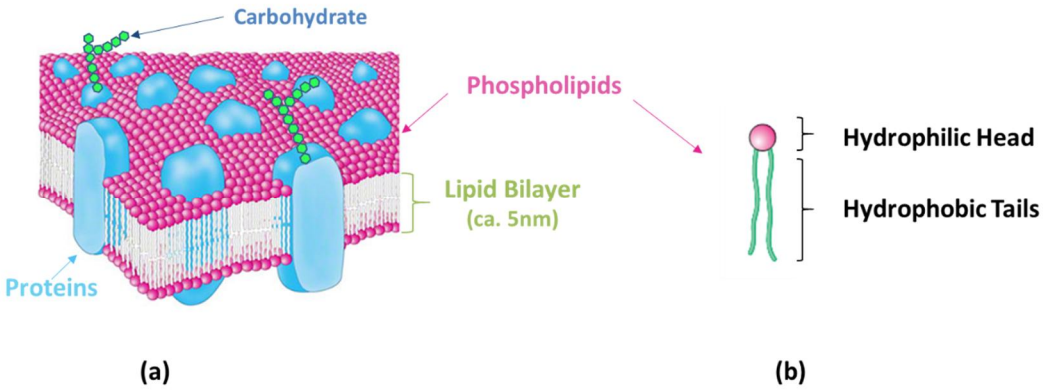

Figure 1.1 Typical views of a cell membrane (a) and phospholipid molecule (b). [6]

Depending on the molecular structure, there are three major types of membrane lipids: phospholipids, glycolipid, and cholesterol. Among them, phospholipids are the most abundant one.[7-8] The phosphatidylcholine (PC), a phospholipid with choline head group, accounts for the largest percentage (ca. 50%) of total lipids by weight in the membrane. [9] For example, the percentage of PC in the membrane of endoplasmic reticulum is 40%, in mitochondrion is 44%, in lung surfactant even rich to 75%.[3]

According to the saturation degree of the hydrophobic chains, the phospholipids can be classified as unsaturated and saturated types. Most of PC molecules have one unsaturated alkyl chain with one or more C=C bond, named as mono- or poly-unsaturated PC, respectively.[9] Figure 1.2 shows the molecular structure of a typical unsaturated phospholipid molecule, l-palmitoyl-2-oleoyl-*sn*-glycero-3-phosphochol, (POPC), in which the choline head group are linked to two fatty acid chains by one glycerol group. Some of typical unsaturated and saturated fatty acid chains in the lipids are shown in Table 1.1. Generally, the C=C double bonds in the unsaturated lipids are in *cis*-configuration.[8] Each *cis*-C=C double bond introduces a rigid kink site and changes the conformation of alkyl chain, that can weaken the van der Waals interaction between two lipids and significantly enhances fluidity of the cell membranes.[4, 10]

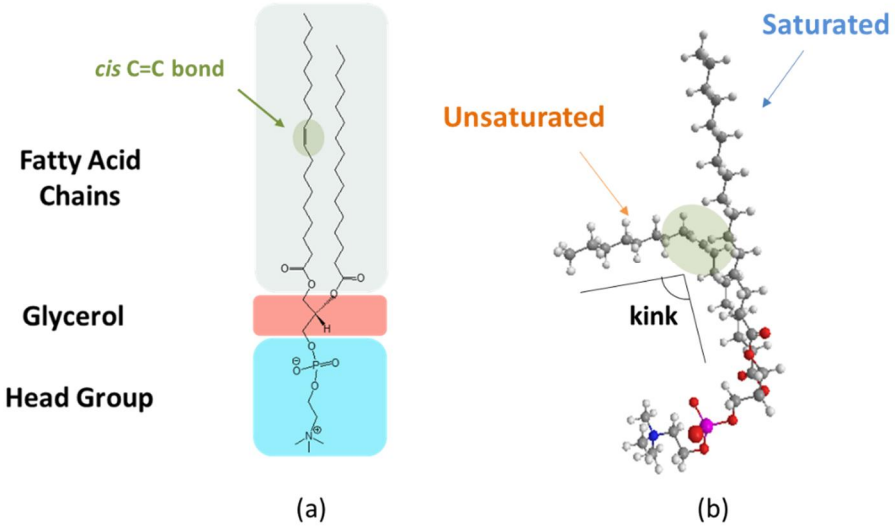

Figure 1.2 Molecular structure of unsaturated phospholipid POPC.

Table 1.1 Fatty Acids That Predominate in Phospholipids [8]

Common Name of Acid	Abbreviation	Chemical Formula
SATURATED FATTY ACIDS		
Myristic	C14:0	$CH_3(CH_2)_{12}COOH$
Palmitic	C16:0	$CH_3(CH_2)_{14}COOH$
Steric	C18:0	$CH_3(CH_2)_{16}COOH$
UNSATURATED FATTY ACIDS		
Oleic	C18:1	$CH_3(CH_2)_7CH=CH_3(CH_2)_7COOH$
Linoleic	C18:2	$CH_3(CH_2)_4CH=CHCH_2CH =CH(CH_2)_7COOH$
Archidonic	C20:4	$CH_3(CH_2)_4(CH=CHCH_2)_3CH =CH(CH_2)_3COOH$

In addition to the fluidity increase of the cell membrane, the *cis*-C=C double bond also significant affect the oxidability of the cell membrane to the oxidants.

1.2 Harmfulness of Lipid Oxidation

The saturated and unsaturated lipids in the cell membrane show different stabilities upon oxidation. Normally, the hydrogen atoms of the methylene groups adjacent to C=C bond (allylic hydrogen atoms) have lower C-H bond energies, especially those for polyunsaturated lipids.[11] These allylic hydrogen atoms attract the reactive oxidant species easily and induce a series of the lipid oxidation reactions.[11] On the contrary, the saturated alkyl chain has no allylic hydrogen atoms and is more resistant to the oxidant species.[11] The modification of lipid structure during oxidation process dramatically decreases the stability of the cell membrane. The products of lipid oxidation may further change the function of the cell membrane including weakening the barrier functions of the membrane[12] and inhibiting the protein synthesis and enzyme activity.[13] Lipid oxidation is known to affect cellular processes. The serious oxidation of the lipids in the cell membrane could cause the imbalance between oxidants and anti-oxidants in the cell, named as oxidative stress. Oxidative stress is known to induce complex modifications to the chemical structure of biomolecules including proteins and DNA.[14-15] It may further induce numerous serious diseases, such as idiopathic pulmonary fibrosis, cancer, atherosclerosis, and Parkinson's disease.[11, 15-18]

In the ambient environment, many species can lead to lipid oxidation, such as ozone (O_3) and free radicals ($\cdot OH$, $O_2^{-}\cdot$).[19-23] Ozone in the ambient is reported to be an important oxidant of the lipid oxidation with high reactivity.[21, 24-26] However, the risk of ozone on human health is often overlooked in our daily life due to its low-concentration and universality in the environment. For example, the surface of the alveoli in lungs is covered by pulmonary surfactants, which efficiently reduces surface tension at the air-liquid interface of the alveoli during expiration and plays an important role in preventing alveolar collapse and pulmonary edema.[15, 26-31] About 25%

of the pulmonary surfactants are unsaturated POPC.[27] Because the alveoli surfaces are exposed to air during the respiration process, both saturated and unsaturated phospholipids can readily interact with oxidant species, such as ozone, in ambient environment. It was found that the amount of unsaturated lipids in the rat pulmonary surfactant significantly decreased after the rats were exposed to ozone (0.8 ppm).[26] It also reported that the unsaturated plasmalogen, phosphotidylethanolamine (PE), in lung surfactant of murine was oxidized by ozone (100 ppb) to form various products that may relate to oxidative stress.[32] Not only the lipids in the lung, but also the lipids in the tissues exposed to the air can be potentially oxidized by ozone.[33-36] For example, the unsaturated constituent of human skin lipids can be easily oxidized by the ozone in the ambient environment. The volatile and less-volatile products may irritate the allergy of the respiratory system and the skin.[34]

1.3 Ozone as Oxidant for Lipid Oxidation

In the atmosphere, many species can be related to lipid oxidation, such as ozone (O_3) and free radicals ($\cdot OH$, $O_2^{-\cdot}$). Generally, the ozone layer in the high altitude is important to protect the livings from the strong radiation of ultraviolet (UV) light in the sunlight. However, near the earth surface, ozone is turned into an evil. Although its concentration is only a few tens of ppb, it is enough to cause the oxidation of lipid with different structures.

The formation of ozone in the atmosphere, including both stratosphere and troposphere, is shown in Figure 1.3.

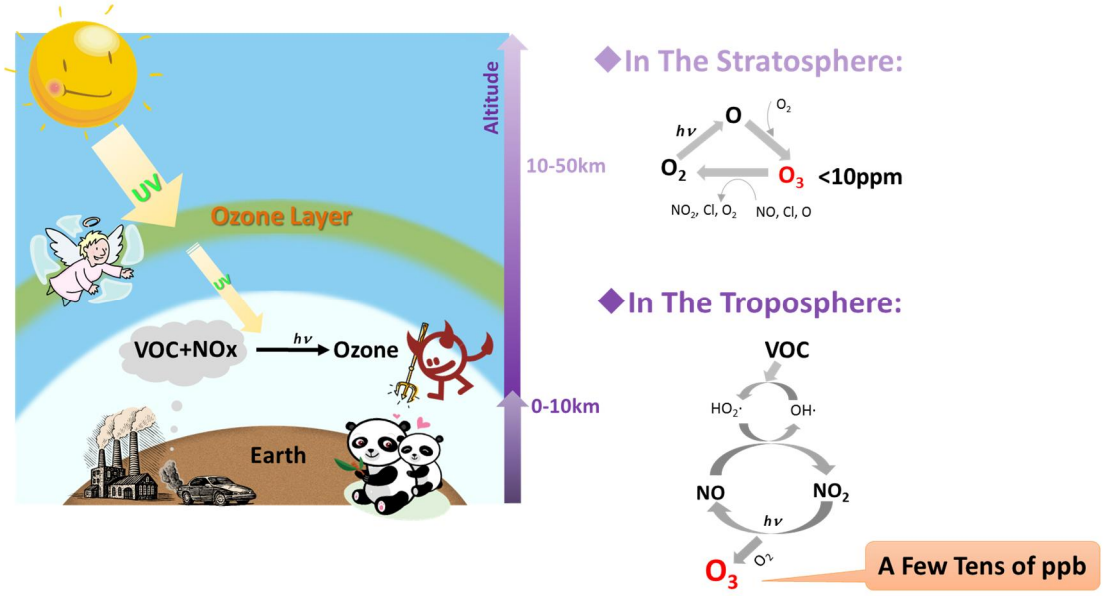

Figure 1.3 The processes of ozone formation in the atmosphere.

Approximately 90% of ozone in atmosphere are present in the stratosphere (10-50 km above earth), and especially concentrated in an ozone layer (20-30 km) with a concentration less than 10 ppm, acting as a protecting shield of the earth by absorbing about 99% of harmful solar UV light (Figure 1.3, left). Ozone in the stratosphere comes from the photolysis of oxygen (O_2). Oxygen is photolyzed by high-energy UV photons to generate many highly reactive oxygen atoms. The oxygen atom combine another oxygen molecule to create ozone (Figure 1.3, right top).[20, 37]

On the other hand, ozone in the troposphere (0-10 km) is produced by different processes from stratosphere where the strong UV is not available. One of the simplified formation mechanisms of ozone in troposphere is shown in Figure 1.3 (right bottom).[20] In this Scheme, O_3 is formed by oxidation of volatile organic compounds (VOC) which come from a number of sources, including organic solvent utilization and the off-gas from the engines and vehicles. The oxidation starts from the reaction of VOC and the hydroxyl radical ($OH^{\cdot}$). $OH^{\cdot}$ with a high reactivity will generate peroxy radicals ($HO_2^{\cdot}$) intermediately. $HO_2^{\cdot}$ then will oxidize nitrogen monoxide (NO) to nitrogen dioxide (NO_2). After that, NO_2 is photolyzed to give an atomic oxygen. Finally, ozone is formed by the reaction of an atomic oxygen and oxygen. In these process, hydroxyl radical ($OH^{\cdot}$) speed up the ozone generation as

catalysis. The concentration of ozone in troposphere is around few tens of ppb. [20, 38-39]

Since last century, the concentration of ozone is induced to abnormally high level by human activities, such as combustion of fossil fuels including gasoline and diesel incompletely. Ozone, though with much less concentration than in the stratosphere, becomes a hazard that is poisonous to all the livings on the earth. One of the well-known ozone induced hazards is the "Los Angeles" smog in the late 1940's, which causes a serious crop injury in Los Angeles County with an estimated loss of $479,495.[20, 40-41] The similar environment problem also occurred in many developed countries. In fact, China is also facing the photochemical smog problem due to highly increased car and factories. Because of the toxicity to human health, ozone level in the environments are detected and regulated by governments. In 2006, the world Health Organization (WHO) Task Group recommended a standard limitation of 0.05 ppm ozone per hour exposure for public health safety.[42] The U.S. federal air quality standard states that ozone exposure (0.12 ppm for 1 h) should not be exceeded more than once per year.[43]

Furthermore, the risk of ozone in indoor environment to human health is often underestimated. In fact, ozone as well as other reactive species are also daily generated indoors from many sources such as a copier, laser printer, and high-voltage electronic instruments. The ozone oxidation products of unsaturated organic compounds are known to induce eye irritation.[36] The trace amount of ozone in indoor environment is enough to cause the oxidation reaction in human body and induce many chronic age-related pathological process.[19] Since ozone is one of the most common species that may cause lipid oxidation even the concentration as low as a few tens of ppb, it is important to understand the reaction mechanism and kinetics of ozone oxidation on lipids in different systems.

1.4 Previous Studies on Lipid Oxidation

1.4.1 Historical Perspective of Studies on Lipid Oxidation

As mentioned above, ozone is known as one of the most powerful oxidants in the atmosphere. The presence of ozone in the ambient causes a potential public health concern. In the past century, the study on lipid oxidation in ozone has been an interest of wide research fields including biological and environmental science.

As early as 1910, Thunberg found iron salts increased the uptake of oxygen in tissues in the phospholipid suspensions.[11] In 1939, Frederik and Bernheim also found metal salt of iron[44], and vanadium [45] could catalyze the oxidation of lipid in the tissues. After that, many oxidants were discovered to induce the lipid oxidation, such as peroxides (H_2O_2), free radical ($OH^{\cdot}$), and ozone.[46]

Generally, the oxidation effects of ozone can be summarized as following[24]: (1) creating free radicals and reactive intermediate; (2) initiating the lipid peroxidation; (3) inducing the loss of activities of biomolecules by oxidizing the functional group; (4) causing the inflammation; (5) inducing secondary processes, such as reactive oxygen species (ROS). It is widely accepted that the biological damages produced by high oxidative ozone through either direct reaction or the formation of free radical and reactive intermediates, or both.[47-48] In spite of the knowledge about the lipid oxidation, lots of questions about the reaction mechanism as well as the effect of products on the membrane function still remain unknown.

The ozonization on lipid is commonly explained by the Criegee mechanism, which is named by Criegee.[48] The three steps in the ozonolysis are shown as following.

Step 1: formation of a primary ozonide. (POZ)

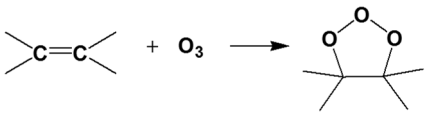

Step2: decomposition of POZ, and generate carbonyl oxide and carbonyl compound.

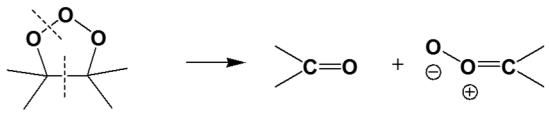

Step3: addition of the carbonyl oxide to carbonyl compound.

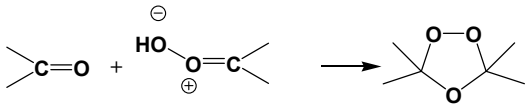

The Criegee mechanism is widely used and further complete in the analysis of C=C bond in unsaturated lipids. This mechanism of ozonolysis is also applied in the organic bulk phase.

In recent decades, many advanced techniques, such as differential scanning calorimetry (DSC), nuclear magnetic resonance (NMR), neutron reflection (NR), mass spectroscopy (MS), molecular dynamic (MD) simulation, as well as vibrational spectroscopy, have been employed to investigate the process of lipid oxidation. A wealth of information about the oxidation reaction has been obtained with the aid of these techniques.

The phase behavior of the lipid membranes containing unsaturated lipid [49] [50] or oxidized lipid [51] were observed by DSC. The information about the lipid structure, such as the chain ordering and interactions between head group, were further measured by the combination with ^{13}C and ^{31}P solid-state nuclear magnetic resonance. It was found only 2% of oxidized lipids has a visible reduction effect on the main transition temperature of DMPC bilayer by ca. 0.2°C. The oxidized lipid have strong distorting effects on the headgroup region of the membrane. [51]

Neutron reflection (NR) is a powerful technique to study the lipid oxidation reaction.[52-54] As shown in Figure 1.4, it is found that both surface pressures of partially deuterated PCs, $Pd_{17}OPC$ and $d_{31}POPC$ (Figure 1.4a), at a fixed surface area increased soon after exposure to ozone (0.1-3.2 ppm) (Figure 1.4b). But only $Pd_{17}OPC$ with deuterated terminal C_9 portion on unsaturated chain showed fast decrease of the reflectivity at interface for neutrons (Figure 1.4c), while $d_{31}POPC$ with saturated chain (deuterated) showed relative stable in O_3. They attributed the increase of the surface pressure to the reorientation of the oxidized tail of the POPC molecule, and the reflectivity for neutron decrease came from the fast loss of C9 portion of the

oleoyl strand from the water surface, at the meanwhile, the palmitoyl chain was impregnable.[52-53]

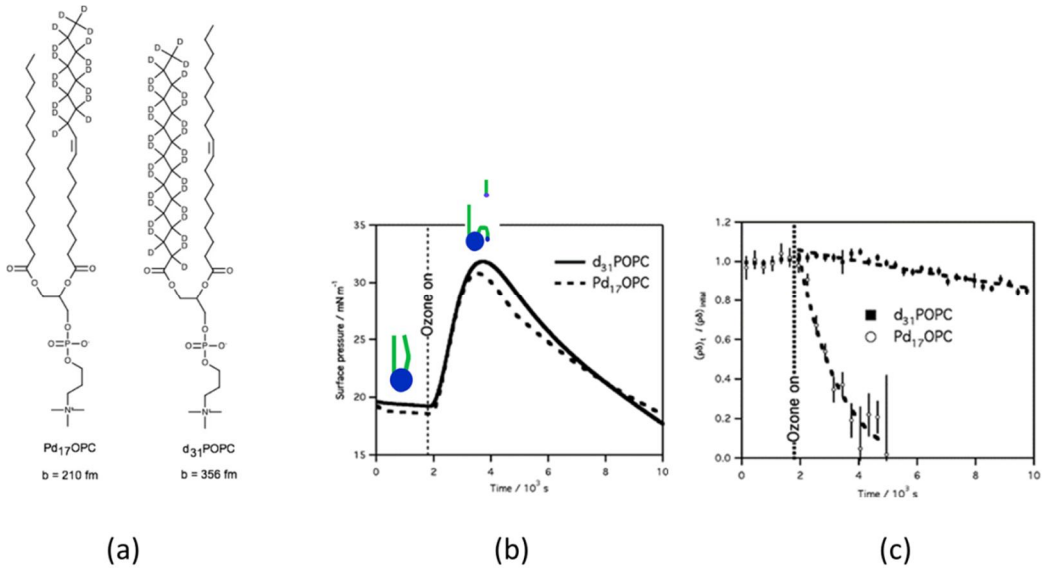

Figure 1.4 The molecule structure of $Pd_{17}OPC$ and $d_{31}POPC$ (a). The change of surface pressure (b) and fitted $\rho\delta$ (c) as a function of time. ρ is the neutron scattering length density, $\delta$is the film thickness, and they are related to the reflectivity of an interface for neutrons.[53]

In past, it is difficult to analyze the lipid oxidation products because the great diversity of the products. Mass spectroscopy in combination with various electron ionization methods can overcome this difficulty by offering both qualitative and quantitative information about the oxidation products. [11, 21, 32, 46, 55-57] MS has been utilized to study the ozone induced dissociation (OzID) over forty years and is proven to be a powerful tool for identifying the species of oxidation products and deducing double bond position in unsaturated lipids.[56, 58-59] MS analysis for the oxidation products from the lipid monolayers on water surface exposed to ozone (0.3~10 ppm) confirmed that the unsaturated moieties in the lipids can be selectively oxidized.[60-62]

Recently, the lipid oxidation studied by MS with *low*-concentration O_3 (similar to the level in ambient air) shows some distinct results.[21, 32, 63-65] Unlike high-concentration O_3 oxidized all the C=C bonds in the lipid, the low-concentration O_3 shows unique oxidation selectivity on the C=C bond position. As shown in Figure1.5, the 1-O-octadec-1'-enyl-2-octadecenoyl-PE (18:0p/18:1-PE) has two kinds of C=C bonds, however, only the vinyl ether bond connected to the glycerol backbone

can be oxidized by O_3 under the concentration of 100 ppb .[32]

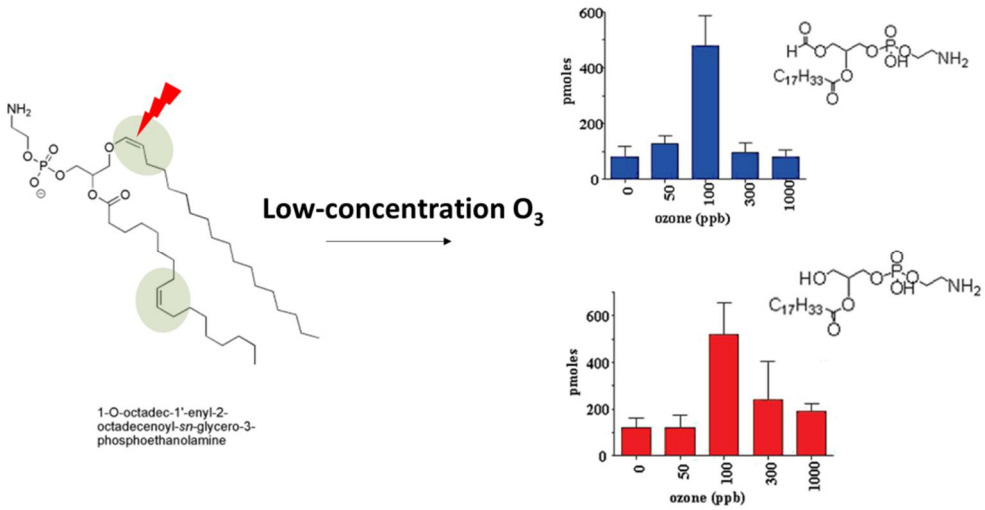

Figure 1.5 The molecule structure of 18:0p/18:1-PE and oxidation products generated by ozone exposure (0,50,100,300, and 1000ppb). (a)1-Formyl-2-octadecenoyl-PE (b)1-hydroxy-2-octadecenoyl-PE

MD simulation has been employed to study the dynamic of lipid oxidation and the effect of oxidized phospholipid on the properties of the mimic-membrane system.[66-74] It is found that the flip-flop in lipid bilayer is efficiently promoted by the presence of lipid oxidation products.[75] The oxidized chain of unsaturated phospholipid was found to reorient to the water surface to adopt an extended conformation (Figure 1.6).[67, 76]

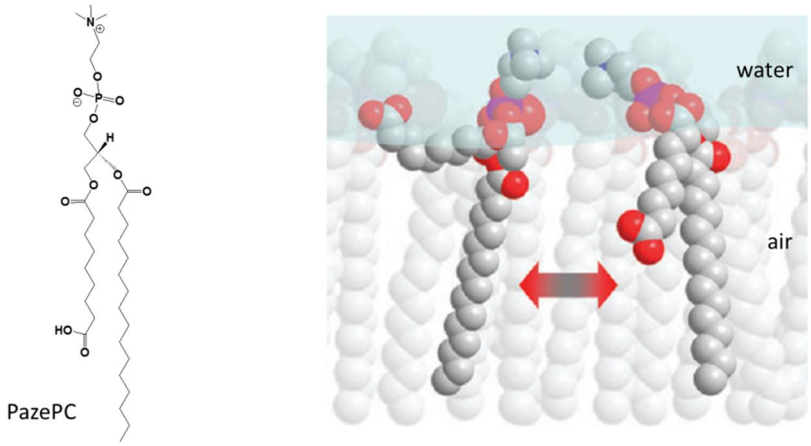

Figure 1.6 The molecule structure of oxidized phospholipid PazePC (left) and the scheme shows the reorientation of the oxidized portion at air-water interface (right).[67, 76]

Vibrational spectroscopy is a traditional and useful tool to study the molecule

structure of the lipid oxidation reaction. The reaction group on the molecule and formation of new species could be deduced by the analysis of the vibrational spectra. [77-78] Dilbeck *et al*. found that the C=C bond on the unsaturated chain of POPC was lost in ozone environment since the decrease in the 3008 cm^{-1} in the spectrum of diffuse reflection infrared Fourier transform spectrometry (DRIFTS), as shown in Figure 1.7. The absorption decrease of methylene group (2920 cm^{-1} and 2850 cm^{-1}) is due to the small volatile fragment removed from the sample. The changes at 2950 cm^{-1} and 2880 cm^{-1} are the evidence of the formation of the secondary ozonide (SOZ), since they are assigned to H-C stretches of the ring carbons of the SOZ. [77] In addition, the modern high-resolution of vibrational spectroscopy is also utilized to detect the Criegee intermediate during ozone oxidation process. The great breakthroughs were reported recently that the Criegee intermediate, rather than other isomers, was confirmed by transient infrared absorption spectroscopy.[79-80]

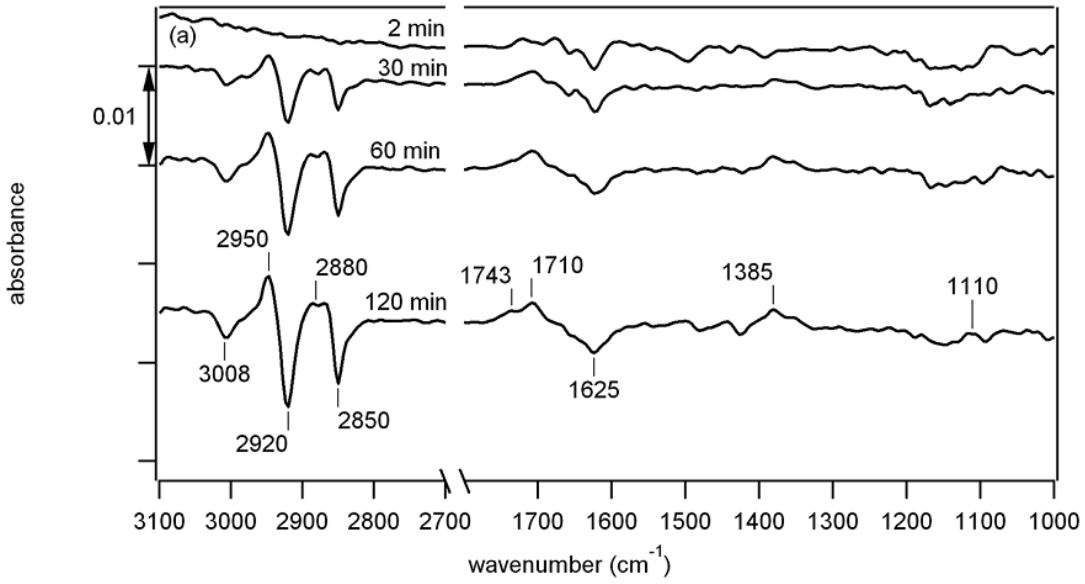

Figure 1.7 DRIFTS spectrum of POPC/ Instant Ocean (IO, a synthetic sea salt) during reaction with 1.2×10^{13} ozone cm^{-3}. Absorbance is normalized by the single beam spectrum of unreacted POPC/IO. [77]

With the aid of its surface selectivity and sensitivity, [81-91] sum frequency generation (SFG) vibrational spectroscopy has been proven to be a powerful tool to study the

unsaturated biomolecule oxidation at interface.[92-96] The surface pressure and surface structures of unsaturated phospholipid monolayers (Figure 1.8) or fatty acid monolayers on the water surface could change with exposure time to the ambient air. It was found that the 18:0 PC was stable, whereas unsaturated PCs degraded in the lab air, but the degradation was habited by changing the air with N_2 (Figure 1.8a). The SFG spectra (Figure 1.8b) shows the structural change of these lipid molecules, the vinyl CH peak decreased with the exposure time, that indicate the cis-double bond in the unsaturated chain was attacked by the oxidants in the air. However, the reaction mechanism was not fully understood.[93]

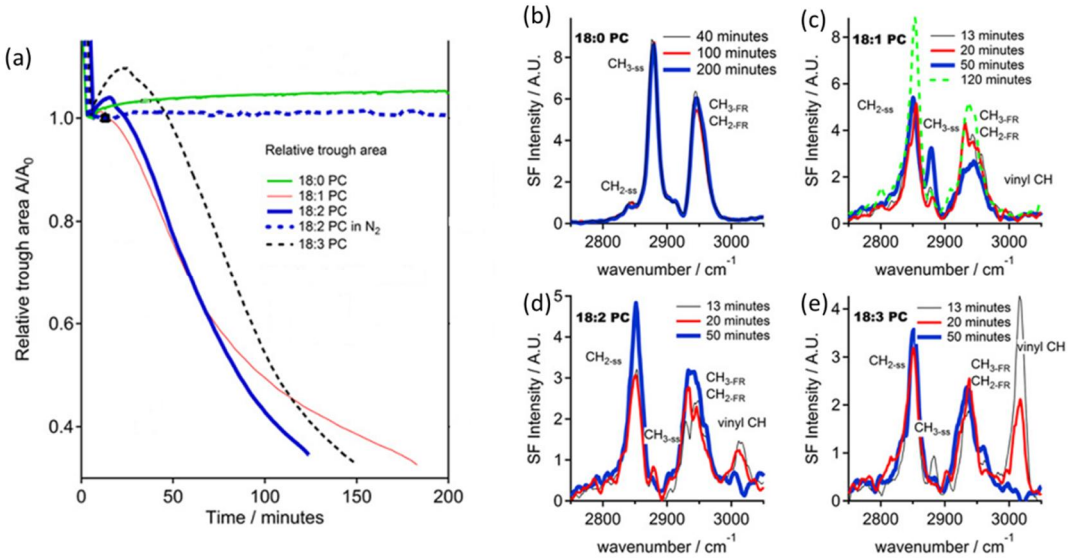

Figure 1.8 (a) Relative trough area of saturated PC (18:0), and unsaturated PCs (18:1, 18:2, 18:3) as a function of time at constant surface pressure. (b)-(e) The SFG spectra of these PCs.[93]

1.4.2 Challenges in Lipid Oxidation Research

In spite of numerous progresses in lipid oxidation research as reviewed above, there are still many challenges in understanding the mechanism of lipid oxidation as well as its influence on biological functions.

One of the challenges is investigation of *low*-concentration ozone induced lipid oxidation reaction. As mentioned above, most of previous studies have used high concentration ozone (0.3-10 ppm which is much higher than that of ozone in ambient

environment (tens of ppb). However, some recent researches have reported that selectivity of the C=C bonds in lipid oxidation reaction shows a dependence on the concentration of ozone.[32] It suggests that the oxidation mechanism or the effect of oxidation on the cellular function can be significantly dependent on the concentration of ozone. Therefore, in order to examine how the lipids especially unsaturated lipids are influenced by the ozone in air, it is essential to study the lipid oxidation under *low*-concentration ozone (ppb level). This is the possible reason why most of previous research works used high-concentration ozone or did not controlled the concentration during the experiments.

Another challenge is acquisition of molecular structure information of the lipid molecules during the oxidation reaction at molecule level. As mentioned above, most of previous works studied the lipid oxidation occurred in solution. In contrast, most of lipid oxidation reactions occur in the cell membrane in nature which is a sheet-like interface between the intracellular and extracellular regions. Therefore, it is very important to study the lipid oxidation reaction at interfaces, such as the lipid monolayer or bilayer systems. Despite some progresses obtained by NR, this technique is generally not sensitive to chemical structure. [52-54] To overcome this problem, the vibrational spectroscopic technique is highly desired. The conventional vibrational spectroscopy such as infrared or Raman spectroscopy, however, is difficult to provide monolayer sensitivity and surface selectivity. In recent years, a few reports have used SFG spectroscopy which is intrinsically surface-specific to study the lipid oxidation reaction. Although the SFG can give the molecular structure information with sub-monolayer sensitivity, however, the present progress by using this advanced surface technique to study lipid oxidation is still very limited. The ozone effect especially the low-concentration ozone effect on the lipids has not been examined by SFG. Similarly, atomic force microscopy (AFM) which can provide the morphological information of the interfaces also a good choice as a supplementary means. By combination of SFG and AFM, the information of both molecular structure and morphology of the lipid monolayer could be obtained.

1.5 Purpose and Outline of This Thesis

The purpose of the present study is to investigate the molecular structure and stability of the phospholipid monolayers in an environment containing a very low-concentration of ozone (20±10 ppb) by various surface-specific techniques. As mentioned above, most of previous research works applied in the high concentration of ozone (0.3-10 ppm), which is much higher than that in ambient atmosphere (few tens of ppb). Moreover, due to lack of surface-specific vibrational spectroscopic method, the structural changes of interfacial lipid molecules in oxidation reaction is still not clear. Hence it is essential to understand the structural changes of interfacial lipid molecules under *low*-concentration ozone.

In this thesis, with respect to the issues mentioned above, the surface molecular structures, stability, and morphology of various phospholipid monolayer systems in low-concentration ozone are investigated by SFG spectroscopy together with other surface characterization methods, including π-A isotherms and atomic force microscopy (AFM).

In Chapter 1, a brief introduction of lipid membrane and lipid oxidation is first described. Then previous studies on the lipid oxidation and mechanism are briefly reviewed. Finally, the purpose and outline of the present thesis are given.

In Chapter 2, a basic theory of nonlinear optical process and SFG process will be introduced. Furthermore, the molecular orientation analysis based on SFG results is given.

In Chapter 3, the details about experiment, including chemicals, sample preparation, control of ozone concentration, and system description about SFG spectroscopy and AFM measurement are given.

In Chapter 4, an unsaturated lipid, 1,2-dioleoyl-*sn*-glycero-3-phosphocholine (DOPC), and a saturated lipid, 1,2-dipalmitoyl(d_{62})-*sn*-glycero-3-phosphorcholine-1,1,2,2-d_4-N,N,N- trimethyl-d_9 (DPPC-d_{75}), are used to prepare pure and mixed monolayers to mimic the cell membrane. The stability and structure of these monolayers exposed to nitrogen, oxygen, ambient laboratory air and an extremely low

concentration of ozone (20±10 ppb) on the water surface behave been explored by π-A isotherm, AFM, and SFG vibrational spectroscopy.

In Chapter 5, the molecular structure of another important unsaturated lipid molecule, 1-palmitoyl-2-oleoyl-*sn*-glycero-3-phosphocholine (POPC) has been studied in details. Stability of the POPC monolayer in low-concentration ozone has been evaluated by π-A isotherm measurements. The molecular structure of the unsaturated portion has also been probed by *in-situ* SFG spectroscopy. A detailed analysis also carried out to verify the oxidation products. Moreover, a possible oxidation mechanism for POPC monolayer by ozone has been proposed. Then, SFG spectroscopy and AFM will be employed to investigate the molecular structure and morphology of monolayers of POPC mixing with 1,2-dipalmitoyl-*sn*-glycero-3-phosphocholine (DPPC). The mixing effect of DPPC and oxidation products on the lipid monolayers are discussed in detail.

In Chapter 6, a general conclusion will be given. In addition, a future prospect on oxidation research of lipid membrane will be briefly presented.

REFERENCE

1. Sadava, D.; Heller, C.; Orians, G.; Purves, W.; Hillis, D., *Life: The Science of Biology*. Sinauer Associates, Inc.: Sunderland, MA, 2008.
2. Singer, S. J.; Nicolson, G. L., Fluid Mosaic Model of Structure of Cell-membranes. *Science* **1972,** *175* (4023), 720-&.
3. Alberts, B.; Johnson, A.; Lewis, J.; Raff, M.; Roberts, K.; Walter, P., *Molecular Biology of the Cell*. Garland Science: New York, 2008.
4. Gennis, R. B., Biomembranes: Molecular Structure and Function. In *Biomembranes*, Springer: New York, 1989.
5. Israelachvili, J. N., *Intermolecular and Surface Forces*. 3rd ed.; Academic Press: 2011.
6. Berg, J. M.; Tymoczko, J. L.; Stryer, L., *Biochemistry, Sixth Edition*. WH Freeman & Co. New York: 2006.
7. Lodish, H.; Berk, A.; Kaiser, C. A.; Krieger, M.; Scott, M. P., *Molecular Cell Biology*. 6th ed.; W. H. Freeman and Company: 2007.
8. Berg, J. M.; Tymoczko, J. L.; Stryer, L.; Jr., G., J. G., *Biochemistry*. 7th ed.; W. H. Freeman and Company: New York, 2011.
9. Van Meer, G.; Voelker, D. R.; Feigenson, G. W., Membrane lipids: where they are and how they behave. *Nature reviews molecular cell biology* **2008,** *9* (2), 112-124.
10. Sadava, D.; Heller, C.; Orians, G.; Purves, W.; Hillis, D., *Life*. 8th ed.; Sinauer Associates, Inc.: Sunderland, MA, 2008.
11. Reis, A.; Spickett, C. M., Chemistry of phospholipid oxidation. *Bba-Biomembranes* **2012,** *1818* (10), 2374-2387.
12. Tai, W.-Y.; Yang, Y.-C.; Lin, H.-J.; Huang, C.-P.; Cheng, Y.-L.; Chen, M.-F.; Yen, H.-L.; Liau, I., Interplay between Structure and Fluidity of Model Lipid Membranes under Oxidative Attack. *The Journal of Physical Chemistry B* **2010,** *114* (47), 15642-15649.
13. Fridovich, S. E.; Porter, N. A., OXIDATION OF ARACHIDONIC-ACID IN MICELLES BY SUPEROXIDE AND HYDROGEN-PEROXIDE. *Journal of Biological Chemistry* **1981,** *256* (1), 260-265.
14. Apel, K.; Hirt, H., Reactive oxygen species: metabolism, oxidative stress, and signal transduction. *Annu. Rev. Plant Biol.* **2004,** *55*, 373-399.
15. Megli, F. M.; Sabatini, K., Mitochondrial phospholipid bilayer structure is ruined after liver oxidative injury in vivo. *FEBS Letters* **2004,** *573* (1-3), 68-72.
16. Roberts, R. A.; Laskin, D. L.; Smith, C. V.; Robertson, F. M.; Allen, E. M. G.; Doorn, J. A.; Slikkerk, W., Nitrative and Oxidative Stress in Toxicology and Disease. *Toxicol. Sci.* **2009,** *112* (1), 4-16.
17. Blokhina, O.; Virolainen, E.; Fagerstedt, K. V., Antioxidants, Oxidative Damage and Oxygen Deprivation Stress: a Review. *Annals of Botany* **2003,** *91* (2), 179-194.
18. Bargagli, E.; Olivieri, C.; Bennett, D.; Prasse, A.; Muller-Quernheim, J.; Rottoli, P., Oxidative stress in the pathogenesis of diffuse lung diseases: A review. *Respir. Med.* **2009,** *103* (9), 1245-1256.
19. Brunekreef, B.; Holgate, S. T., Air pollution and health. *Lancet* **2002,** *360* (9341), 1233-1242.
20. Finlayson-Pitts, B. J.; Jr., P., J. N. , *Chemistry of the Upper and Lower Atmosphere: Theory, Experiments, and Applications*. Academic Press: San Diego, 2000.
21. Cohen, S. L., Ozone in Ambient Air as a Source of Adventitious Oxidation. A Mass Spectrometric Study. *Anal Chem* **2006,** *78* (13), 4352-4362.
22. Kelly, F. J.; Mudway, I.; Krishna, M. T.; Holgate, S. T., The free radical basis of air pullution: focus on

ozone. *Respir. Med.* **1995,** *89* (10), 647-656.

23. Pratt, D. A.; Tallman, K. A.; Porter, N. A., Free Radical Oxidation of Polyunsaturated Lipids: New Mechanistic Insights and the Development of Peroxyl Radical Clocks. *Accounts of Chemical Research* **2011,** *44* (6), 458-467.

24. Mustafa, M. G., Biochemical basis of ozone toxicity. *Free Radical Biology and Medicine* **1990,** *9* (3), 245-265.

25. Finlayson-Pitts, B. J., Reactions at surfaces in the atmosphere: integration of experiments and theory as necessary (but not necessarily sufficient) for predicting the physical chemistry of aerosols. *Phys Chem Chem Phys* **2009,** *11* (36), 7760-7779.

26. Finlayson-Pitts, B.; Mautz, W.; Lai, C.; Bufalino, C.; Messer, K.; Mestas, J.; Koch, H.; Lucio, L., Are changes in breathing pattern on exposure to ozone related to changes in pulmonary surfactant? *Inhalation toxicology* **1994,** *6* (3), 267-287.

27. King, R., Pulmonary surfactant. *Journal of Applied Physiology* **1982,** *53* (1), 1-8.

28. Ciencewicki, J.; Trivedi, S.; Kleeberger, S. R., Oxidants and the pathogenesis of lung diseases. *Journal of Allergy and Clinical Immunology* **2008,** *122* (3), 456-468.

29. Pérez-Gil, J., Structure of pulmonary surfactant membranes and films: The role of proteins and lipid–protein interactions. *Biochimica et Biophysica Acta (BBA) - Biomembranes* **2008,** *1778* (7–8), 1676-1695.

30. Perez-Gil, J.; Weaver, T. E., Pulmonary surfactant pathophysiology: current models and open questions. *Physiology* **2010,** *25* (3), 132-141.

31. Pryor, W. A., Mechanisms of radical formation from reactions of ozone with target molecules in the lung. *Free Radical Biology and Medicine* **1994,** *17* (5), 451-465.

32. hoWynalda, K. M.; Murphy, R. C., Low-concentration ozone reacts with plasmalogen glycerophosphoethanolamine lipids in lung surfactant. *Chemical research in toxicology* **2009,** *23* (1), 108-117.

33. Darley, E. F.; Middleton, J. T.; Garber, M. J., Phytotoxicity of Gas Mixtures, Plant Damage and Eye Irritation from Ozone-Hydrocarbon Reactions. *Journal of Agricultural and Food Chemistry* **1960,** *8* (6), 483-485.

34. Wisthaler, A.; Weschler, C. J., Reactions of ozone with human skin lipids: Sources of carbonyls, dicarbonyls, and hydroxycarbonyls in indoor air. *Proceedings of the National Academy of Sciences* **2010,** *107* (15), 6568.

35. Pandrangi, L. S.; Morrison, G. C., Ozone interactions with human hair: Ozone uptake rates and product formation. *Atmospheric Environment* **2008,** *42* (20), 5079-5089.

36. Wolkoff, P.; Nojgaard, J. K.; Troiano, P.; Piccoli, B., Eye complaints in the office environment: precorneal tear film integrity influenced by eye blinking efficiency. *Occup. Environ. Med.* **2005,** *62* (1), 4-12.

37. Staehelin, J.; Harris, N. R. P.; Appenzeller, C.; Eberhard, J., Ozone trends: A review. *Reviews of Geophysics* **2001,** *39* (2), 231-290.

38. Seinfeld, J.; Pandis, S., *Atmospheric chemistry and physics: from air pollution to climate change*. 2nd ed. ed.; John Wiley & Sons, Inc.: Hoboken, 2006.

39. Warneck, P., *Chemistry of the Natural Atmosphere*. Academic Press: San Diego, 2000.

40. Middleton, J.; Kendrick, J.; Schwalm, H., Smog in the south coastal area: Injury to herbaceous plants in the affected area found to be result of air pollution by gases and aerosols. *California agriculture* **1950,** *4* (11), 7-10.

41. Haagen-Smit, A., Chemistry and physiology of Los Angeles smog. *Industrial & Engineering Chemistry* **1952,** *44* (6), 1342-1346.

42. Team, W. H. O. O. a. E. H., WHO Air quality guidelines global update 2005: particulate matter, ozone, nitrogen dioxide and sulfur dioxide. World Health Organization: Geneva 2006.

43. Mautz, W. J.; Finlayson-pitts, B. J.; Messer, K.; Kleinman, M. T.; Norgren, M. B.; Quirion, J., Effects of ozone combined with components of acid fogs on breathing pattern, metabolic rate, pulmonary surfactant composition, and lung injury in rats. *Inhalation Toxicology* **1991,** *3* (1), 1-25.

44. Elliott, K.; Libet, B., Oxidation of phospholipid catalyzed by iron compounds with ascorbic acid. *Journal of Biological Chemistry* **1944,** *152* (3), 617-626.

45. Bernheim, F.; Bernheim, M. L. C., THE ACTION OF VANADIUM ON THE OXIDATION OF PHOSPHOLIPIDS BY CERTAIN TISSUES. *Journal of Biological Chemistry* **1939,** *127* (2), 353-360.

46. Yin, H.; Xu, L.; Porter, N. A., Free radical lipid peroxidation: mechanisms and analysis. *Chem Rev* **2011,** *111* (10), 5944-5972.

47. Spiteller, G., The Important Role of Lipid Peroxidation Processes in Aging and Age Dependent Diseases. *Molecular Biotechnology* **2007,** *37* (1), 5-12.

48. Criegee, R., Mechanism of ozonolysis. *Angewandte Chemie International Edition in English* **1975,** *14* (11), 745-752.

49. Fritzsching, K. J.; Kim, J.; Holland, G. P., Probing lipid–cholesterol interactions in DOPC/eSM/Chol and DOPC/DPPC/Chol model lipid rafts with DSC and 13C solid-state NMR. *Biochimica et Biophysica Acta (BBA) - Biomembranes* **2013,** *1828* (8), 1889-1898.

50. Svetlovics, James A.; Wheaten, Sterling A.; Almeida, Paulo F., Phase Separation and Fluctuations in Mixtures of a Saturated and an Unsaturated Phospholipid. *Biophys J* **2012,** *102* (11), 2526-2535.

51. Wallgren, M.; Dat Pham, Q.; Lidman, M.; Kinnunen, P. K. J.; Hof, M.; Gröbner, G., Impact of Oxidized Phospholipids on Membrane Organization. *Biophys J* **2013,** *104* (2, Supplement 1), 249a.

52. Thompson, K. C.; Rennie, A. R.; King, M. D.; Hardman, S. J. O.; Lucas, C. O. M.; Pfrang, C.; Hughes, B. R.; Hughes, A. V., Reaction of a Phospholipid Monolayer with Gas-Phase Ozone at the Air− Water Interface: Measurement of Surface Excess and Surface Pressure in Real Time. *Langmuir* **2010,** *26*, 17295-17303.

53. Thompson, K. C.; Jones, S. H.; Rennie, A. R.; King, M. D.; Ward, A. D.; Hughes, B. R.; Lucas, C. O. M.; Campbell, R. A.; Hughes, A. V., Degradation and Rearrangement of a Lung Surfactant Lipid at the Air–Water Interface during Exposure to the Pollutant Gas Ozone. *Langmuir* **2013,** *29* (14), 4594-4602.

54. Smith, H. L.; Howland, M. C.; Szmodis, A. W.; Li, Q.; Daemen, L. L.; Parikh, A. N.; Majewski, J., Early Stages of Oxidative Stress-Induced Membrane Permeabilization: A Neutron Reflectometry Study. *J Am Chem Soc* **2009,** *131* (10), 3631-3638.

55. Reis, A.; Domingues, M. R. M.; Amado, F. M. L.; Ferrer-Correia, A. J. V.; Domingues, P., Separation of peroxidation products of diacyl-phosphatidylcholines by reversed-phase liquid chromatography-mass spectrometry. *Biomed. Chromatogr.* **2005,** *19* (2), 129-137.

56. Brown, S. H. J.; Mitchell, T. W.; Blanksby, S. J., Analysis of unsaturated lipids by ozone-induced dissociation. *Biochimica et Biophysica Acta (BBA) - Molecular and Cell Biology of Lipids* **2011,** *1811* (11), 807-817.

57. Kim, H. I.; Kim, H.; Shin, Y. S.; Beegle, L. W.; Goddard, W. A.; Heath, J. R.; Kanik, I.; Beauchamp, J., Time Resolved Studies of Interfacial Reactions of Ozone with Pulmonary Phospholipid Surfactants Using Field Induced Droplet Ionization Mass Spectrometry. *The Journal of Physical Chemistry B* **2010,** *114* (29), 9496-9503.

58. Thomas, M. C.; Mitchell, T. W.; Harman, D. G.; Deeley, J. M.; Nealon, J. R.; Blanksby, S. J., Ozone-Induced Dissociation: Elucidation of Double Bond Position within Mass-Selected Lipid Ions. *Anal Chem* **2007,** *80* (1), 303-311.

59. Thomas, M. C.; Mitchell, T. W.; Harman, D. G.; Deeley, J. M.; Murphy, R. C.; Blanksby, S. J., Elucidation of Double Bond Position in Unsaturated Lipids by Ozone Electrospray Ionization Mass Spectrometry. *Anal Chem* **2007,** *79* (13), 5013-5022.

60. Lai, C. C.; Finlayson-Pitts, B. J.; Willis, W. V., Formation of secondary ozonides from the reaction of an unsaturated phosphatidylcholine with ozone. *Chemical research in toxicology* **1990,** *3* (6), 517-523.

61. Lai, C.; Yang, S.; Finlayson-Pitts, B., Interactions of monolayers of unsaturated phosphocholines with ozone at the air-water interface. *Langmuir* **1994,** *10* (12), 4637-4644.

62. Uhlson, C.; Harrison, K.; Allen, C. B.; Ahmad, S.; White, C. W.; Murphy, R. C., Oxidized Phospholipids Derived from Ozone-Treated Lung Surfactant Extract Reduce Macrophage and Epithelial Cell Viability. *Chemical research in toxicology* **2002,** *15* (7), 896-906.

63. Ellis, S. R.; Hughes, J. R.; Mitchell, T. W.; Blanksby, S. J., Using ambient ozone for assignment of double bond position in unsaturated lipids. *Analyst* **2012,** *137* (5), 1100-1110.

64. Zhou, Y.; Park, H.; Kim, P.; Jiang, Y.; Costello, C. E., Surface Oxidation under Ambient Air – Not Only a Fast and Economical Method to Identify Double Bond Positions in Unsaturated Lipids But Also a Reminder of Proper Lipid Processing. *Anal Chem* **2014**.

65. Wadia, Y.; Tobias, D. J.; Stafford, R.; Finlayson-Pitts, B. J., Real-Time Monitoring of the Kinetics and Gas-Phase Products of the Reaction of Ozone with an Unsaturated Phospholipid at the Air−Water Interface. *Langmuir* **2000,** *16* (24), 9321-9330.

66. Jurkiewicz, P.; Olżyńska, A.; Cwiklik, L.; Conte, E.; Jungwirth, P.; Megli, F. M.; Hof, M., Biophysics of lipid bilayers containing oxidatively modified phospholipids: Insights from fluorescence and EPR experiments and from MD simulations. *Biochimica et Biophysica Acta (BBA) - Biomembranes* **2012,** *1818* (10), 2388-2402.

67. Volinsky, R.; Kinnunen, P. K. J., Oxidized phosphatidylcholines in membrane-level cellular signaling: from biophysics to physiology and molecular pathology. *Febs J.* **2013,** *280* (12), 2806-2816.

68. Cwiklik, L.; Jungwirth, P., Massive oxidation of phospholipid membranes leads to pore creation and bilayer disintegration. *Chem Phys Lett* **2010,** *486* (4), 99-103.

69. Khabiri, M.; Roeselova, M.; Cwiklik, L., Properties of oxidized phospholipid monolayers: An atomistic molecular dynamics study. *Chem Phys Lett* **2012,** *519–520* (0), 93-99.

70. Wong-Ekkabut, J.; Xu, Z. T.; Triampo, W.; Tang, I. M.; Tieleman, D. P.; Monticelli, L., Effect of lipid peroxidation on the properties of lipid bilayers: A molecular dynamics study. *Biophys J* **2007,** *93* (12), 4225-4236.

71. Huynh, L.; Perrot, N.; Beswick, V.; Rosilio, V.; Curmi, P. A.; Sanson, A.; Jamin, N., Structural Properties of POPC Monolayers under Lateral Compression: Computer Simulations Analysis. *Langmuir* **2013,** *30* (2), 564-573.

72. Murzyn, K.; Róg, T.; Jezierski, G.; Takaoka, Y.; Pasenkiewicz-Gierula, M., Effects of phospholipid unsaturation on the membrane/water interface: a molecular simulation study. *Biophys J* **2001,** *81* (1), 170-183.

73. Vieceli, J.; Roeselová, M.; Potter, N.; Dang, L. X.; Garrett, B. C.; Tobias, D. J., Molecular Dynamics Simulations of Atmospheric Oxidants at the Air−Water Interface: Solvation and Accommodation of OH and O3. *The Journal of Physical Chemistry B* **2005,** *109* (33), 15876-15892.

74. Beranova, L.; Cwiklik, L.; Jurkiewicz, P.; Hof, M.; Jungwirth, P., Oxidation changes physical

properties of phospholipid bilayers: fluorescence spectroscopy and molecular simulations. *Langmuir* **2010,** *26* (9), 6140-6144.

75. Volinsky, R.; Cwiklik, L.; Jurkiewicz, P.; Hof, M.; Jungwirth, P.; Kinnunen, Paavo K. J., Oxidized Phosphatidylcholines Facilitate Phospholipid Flip-Flop in Liposomes. *Biophys J* **2011,** *101* (6), 1376-1384.

76. Khandelia, H.; Mouritsen, O. G., Lipid gymnastics: evidence of complete acyl chain reversal in oxidized phospholipids from molecular simulations. *Biophys J* **2009,** *96* (7), 2734-2743.

77. Dilbeck, C. W.; Finlayson-Pitts, B. J., Heterogeneous oxidation of a phosphocholine on synthetic sea salt by ozone at room temperature. *Phys Chem Chem Phys* **2013,** *15* (6), 1990-2002.

78. Dubowski, Y.; Vieceli, J.; Tobias, D. J.; Gomez, A.; Lin, A.; Nizkorodov, S. A.; McIntire, T. M.; Finlayson-Pitts, B. J., Interaction of gas-phase ozone at 296 K with unsaturated self-assembled monolayers: A new look at an old system. *The Journal of Physical Chemistry A* **2004,** *108* (47), 10473-10485.

79. Su, Y.-T.; Huang, Y.-H.; Witek, H. A.; Lee, Y.-P., Infrared Absorption Spectrum of the Simplest Criegee Intermediate CH2OO. *Science* **2013,** *340* (6129), 174-176.

80. Su, Y.-T.; Lin, H.-Y.; Putikam, R.; Matsui, H.; Lin, M. C.; Lee, Y.-P., Extremely rapid self-reaction of the simplest Criegee intermediate CH2OO and its implications in atmospheric chemistry. *Nat Chem* **2014,** *6* (6), 477-483.

81. Shen, Y.-R., *The principles of nonlinear optics*. Wiley-Interscience: New York, 1984.

82. Bain, C. D., Sum-frequency vibrational spectroscopy of the solid/liquid interface. *J. Chem. Soc., Faraday Trans.* **1995,** *91* (9), 1281-1296.

83. Miranda, P. B.; Shen, Y. R., Liquid Interfaces: A Study by Sum-Frequency Vibrational Spectroscopy. *The Journal of Physical Chemistry B* **1999,** *103* (17), 3292-3307.

84. Richmond, G., Molecular bonding and interactions at aqueous surfaces as probed by vibrational sum frequency spectroscopy. *Chem Rev* **2002,** *102* (8), 2693-2724.

85. Holman, J.; Davies, P. B.; Nishida, T.; Ye, S.; Neivandt, D. J., Sum Frequency Generation from Langmuir−Blodgett Multilayer Films on Metal and Dielectric Substrates. *The Journal of Physical Chemistry B* **2005,** *109* (40), 18723-18732.

86. Bonn, M.; Campen, R. K., Optical methods for the study of dynamics in biological membrane models. *Surf Sci* **2009,** *603* (10), 1945-1952.

87. Zhang, C.; Myers, J. N.; Chen, Z., Elucidation of molecular structures at buried polymer interfaces and biological interfaces using sum frequency generation vibrational spectroscopy. *Soft Matter* **2013,** *9* (19), 4738-4761.

88. Nihonyanagi, S.; Mondal, J. A.; Yamaguchi, S.; Tahara, T., Structure and Dynamics of Interfacial Water Studied by Heterodyne-Detected Vibrational Sum-Frequency Generation. *Annu Rev Phys Chem* **2013,** *64*, 579-603.

89. Ye, S.; Uosaki, K., Sum Frequency Generation (SFG) Evaluation of the Chemically Modified Solid Surface. In *Encyclopedia of Electrochemistry*, Wiley-VCH Verlag GmbH & Co. KGaA: 2007.

90. Ye, S.; Osawa, M., Molecular structures on solid substrates probed by sum frequency generation (SFG) vibration spectroscopy. *Chem Lett* **2009,** *38* (5), 386-391.

91. Ye, S.; Tong, Y.; Ge, A.; Qiao, L.; Davies, P. B., Interfacial Structure of Soft Matter Probed by SFG Spectroscopy. *The Chemical Record* **2014,** *14*, 794-805.

92. Stottrup, B. L.; Stevens, D. S.; Keller, S. L., Miscibility of Ternary Mixtures of Phospholipids and Cholesterol in Monolayers, and Application to Bilayer Systems. *Biophys J* **2005,** *88* (1), 269-276.

93. Liljeblad, J. F. D.; Bulone, V.; Tyrode, E.; Rutland, M. W.; Johnson, C. M., Phospholipid monolayers probed by vibrational sum frequency spectroscopy: instability of unsaturated phospholipids. *Biophys J* **2010,** *98* (10), L50-L52.

94. Tyrode, E.; Niga, P.; Johnson, M.; Rutland, M. W., Molecular Structure upon Compression and Stability toward Oxidation of Langmuir Films of Unsaturated Fatty Acids: A Vibrational Sum Frequency Spectroscopy Study. *Langmuir* **2010,** *26* (17), 14024-14031.

95. Stokes, G. Y.; Buchbinder, A. M.; Gibbs-Davis, J. M.; Scheidt, K. A.; Geiger, F. M., Chemically diverse environmental interfaces and their reactions with ozone studied by sum frequency generation. *Vib Spectrosc* **2009,** *50* (1), 86-98.

96. Kleber, J.; Kristian, L.; Friedrichs, G., Quantitative Time-Resolved Vibrational Sum Frequency Generation Spectroscopy as a Tool for Thin Film Kinetic Studies: New Insights into Oleic Acid Monolayer Oxidation. *The Journal of Physical Chemistry A* **2013,** *117* (33), 7863-7875.

Chapter 2

SFG Theory

Unlike the conventional linear optical techniques such as IR and Raman vibrational spectroscopy, which lack the intrinsic surface specificity, the second-order nonlinear optical technique, sum frequency generation (SFG) spectroscopy, has unique advantages on the interfacial studies.[1-4] In the present thesis, SFG spectroscopy is the main experimental technique to obtain the information of the molecular structure at the interfaces.

In this chapter, theoretical background of the SFG technique is briefly described. At the beginning, the intrinsically surface-specific features of the second-order nonlinear optical techniques will be introduced. Then, the basic SFG process at the interface will be discussed. After that, the analysis of the SFG spectra as well as the molecular orientation will be described.

2.1 General Theory of Nonlinear Optics

When putting a molecule in an intense electric field ($\boldsymbol{E}$),such as irradiation by an intense laser, the charge in the molecule will separate to induce a dipole. The induced dipole can be expressed as:

$$\boldsymbol{\mu} = \boldsymbol{\mu}^0 + \alpha : \boldsymbol{E} + \beta : \boldsymbol{EE} + \gamma : \boldsymbol{EEE} + \cdots \quad (2\text{-}1)$$

where $\boldsymbol{\mu}$ is the dipole moment of the molecule. $\boldsymbol{\mu}^0$ is the static dipole moment. α is the linear polarizability which is second rank tensor. β and γ are the first and second hyperpolarizabilities of the molecule, representing the non-linear response to the field, with third and fourth rank tensors, respectively. The symbolic notation $\beta : \boldsymbol{EE}$ means $\sum_i \sum_{j,k} \beta_{ijk} E_j E_k$, where the tensor element β_{ijk} represents Cartesian component i ($i = x, y, z$) of the hyperpolarizability induced by Cartesian components j and k ($j, k = x, y, z$) of the electric field, respectively. These non-linear responses to the field, as shown in terms including high-order (≥ 2) of $\boldsymbol{E}$, are the theoretical origin of the second, third, and higher order non-linear effects.

In macroscopic molecular system, such as a bulk material, one may use the term of polarization to express the average dipole moment in unit volume, as shown in following equation,

$$\begin{aligned}\boldsymbol{P} &= \boldsymbol{N\langle\mu\rangle} \\ &= \boldsymbol{P^{(0)}} + \boldsymbol{P^{(1)}} + \boldsymbol{P^{(2)}} + \boldsymbol{P^{(3)}} + \cdots \\ &= \boldsymbol{P^{(0)}} + \varepsilon_0(\chi^{(1)}\!:\boldsymbol{E} + \chi^{(2)}\!:\boldsymbol{EE} + \chi^{(3)}\!:\boldsymbol{EEE} + \cdots) \qquad (2\text{-}2)\end{aligned}$$

Where, N is the molecular number density. $\langle\ \ \rangle$ is the ensemble average over all the dipoles. ε_0 is vacuum permittivity. $\chi^{(1)}$, $\chi^{(2)}$, and $\chi^{(3)}$ are the linear, second order and third order nonlinear susceptibilities, respectively The term $\boldsymbol{P^{(0)}}$ is the static polarization which is independent of the electric field. The value of the high-order terms of χ are several orders lower than that of the linear term. Therefore, the high-order terms of polarization are often ignored in weak external field. However, when the external field is strong enough (such as the external field induced by the laser pulse), the response to the high-order nonlinear susceptibilities becomes substantial. In this thesis, we focus on the second non-linear optical process, because it is the fundamental for SFG spectroscopy.

If the total field consist of two electric fields such as two laser beams of $\boldsymbol{E_1} = E_1\,cos(\omega_1 t)$ and $\boldsymbol{E_2} = E_2\,cos(\omega_2 t)$, then the second order non-linear polarization $\boldsymbol{P^{(2)}}$ can be expressed as:

$$\begin{aligned}\boldsymbol{P^{(2)}} &= \varepsilon_0\chi^{(2)} : [E_1 + E_2]^2 \\ &= \varepsilon_0\chi^{(2)} : [E_1\,cos(\omega_1 t) + E_2\,cos(\omega_2 t)]^2 \\ &= \tfrac{1}{2}\varepsilon_0\chi^{(2)} : [E_1^2\,(1 + cos(2\omega_1)\,t) + E_2^2(1 + cos(2\omega_2)\,t)] \\ &\quad + \varepsilon_0\chi^{(2)} : E_1E_2[cos(\omega_1 + \omega_2)\,t + cos(\omega_1 - \omega_2)\,t] \qquad (2\text{-}3)\end{aligned}$$

The $\boldsymbol{P^{(2)}}$ contains the terms with frequencies of $2\omega_1$, $2\omega_2$, $\omega_1 + \omega_2$, and $\omega_1 - \omega_2$, which represents the oscillating polarization emit lights at the double, sum and difference frequency of the two applied electric fields, respectively. These are the origins of second harmonic generation (SHG), sum frequency generation (SFG), and difference frequency generation (DFG) processes, respectively.

Moreover, for the medium with inversion symmetry, optical properties are not changed upon inversion operation. Because the susceptibility $\chi^{(n)}$ contains the optical properties of the material, after inversion operation, the $\chi^{(n)}$ should keep constant. So $\chi^{(n)}$ obey the equation:

$$\chi^{(n)} = (-1)^{(n+1)}\chi^{(n)} \tag{2-4}$$

Where, *n* is the order of non-linear susceptibilities.

For the centrosymmetric medium as shown in figure 2.1, such as bulk liquid, gases, or centrosymmetric solid, the second order susceptibility $\chi^{(2)}$ should satisfy the equation (2-4), that is $\chi^{(2)} = -\chi^{(2)}$, so the $\chi^{(2)}$ must be zero, which means the medium is SFG inactive. On the other hand, for media without inversion symmetry, $\chi^{(2)}$ does not need to obey the Equation (2-4). The non-zero $\chi^{(2)}$ means that the medium is SFG active.

The interface is the boundary between two different media, so the symmetry of the interface is naturally broken. Thus, SFG is active at the interface while it is inactive in the bulk. That is the reason why SFG has intrinsically surface-specific feature. On the other hand, the odd-order susceptibilities such as linear susceptibility $\chi^{(1)}$ have no such surface-specific feature. Therefore, the linear spectroscopy does not have the intrinsically interface selectivity.

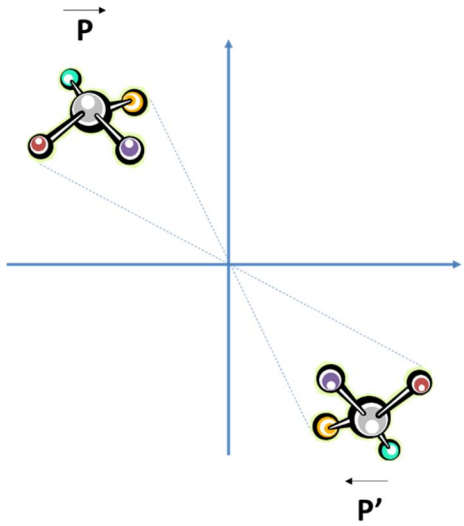

Figure 2.1 Scheme of the bulk phase with inversion symmetry

2.2 Vibrational SFG Process

In the common vibrational SFG process, two laser beams oscillating at visible (ω_{vis}, the ω represents "wavenumber" in the present thesis), and infrared (ω_{IR}) frequencies are spatially and temporally overlapped at interface to generate a sum frequency beam. When the infrared frequency is equal to the vibrational transition frequency of the interfacial molecules, the SFG intensity will be resonantly enhanced. As a result, we can obtain the vibrational information about the interfacial molecules from the SFG spectra. SFG process can be regarded as an infrared excitation followed by an anti-Stokes Raman transition as shown in Figure 2.2.[1]

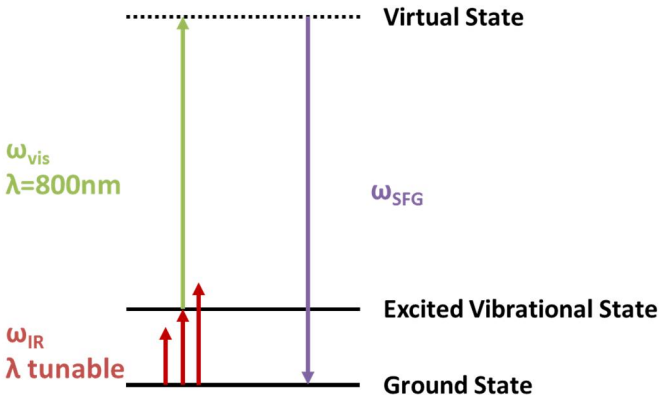

Figure 2.2 Energy-level diagram of SFG process

Based on the law of energy conservation, the frequency of SFG photon is equal to the sum of the infrared and visible photons, thus

$$\omega_{SFG} = \omega_{vis} + \omega_{IR} \tag{2-5}$$

On the other hand, according to the law of momentum conservation, the angular momentum parallel to the surface is conserved, so

$$p_{\parallel,SFG} = p_{\parallel,vis} + p_{\parallel,IR} \tag{2-6}$$

where $p_{\|}$ is the component of the momentum parallel to the surface.

Since

$$\omega = 1/\lambda \tag{2-7}$$

and the momentum of photon is

$$p = h\nu/c = h/\lambda \tag{2-8}$$

where λ is the wavelength in centimeter, Equations 2-5 and 2-6 can be expressed as:

$$\frac{1}{\lambda_{SFG}} = \frac{1}{\lambda_{vis}} + \frac{1}{\lambda_{IR}} \tag{2-9}$$

$$\frac{sin\theta_{SFG}}{\lambda_{SFG}} = \frac{sin\theta_{vis}}{\lambda_{vis}} + \frac{sin\theta_{IR}}{\lambda_{IR}} \tag{2-10}$$

where the θ_{SFG}, θ_{vis}, and θ_{IR} are the emitting angle of SFG photon and incident angles of visible and IR photons with respect to the surface normal, respectively. Therefore, the wavelength (λ_{SFG}) and emitting direction (θ_{SFG}) of the SFG photon can be calculated by the Equation (2-9) and (2-10).

The co-propagating geometry with visible beam and IR beam incident from same quadrant of incident plane is widely used in SFG setup. The SFG scheme with co-propagating geometry used in this thesis is showed in Figure 2.3.

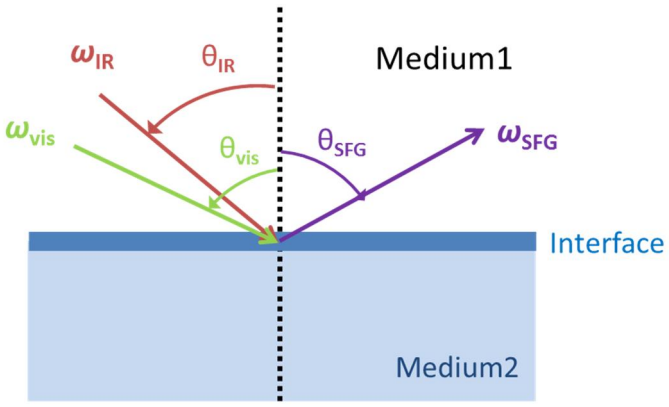

Figure 2.3 SFG with co-propagating geometry.

Assuming the values of both ω_{SFG} and ω_{vis} are far away from the electronic resonance frequency of the molecule, $\chi^{(2)}_{ijk}$ can be expressed as:

$$\chi^{(2)}_{ijk} \propto \frac{N M_{ij} A_k}{\hbar(\omega_{IR} - \omega_n + i\Gamma_n)} \tag{2-11}$$

where ω_n and Γ_n are the resonant frequency and damping constant of the *nth* vibrational mode, respectively. The *i, j* and *k* are the macroscopic susceptibility tensors that mentioned in section 2.1. M_{ij} is the Raman polarizavility tensor. A_k is the IR dipole moment of the *nth* vibrational mode. In order to generate SFG signal, both M_{ij} and A_k must be nonzero, in another word, both Raman and IR must be active.

As mentioned above, when the frequency of the tunable IR beam (ω_{IR}) is equal toω_n, $\chi^{(2)}_{ijk}$ is resonantly enhanced, which is the origin of the SFG peak in the spectrum. In order to obtain SFG spectrum, the IR frequency is scanned or broadband IR pulse is used. And by measuring the intensity of SFG signal as a function of IR frequency, the vibrational mode of the molecules at the surface or interface can be shown in the SFG spectrum.

2.3 SFG Spectral Analysis

As shown in Equation 2.12, the SFG intensity is proportional to the intensities of the incident visible and IR beams and the square of the second-order nonlinear susceptibilities ($\chi^{(2)}_{ijk}$) of the interfacial molecular system.[5]

$$I(\omega_{SFG}) \propto \left|\chi^{(2)}_{ijk}\right|^2 I(\omega_{vis}) I(\omega_{IR}) \tag{2-12}$$

It can also be expressed as:

$$I(\omega_{SFG}) = \frac{8\pi^3 \omega_{SFG}{}^2 sec^2\theta_{SFG}}{c_0^3 n_1(\omega_{SFG}) n_1(\omega_{VIS}) n_1(\omega_{IR})} \left|\chi^{(2)}_{eff}\right|^2 I(\omega_{vis}) I(\omega_{IR}) \tag{2-13}$$

where $I(\omega_i)$ is the intensity of the laser beams at frequency ω_i. $n_1(\omega_i)$ is the refractive index of the bulk medium at frequency ω_i. $\chi^{(2)}_{eff}$ is the effective second-order nonlinear susceptibility, which is the second-order nonlinear susceptibility ($\chi^{(2)}_{ijk}$) corrected by Fresnel factor. $\chi^{(2)}_{eff}$ can be described as:

$$\chi^{(2)}_{eff} = [\boldsymbol{L}(\omega_{SFG}) \cdot \vec{e}(\omega_{SFG})]: \chi^{(2)}_{ijk}[\boldsymbol{L}(\omega_{vis}) \cdot \vec{e}(\omega_{vis})][\boldsymbol{L}(\omega_{IR}) \cdot \vec{e}(\omega_{IR})] \quad (2\text{-}14)$$

where $\boldsymbol{L}(\omega_i)$ is the Fresnel factor at frequency ω_i. The Fresnel factor is considered as a filed correction to determine the absolute value of $\chi^{(2)}$. For a thin layer between medium 1 and 2, the Fresnel factors are given by[6]

$$L_{xx}(\omega_i) = \frac{2n_1(\omega)cos\theta_2}{n_1(\omega)cos\theta_2 + n_2(\omega)cos\theta_1} \quad (2\text{-}15)$$

$$L_{yy}(\omega_i) = \frac{2n_1(\omega)cos\theta_1}{n_1(\omega)cos\theta_1 + n_2(\omega)cos\theta_2} \quad (2\text{-}16)$$

$$L_{zz}(\omega_i) = \frac{2n_2(\omega)cos\theta_1}{n_1(\omega)cos\theta_2 + n_2(\omega)cos\theta_1}\left(\frac{n_1(\omega)}{n_m(\omega)}\right)^2 \quad (2\text{-}17)$$

Where n_1 and n_2 are the refractive indices of media 1 and 2 respectively. $n_m(\omega)$ is the effective refractive index of the interface layer at frequency ω_i. A slab model is usually used for the calculation of $n_m(\omega)$,[6]

$$n_m = \sqrt{\frac{n^2(n^2+5)}{4n^2+2}} \quad (2\text{-}18)$$

where *n* is the refractive index of the bulk.

As mentioned above, $\chi^{(2)}$ is a 3rd rank tensor and has 3^3=27 elements. Generally, the number of non-zero $\chi^{(2)}$ can be reduced under symmetry constraints. For example, an achiral azimuthally isotropic interface, there are seven achiral non-zero components, $\chi^{(2)}_{xxz} = \chi^{(2)}_{yyz}$, $\chi^{(2)}_{xzx} = \chi^{(2)}_{yzy}$, $\chi^{(2)}_{zxx} = \chi^{(2)}_{zyy}$, and $\chi^{(2)}_{zzz}$.[6] The $\chi^{(2)}_{eff}$ is dependent on the

experimental geometry and polarization combination, since they are related to the Fresnel factors. These achiral terms can be probed by *ssp* (*s*-SFG beam, *s*-visible beam, *p*-IR beam), *sps*, *pss*, and *ppp* polarization combinations. For co-propagating geometry, the relationship between $\chi_{\mathrm{eff}}^{(2)}$ and $\chi_{\mathrm{ijk}}^{(2)}$ (i, j, k = x, y, z) with different polarization combinations are shown as following:[6-7]

$$\chi_{eff,ssp}^{(2)} = L_{yy}(\omega_{SFG})L_{yy}(\omega_{vis})L_{zz}(\omega_{IR})sin\theta_{IR}\chi_{\mathrm{yyz}}^{(2)} \quad (2\text{-}19)$$

$$\chi_{eff,sps}^{(2)} = L_{yy}(\omega_{SFG})L_{zz}(\omega_{vis})L_{yy}(\omega_{IR})sin\theta_{vis}\chi_{\mathrm{yzy}}^{(2)} \quad (2\text{-}20)$$

$$\chi_{eff,pss}^{(2)} = L_{zz}(\omega_{SFG})L_{yy}(\omega_{vis})L_{yy}(\omega_{IR})sin\theta_{SFG}\chi_{\mathrm{zyy}}^{(2)} \quad (2\text{-}21)$$

$$\begin{aligned}\chi_{eff,ppp}^{(2)} = &-L_{xx}(\omega_{SFG})L_{xx}(\omega_{vis})L_{zz}(\omega_{IR})cos\theta_{SFG}cos\theta sin\theta_{IR}\chi_{\mathrm{xxz}}^{(2)}\\ &-L_{xx}(\omega_{SFG})L_{zz}(\omega_{vis})L_{xx}(\omega_{IR})cos\theta_{SFG}sin\theta_{vis}cos\theta_{IR}\chi_{\mathrm{xzx}}^{(2)}\\ &+L_{zz}(\omega_{SFG})L_{xx}(\omega_{vis})L_{xx}(\omega_{IR})sin\theta_{SFG}cos\theta_{vis}cos\theta_{IR}\chi_{\mathrm{zxx}}^{(2)}\\ &+L_{zz}(\omega_{SFG})L_{zz}(\omega_{vis})L_{zz}(\omega_{IR})sin\theta_{SFG}sin\theta_{vis}sin\theta_{IR}\chi_{\mathrm{zzz}}^{(2)}\end{aligned} \quad (2\text{-}22)$$

Generally, the conventional SFG intensity can be expressed by a Lorentzian model:[6, 8]

$$I_{SFG} \propto \left|\chi^{(2)}\right|^2 = \left|\chi_{NR}^{(2)} + \chi_{Res}^{(2)}\right|^2 = \left|A_{NR}e^{i\phi_{NR}} + \sum_n \frac{A_n}{\omega_{IR}-\omega_n+i\Gamma_n}\right|^2 \quad (2\text{-}23)$$

where $\chi_{NR}^{(2)}$ and $\chi_{Res}^{(2)}$ are the nonresonant and resonant second-order nonlinear susceptibilities, respectively. A_{NR} and ϕ_{NR} are the amplitude and phase of nonresonant susceptibility. A_n, ω_n, and Γ_n are the amplitude, frequency, and line width of the *nth* vibrational mode of the molecule. By fitting the SFG spectrum, we can get the value of A_n, ω_n, and Γ_n, that contains the information of the molecule structure.[9-15]

2.4 Molecular Orientation Analysis

Much information can be deduced from SFG spectra, such as surface density, relative orientation, conformation ordering, and surface dynamics. In this section, the analysis of molecular orientation on the basis of SFG results will be described. Since the orientation analysis of alkyl chain will be frequently used in the following chapters, the analysis of orientation of methyl group (CH_3) is taken as an example.

As mentioned above, for an achiral azimuthally isotropic interface, there are seven non-zero components of the second-order nonlinear susceptibility:

$$\chi^{(2)}_{yyz} = \chi^{(2)}_{xxz}, \chi^{(2)}_{yzy} = \chi^{(2)}_{xzx}, \chi^{(2)}_{zyy} = \chi^{(2)}_{zxx}, \chi^{(2)}_{zzz}.^{6} \quad (2\text{-}24)$$

The orientation angle of the terminal CH_3 group (θ) is defined as the angle between the surface normal and the symmetric axis of the CH_3 group. A scheme of the molecule orientation is given in Figure 2.4.

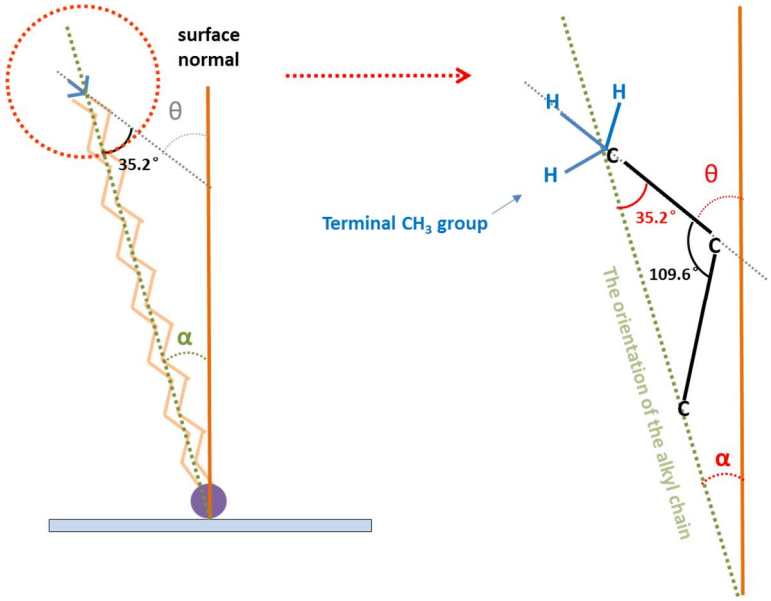

Figure 2.4 The orientation of terminal CH_3 group (θ) and alkyl chain (α)

Considering the CH_3 group has C_{3v} symmetry, the second-order nonlinear susceptibility for the symmetric and asymmetric C–H stretching modes of CH_3 group

can be expressed as :[7, 16]

$$\chi^{(2)}_{yyz,s} = \chi^{(2)}_{xxz,s} = \frac{1}{2}N\beta_{ccc}[\langle cos\theta\rangle(1+r) - \langle cos^3\theta\rangle(1-r)] \quad (2\text{-}25)$$

$$\chi^{(2)}_{yzy,s} = \chi^{(2)}_{xzx,s} = \chi^{(2)}_{zyy,s} = \chi^{(2)}_{zxx,s} = \frac{1}{2}N\beta_{ccc}[\langle cos\theta\rangle - \langle cos^3\theta\rangle](1-r) \quad (2\text{-}26)$$

$$\chi^{(2)}_{zzz,s} = N\beta_{ccc}[r\langle cos\theta\rangle + \langle cos^3\theta\rangle(1-r)] \quad (2\text{-}27)$$

$$\chi^{(2)}_{yyz,as} = \chi^{(2)}_{xxz,as} = -N\beta_{caa}(\langle cos\theta\rangle - \langle cos^3\theta\rangle) \quad (2\text{-}28)$$

$$\chi^{(2)}_{yzy,as} = \chi^{(2)}_{xzx,as} = \chi^{(2)}_{zyy,as} = \chi^{(2)}_{zxx,as} = N\beta_{caa}\langle cos^3\theta\rangle \quad (2\text{-}29)$$

$$\chi^{(2)}_{zzz,as} = N\beta_{caa}[\langle cos\theta\rangle - \langle cos^3\theta\rangle] \quad (2\text{-}30)$$

Where, N is the surface density of the CH_3 group. β_{ccc} and β_{caa} are the hyperpolarizabilities of the CH_3 group. The factor r is the ratio of β_{aac}/β_{ccc}. The operator $\langle\ \ \rangle$ is the ensemble average of the orientation angle of the surface group under the distribution function *f(θ)* as shown in following equation[17-18]

$$\langle F(\theta)\rangle = \int_{-\pi}^{\pi} F(\theta)f(\theta)sin\theta d\theta \quad (2\text{-}31)$$

Normally, the Gaussian function is employed for the distribution:

$$f(\theta) = \frac{1}{\sigma\sqrt{2\pi}}exp\left[-\frac{(\theta-\theta_0)^2}{2\sigma^2}\right] \quad (2\text{-}32)$$

where θ_0 and σ^2 are the mean orientation angle and variance, respectively. In case of $\sigma = 0°$, the Gaussian function can be simplified to the δ-distribution. With the δ-distribution, all terminal methyl groups are supposed to have the same orientation angle.

$\chi^{(2)}_{yyz}$ and $\chi^{(2)}_{yzy}$ are directly related to *ssp* and *sps* polarization combinations, respectively. Thus, their values can be deduced from SFG spectra. Combining the *ssp* and *sps* spectra and Equations (2-28) and (2-29), the orientation angle θ can be calculated after considering Fresnel coefficients.[18] If only *ssp* spectrum is available,

Equations (2-25) and (2-28) can be used to estimate the orientation angle of CH_3 group.[18] If hydrocarbon chains on surface are in all-trans conformation, their tilt angle (α) with respect to the surface normal can be calculated by:

$$\alpha = |35.2° - \theta|.^{18} \quad (2\text{-}33)$$

REFERENCE

1. Shen, Y.-R., *The principles of nonlinear optics*. Wiley-Interscience: New York, 1984.
2. Ye, S.; Uosaki, K., Sum Frequency Generation (SFG) Evaluation of the Chemically Modified Solid Surface. In *Encyclopedia of Electrochemistry*, Wiley-VCH Verlag GmbH & Co. KGaA: 2007.
3. Ye, S.; Osawa, M., Molecular structures on solid substrates probed by sum frequency generation (SFG) vibration spectroscopy. *Chem Lett* **2009,** *38* (5), 386-391.
4. Ye, S.; Tong, Y.; Ge, A.; Qiao, L.; Davies, P. B., Interfacial Structure of Soft Matter Probed by SFG Spectroscopy. *The Chemical Record* **2014,** *14*, 794-805.
5. Shen, Y. R.; Ostroverkhov, V., Sum-frequency vibrational spectroscopy on water interfaces: Polar orientation of water molecules at interfaces. *Chem Rev* **2006,** *106* (4), 1140-1154.
6. Zhuang, X.; Miranda, P.; Kim, D.; Shen, Y., Mapping molecular orientation and conformation at interfaces by surface nonlinear optics. *Phys. Rev. B* **1999,** *59* (19), 12632.
7. Wang, H. F.; Gan, W.; Lu, R.; Rao, Y.; Wu, B. H., Quantitative spectral and orientational analysis in surface sum frequency generation vibrational spectroscopy (SFG-VS). *Int. Rev. Phys. Chem.* **2005,** *24* (2), 191-256.
8. Shen, Y., Phase-Sensitive Sum-Frequency Spectroscopy. *Annu. Rev. Phys. Chem.* **2013,** *64*, 129-150.
9. Ye, S.; Noda, H.; Morita, S.; Uosaki, K.; Osawa, M., Surface Molecular Structures of Langmuir−Blodgett Films of Stearic Acid on Solid Substrates Studied by Sum Frequency Generation Spectroscopy. *Langmuir* **2003,** *19* (6), 2238-2242.
10. Ye, S.; Noda, H.; Nishida, T.; Morita, S.; Osawa, M., Cd2+-Induced Interfacial Structural Changes of Langmuir−Blodgett Films of Stearic Acid on Solid Substrates: A Sum Frequency Generation Study. *Langmuir* **2003,** *20* (2), 357-365.
11. Tong, Y.; Li, N.; Liu, H.; Ge, A.; Osawa, M.; Ye, S., Mechanistic Studies by Sum-Frequency Generation Spectroscopy: Hydrolysis of a Supported Phospholipid Bilayer by Phospholipase A2. *Angewandte Chemie International Edition* **2010,** *49* (13), 2319-2323.
12. Yu, L.; Liu, H.; Wang, Y.; Kuwata, N.; Osawa, M.; Kawamura, J.; Ye, S., Preferential Adsorption of Solvents on the Cathode Surface of Lithium Ion Batteries. *Angewandte Chemie International Edition* **2013,** *52* (22), 5753-5756.
13. Ge, A.; Wu, H.; Darwish, T. A.; James, M.; Osawa, M.; Ye, S., Structure and Lateral Interaction in Mixed Monolayers of Dioctadecyldimethylammonium Chloride (DOAC) and Stearyl Alcohol. *Langmuir* **2013**.
14. Wu, H.; Yu, L.; Tong, Y.; Ge, A.; Yau, S.; Osawa, M.; Ye, S., Enzyme-catalyzed hydrolysis of the supported phospholipid bilayers studied by atomic force microscopy. *Biochimica et Biophysica Acta (BBA) - Biomembranes* **2013,** *1828* (2), 642-651.
15. Qiao, L.; Ge, A.; Osawa, M.; Ye, S., Structure and stability studies of mixed monolayers of saturated

and unsaturated phospholipids under low-level ozone. *Phys Chem Chem Phys* **2013,** *15* (41), 17775-17785.

16. Hirose, C.; Akamatsu, N.; Domen, K., Formulas for the analysis of surface sum‐frequency generation spectrum by CH stretching modes of methyl and methylene groups. *J. Chem. Phys.* **1992,** *96*, 997.

17. Wang, J.; Paszti, Z.; Mark, A.; Chen, Z., Measuring polymer surface ordering differences in air and water by sum frequency generation vibrational spectroscopy. *J. Am. Chem. Soc.* **2002,** *124* (24), 7016-7023.

18. Ye, S.; Morita, S.; Li, G.; Noda, H.; Tanaka, M.; Uosaki, K.; Osawa, M., Structural changes in poly (2-methoxyethyl acrylate) thin films induced by absorption of bisphenol A. An infrared and sum frequency generation (SFG) study. *Macromolecules* **2003,** *36* (15), 5694-5703.

Chapter 3

Experimental

3.1 Chemicals

3.1.1 Saturated and Unsaturated Phospholipids

Saturated phospholipids 1,2-dipalmitoyl-*sn*-glycero-3-phosphocholine (DPPC) and unsaturated phospholipids 1,2-dioleoyl-*sn*-glycero-3-phosphocholine (DOPC), l-palmitoyl-2-oleoyl-*sn*-glycero-3-phosphocholine (POPC) were used in this thesis. The deuterated form 1,2-dipalmitoyl-d_{62}-*sn*-glycero-3-phosphorcholine-1,1,2,2-d_4-N,N,N-trimethyl-d_9 (DPPC-d_{75}), and 1-palmitoyl-d_{31}-2-oleoyl-*sn*-glycero-3-phosphocholine (DPPC-d_{75}) were also used. All the lipids were purchased from Avanti Polar Lipids with the purity of >99%. The 1mM lipid solutions were prepared in chloroform (Nacalai Tesque, Inc. All chemicals were used without further purification. [1-2]

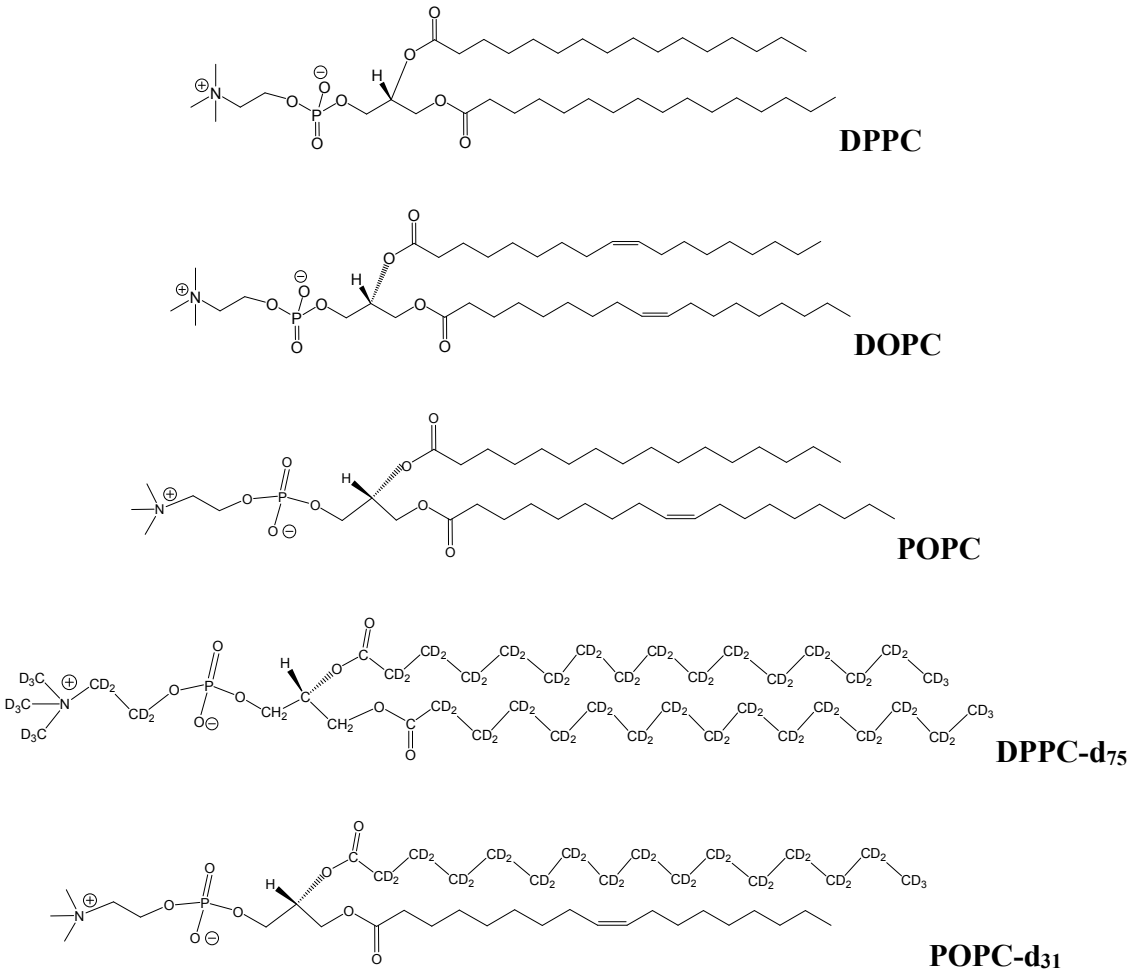

Figure 3.1 Molecular structures of DPPC, DOPC, POPC, DPPC-d_{75}, and POPC-d_{31}.

3.1.2 Expected Products of Phospholipid Oxidation Reaction

1-palmitoyl-2-azelaoyl-*sn*-glycero-3-phosphocholine (PAzPC), 1-palmitoyl-2-(9'-oxo-nonanoyl)-*sn*-glycero-3-phosphocholine (POnPC) of >99% purity were purchased from Avanti Polar Lipids. 1-nonanal ($CH_3(CH_2)_7CHO$) of >95.0% purity was purchased from Kanto chemical Co., Inc. Nonanoic acid ($CH_3(CH_2)_7COOH$) of >98.0% purity was purchased from Tokyo Chemical Industry Co., Ltd. The solutions with the concentration of 1mM were prepared in chloroform (Nacalai Tesque, Inc.). All chemicals were used without further purification.

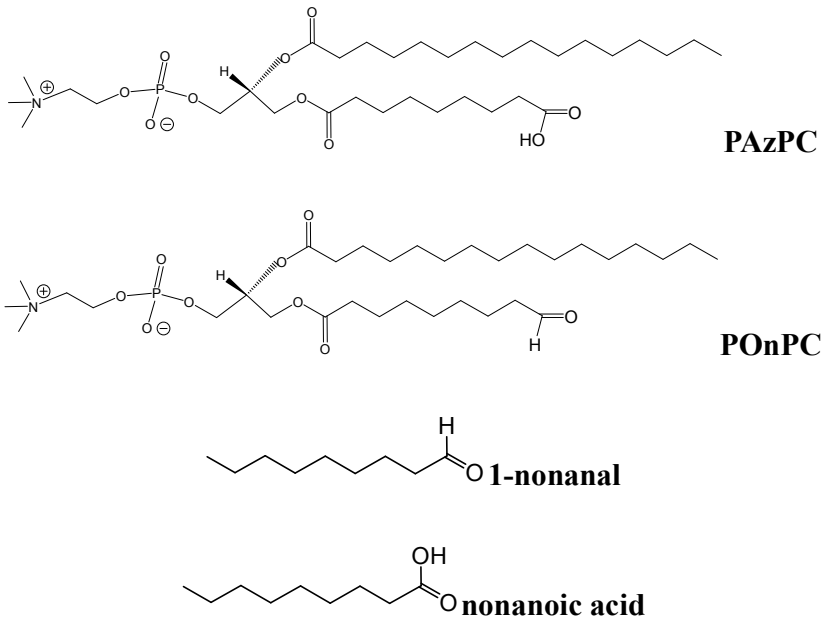

Figure 3.2 Molecular structures of oxidized phospholipids PAzPC and POnPC, and their counterpart residues 1-nonanal and nonanoic acid.

3.2 Sample Preparations

3.2.1 Mixed Phospholipids Solutions

DPPC-d_{75} - DOPC and DPPC - POPC mixed monolayers were prepared with the different molar ratios of DPPC-d_{75} to DOPC or DPPC to POPC of 3:1, 1:1 and 1:3 in chloroform. All solutions contained unsaturated lipids were prepared in a glove chamber filled with argon, with a volume of <1ml/bottle, usually used in a period shorter than one week in the ambient environment and protected by argon again every time after exposure to air.

3.2.2 Phospholipid Monolayer at Air-Water Interface[1]

The monolayers were prepared by spreading a certain volume of the solutions on the surface of pure water (Mill-Q, resistivity > 18.2 MΩcm) in a Langmuir-Blodgett (LB) trough (100mm×366mm, FSD-500, USI, of 140mm×70mm, KSV NIMA-102M) at 22℃ or 24. After the solvent had completely evaporated in 15 min, the π-A isotherm was recorded by compressing a PTFE barrier at the speed of 0.15 mm/sec for USI trough and 20 cm^2/min for NIMA trough.[3-4] The LB trough was placed in a sealed chamber (volume ca.9.5L) purged with different gases for special purposes.

Ozone flow was provided by an ozone generator (SK2002C, Syoken Co., Ltd., Japan) and mixed with the nitrogen (AIR-TECH, >99%) at a flow-rate of 10 L/min. And its concentration in the chamber was controlled to ca. 20 ppb as detected by an Aeroqual Series 200 portable monitor with an ozone R10 sensor head (Aeroqual Limited, New Zealand), which has a detection range from 0 to 150 ppb with a resolution of 1 ppb. It should be mentioned that the exact concentration of ozone in the chamber was not exactly controlled in the present study and usually ± 10 ppb fluctuations were present. The chamber volume is 9.5 L. The system can adjust the ozone concentration in range of 20 ± 10ppb in a period of ca. 3 ~ 5 min. The concentration of ozone was similar or slightly higher than the local environmental level including our laboratory atmosphere (typically ca. 10 ppb). To avoid any potential photochemical reactions, all the experiment were done in dark.

3.2.3 Monolayer Deposition on Solid Substrate

In order to evaluate the structure and morphology of the monolayers on the water surface after exposure to various environments, the monolayers after the exposures were transferred to a SiO_2 thin-film (~20 nm) covered CaF_2 surface or a freshly cleaved mica surface at a surface pressure of 15 mN/m or 30 mN/m by a vertical dipping procedure and characterized by SFG and AFM measurements. [5-8] The transfer ratios were close to 1.0.

3.3 Characterization Methods

3.3.1 π-A Isotherms

The surface pressure-area (π-A) isotherms of the monolayer at the gas-water interface can be obtained by a Wilhelmy plate on a LB trough. When a monolayer is compressed on water surface, the surface tension is reduced. The reduction of surface tension is defined as surface. The sum of surface tension and surface pressure is equal to absolute surface tension of water, i.e., 72.8 mN/m at the condition of 298 K, 1 atmosphere. The change of the water surface tension (or surface pressure) is measured by suspending a paper plate across the air/water interface and measuring the force by a balance. The experiment setup of π-A isotherms is shown in Figure 3.3.

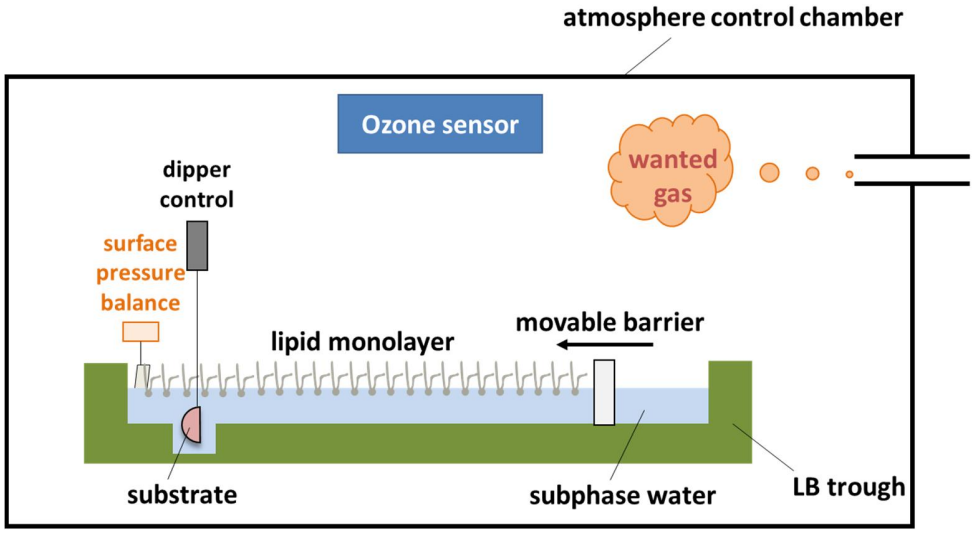

Figure 3.3. Scheme of a LB trough in the sealed chamber with surface pressure, dipper, and atmosphere control.

The monolayer is compressed by a movable barrier and transferred onto a substrate (CaF_2 prism or mica) by the vertical dipping method. The temperature of the subphase water is controlled by a chiller.

3.3.2 Monolayer Stability under Different Atmospheres

The monolayer stability was evaluated by the change in the surface area as a function of the exposure time to various environments at a constant surface pressure. As mentioned before, because the LB trough was placed in a sealed chamber, the atmosphere can be controlled easily. As shown in the Figure 3.4, the chamber fully filled with nitrogen immediately after the solution was spread. Then, the monolayer is compressed to the target surface pressure. About 1 hour later, the atmosphere in the chamber was changed by purging extremely low-concentration ozone. The surface area was recorded from the beginning to the end of the experiment.

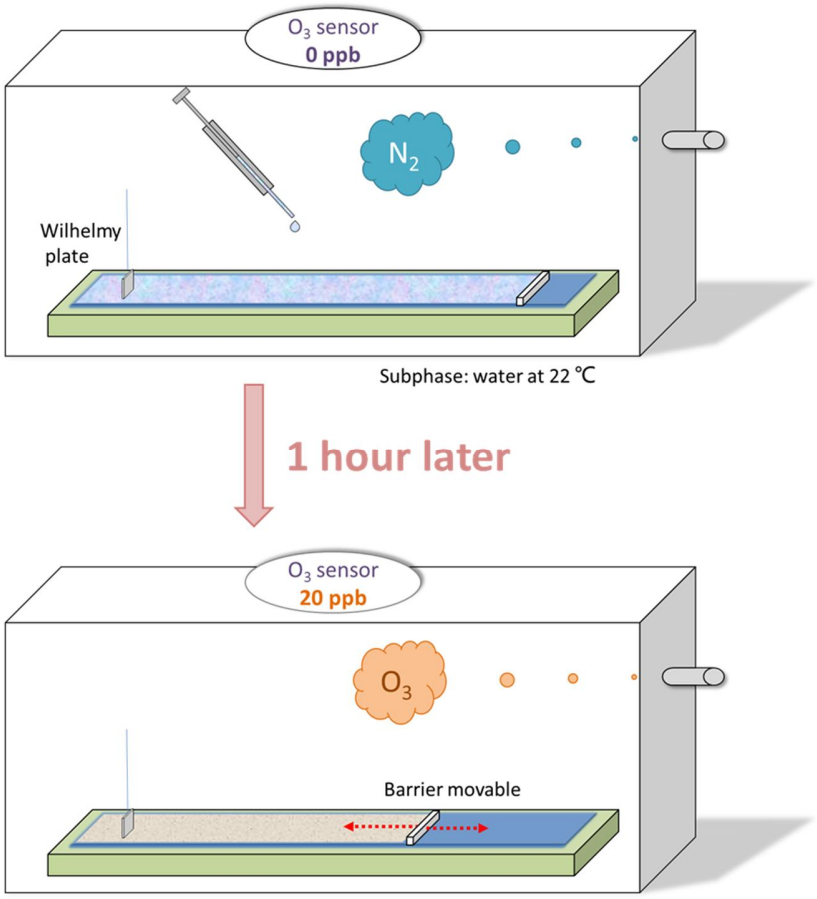

Figure 3.4. Stability measurement of the monolayer on a LB trough at a constant surface pressure.

3.3.3 SFG Vibrational Spectroscopy

The theory of SFG spectroscopy is introduced in chapter 2 in detail. Here gives the information about the laser system and the sample measurement.

(1) The Width and Resolution of SFG Spectrum

A broad-band femtosecond IR pulse SFG system with all-solid lasers is used in the present thesis. For a Gaussian pulse, the full width at half maximum (FWHM) of the temporal intensity profile (Δt) and the spectral intensity profile ($\Delta \nu$, frequency rather than circular frequency) are restrained by the minimum time-bandwidth product (TBWP):[9]

$$\Delta t \Delta \nu \geq 0.441 \quad (3\text{-}1)$$

For example, for a transform-limited Gaussian pulses with a duration of $\Delta t = 120$ *fs* centered at 3500 nm (IR pulse, normally used in C-H stretching region), the $\Delta \nu$ would be 3.68×10^{12} Hz, and $\Delta \omega = 123$ cm^{-1} (broadband). On the other hand, for a pulse of $\Delta t = 10$ *ps* ($10*10^{-12}$ sec) centered at 800 nm, $\Delta \omega = 1.47$ cm^{-1}(narrowband). Therefore, by combining femtosecond IR pulse and picosecond visible pulse, the SFG spectrum with a width (FWHM) more than 100 cm^{-1} and a spectral resolution of a few wavenumbers can be obtained.

(2) Laser System

Figure 3.5 shows the broad-band *fs* SFG system used in this thesis. Generally, it contains a Ti:Sapphire oscillator (MaiTai, Spec. Phys.), a regenerative amplifier (Spitfire Pro, Spec. Phys.), a pump laser (Empower, Spec. Phys.), an optical parametric generation (OPG)/amplification (OPA) (Travelling-wave Optical Parametric Amplifier of Super-fluorescence, TOPAS, Light Conversion Inc.) for IR beam, and a home-made spectra shaper.

In Ti:Sapphire oscillator, there are two diodes which can convert electric current to continue wave (cw) laser beam at 808±3nm (2*3W). This cw laser beam pumps the $Nd:YNO_4$ laser and gives a output beam at 1064nm. Then a LBO crystal further converts that output beam to 532nm (>5W, cw). Finally, the 532nm laser beam pumps the Ti:Sapphire crystal, and generates a mode locked 40MHz pulse train centered at 800nm with pulse duration of about 100*fs*.

After that, this 532nm laser beam seeds the regenerative amplifier system. The fundamental of the amplification process is the technique of chirped pulse amplification (CPA). It consists of three procedures, stretching the seed beam (532nm beam from MaiTai) in time domain, regenerating and amplifying the intensity of seed beam by a green pump laser (532.5nm) of Empower, and compressing the amplified pulse to its original time duration by a grating-based compressor. Typically, the output energy of the Spitfire Pro is around 2.1 mJ per pulse (800nm, ca.120 fs, 1 kHz).

Then, the regenerative amplifiers output is divided to two beam with equal energy. One beam is used to generate a narrow band (ca. 10cm^{-1}, in frequency domain) visible beam with time duration of ca. 10ps by a home-made pulse shaper. The other one is used to pump an OPG/OPA system and generate a single beam and an idler beam. Then these two beams pass through a non-linear crystal ($AgGaS_2$), by a difference frequency generation (DFG) process, to generate a tunable mid-IR beam with the wavelength between 2.5 to 10μm (4000-1000cm^{-1} wavenumber) and a FWHM of ca. 150 cm^{-1}.

The SFG setup with co-propagating geometry was used. The incidence angles for IR and visible beams are 50° and 70°, respectively. These two beams are spatially and temporally overlapped on the sample surface. The sample stage consists of several mounts which can adjust XY axis, Z axis, rotation, and tilt of the stages. The SFG signal is detected by a CCD detector (DU420-BV, Andor Technology) attached to a spectrograph (MS3504, Solar-TII, f = 35 cm, 1200 grooves/mm for visible region).

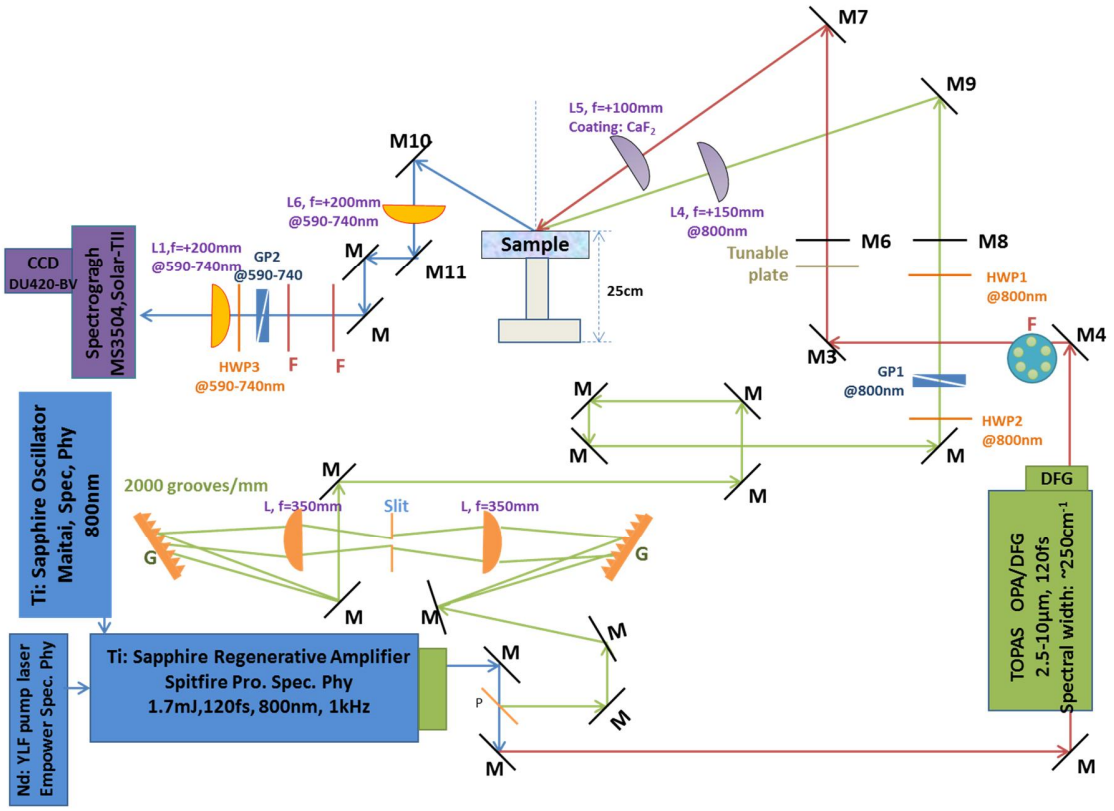

Figure 3.5. Scheme of the broad-band SFG setup. A laser system (in color of blue and green), pulse shaper (orange), sample stage (grey), and detection devices (purple). In the pulse shaper, the gratings and the slit are placed in the focal plane of the lens. The visible beam pass is in green, IR beam pass is in red, and SFG beam pass is in blue. Abbreviations: M mirror, L lens, HWP half wave plate, GP Glan prism, F filter, and HWP half wave plate.

(3) The Ex-situ and In-situ SFG Measurements

For the ex-situ SFG measurement, the phospholipid monolayers were transferred onto the surface of CaF2 substrate firstly, and then measured by SFG in air, as described in Section 3.2.3. For the in-situ SFG measurement, however, Langmuir monolayers on the water surface were detected by SFG directly. As shown in Figure 3.6, the NIMALB trough was fixed on the SFG sample stage. A surface height detector (KEYENCE SI-F10, resolution 10nm) was set upon the water surface to monitor the water evaporation. Unlike the ex-situ measurement, in which the LB trough was put in a chamber, the LB trough in in-situ measurement was exposed to ambient air containing trace amount of ozone (ca. 20ppb). Because the humility and the atmospheric pressure in the SFG room are constant, the water height decreases with constancy speed. Since the initial height of the water surface in the LB trough for each SFG probe is same and the accumulation time was 6min

for every spectrum, the effect of the water evaporation on the SFG signals can be ignored, and thus the SFG intensities are comparable. The alignment of the lens in each beam path should be adjusted patiently, especially the visible beam. The overlapping position for the two incident beam on the water surface should close to the focus of the lens in each beam path as much as possible, but noting to avoid burning the sample, usually shown as a bright white light.

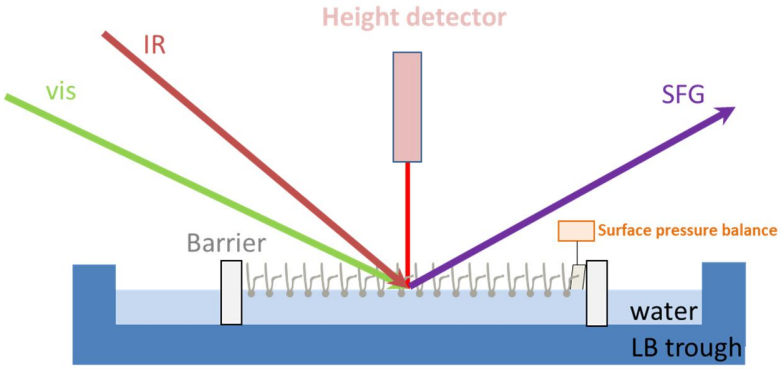

Figure 3.6 The experimental setup for in-situ SFG measurement.

3.3.4 Atomic Force Microscopy (AFM)

An Agilent 5500 atomic force microscope (Agilent Technologies) was used in air at room temperature (ca. 25℃). The tapping mode was used at the scan rate of 1 Hz using a SiN cantilever (OMCL-AC160TS-C2, Olympus)with the stiffness of 42N/m and resonant frequency of 300 kHz All the AFM measurements were carried out in the laboratory without further environment control. The Scanning Probe Image Processor SPIP 5.0.6 (Image Metrology A/s, Denmark) was used to analyze the AFM images.[8, 10]

REFERENCES

1. Qiao, L.; Ge, A.; Osawa, M.; Ye, S., Structure and stability studies of mixed monolayers of saturated and unsaturated phospholipids under low-level ozone. *Phys Chem Chem Phys* **2013,** *15* (41), 17775-17785.

2. Ye, S.; Tong, Y.; Ge, A.; Qiao, L.; Davies, P. B., Interfacial Structure of Soft Matter Probed by SFG Spectroscopy. *The Chemical Record* **2014,** *14*, 794-805.

3. Ye, S.; Noda, H.; Morita, S.; Uosaki, K.; Osawa, M., Surface molecular structures of Langmuir-Blodgett films of stearic acid on the solid substrate studied by sum frequency generation spectroscopy. *Langmuir* **2003,** *19*, 2238-2242.

4. Ye, S.; Noda, H.; Nishida, T.; Morita, S.; Osawa, M., Cd^{2+}-induced interfacial structural changes of Langmuir-Blodgett films of stearic acid on solid substrates: A sum frequency generation study. *Langmuir* **2004,** *20*, 357-365.

5. Ye, S.; Noda, H.; Nishida, T.; Morita, S.; Osawa, M., Cd2+-Induced Interfacial Structural Changes of Langmuir−Blodgett Films of Stearic Acid on Solid Substrates: A Sum Frequency Generation Study. *Langmuir* **2003,** *20* (2), 357-365.

6. Ye, S.; Noda, H.; Morita, S.; Uosaki, K.; Osawa, M., Surface Molecular Structures of Langmuir−Blodgett Films of Stearic Acid on Solid Substrates Studied by Sum Frequency Generation Spectroscopy. *Langmuir* **2003,** *19* (6), 2238-2242.

7. Tong, Y.; Li, N.; Liu, H.; Ge, A.; Osawa, M.; Ye, S., Mechanistic Studies by Sum-Frequency Generation Spectroscopy: Hydrolysis of a Supported Phospholipid Bilayer by Phospholipase A2. *Angewandte Chemie International Edition* **2010,** *49* (13), 2319-2323.

8. Wu, H.; Yu, L.; Tong, Y.; Ge, A.; Yau, S.; Osawa, M.; Ye, S., Enzyme-catalyzed hydrolysis of the supported phospholipid bilayers studied by atomic force microscopy. *Biochimica et Biophysica Acta (BBA) - Biomembranes* **2013,** *1828* (2), 642-651.

9. Ye, S.; Uosaki, K., Sum Frequency Generation (SFG) Evaluation of the Chemically Modified Solid Surface. In *Encyclopedia of Electrochemistry*, Wiley-VCH Verlag GmbH & Co. KGaA: 2007.

10. Ge, A.; Wu, H.; Darwish, T. A.; James, M.; Osawa, M.; Ye, S., Structure and Lateral Interaction in Mixed Monolayers of Dioctadecyldimethylammonium Chloride (DOAC) and Stearyl Alcohol. *Langmuir* **2013**.

Chapter 4

Structure and Stability Studies on DOPC Monolayer and DPPC-DOPC Mixed Monolayers in Low-level Ozone

4.1 Introduction

As mentioned in Chapter 1, the chain length and saturation degree of the phospholipids can significantly influence the density, fluidity and phase transition behaviors of the cell membranes.[1] An appropriate ratio of saturated and unsaturated phospholipids is regarded as an important feature for a certain membrane. Furthermore, the stability of the membranes is essential to maintain a good biological function for the membrane. The heavy oxidation of the lipids in the cell membrane could cause oxidative stress which may further induce various serious diseases, such as cancer, atherosclerosis, and Parkinson's disease.[2-3] Since the stabilities of the saturated and unsaturated lipids are different with respect to oxidation, the functionality of the membranes could be considerably affected, especially in an environment contaminated by oxidants such as ozone, which is a universal air pollutant. The concentration of ozone at the earth surface of troposphere are usually few tens of ppb, mainly formed upon photochemical reaction of nitrogen oxide (NO_x) and volatile organic compounds (VOC) with UV light. It is an urgent issue to determine the influence of the lipid oxidation in an ambient environment containing a low concentration of ozone on the membrane's structure and function. And it is highly expected to investigate the stability of lipid molecules under the similar indoor environment since the reaction rate and oxidation selectivity can significantly affect by the ozone concentration.

In this chapter, an unsaturated lipid, 1,2-dioleoyl-*sn*-glycero-3-phosphocholine (DOPC), and a saturated lipid, 1,2-dipalmitoyl(d_{62})-*sn*-glycero-3-phosphorcholine- -1,1,2,2-d_4-N,N,N- trimethyl-d_9 (DPPC-d_{75}), were used to prepare single and binary mixed monolayers to mimic the cell membrane. The deuterated DPPC was used in order to distinguish the vibrational contribution from DOPC in the DPPC/DOPC

mixed monolayer.

The stability and structure of these monolayers exposed to nitrogen, oxygen, lab air and an extremely low concentration of ozone (20±10 ppb) on the water surface were explored by π-A isotherm, sum frequency generation (SFG) vibrational spectroscopy and atomic force microscopy (AFM). AFM was used to probe the morphological changes induced by the ozone exposure. SFG spectroscopy, which is known for its excellent surface sensitivity and selectivity,[4-12] was employed to probe the structural changes in these monolayers exposed to different environments at a molecular level. The combination of the three techniques gives some new insights of lipid oxidation of DPPC-DOPC mixed monolayer.

Our experiments demonstrated that the unsaturated DOPC in the pure/mixed monolayers become unstable after exposure to a low concentration of ozone or even to ambient laboratory atmosphere, which has a similar ozone level, but stable in nitrogen or oxygen. The saturated DPPC is stable in all environments. These results suggest that the unsaturated phospholipids can be selectively oxidized by a trace amount of ozone in the ambient environment. The differences in the reaction mechanism, structural changes and oxidation products between the DOPC monolayer and DPPC-d_{75}/DOPC mixed monolayers have been discussed based on our observations. And the oxidation of DOPC is affected by the presence of DPPC. The present study provides important information about the physicochemical properties of the model cell membranes with unsaturated phospholipids in the normal environment with an extremely *low* ozone concentration.

4.2 Experimental

In this chapter, one saturated lipid DPPC-d_{75} and one unsaturated lipid DOPC were chosen to mimic the cell membrane. Their molecular structures area shown in Figure 4.1. See more details about the chemicals in Chapter 3.

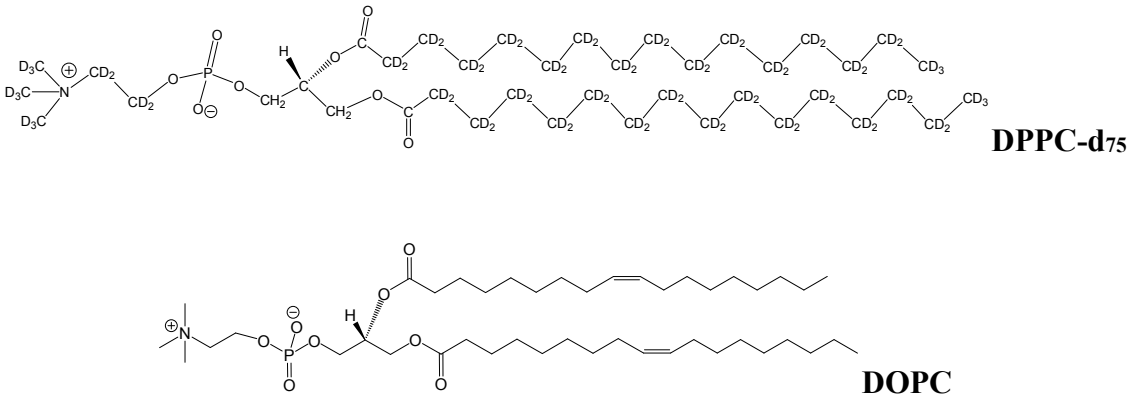

Figure 4.1 Molecular structures of DPPC-d_{75}, and DOPC.

Langmuir-Blodgett (LB) trough (100 mm×366 mm, FSD-500, USI) was used to measure the π-A isotherms, the stability of the monolayer in different atmosphere, and transfer the monolayer to mica or CaF_2 prism surface. For the latter two experiments, the surface pressure was controlled at 30 mN/m. The temperature of the water subphase is 22℃.

Details for the measurements of the π-A isotherms, AFM and SFG have been given in Chapter 3.

4.3 Results and Discussion

4.3.1 π-A Isotherms

Figure 4.2 shows the π-A isotherms of the DPPC-d_{75}, DOPC and DPPC-d_{75}/DOPC binary mixtures with molar ratios of 3:1, 1:1, and 1:3 in a nitrogen environment. The surface pressure for the DPPC-d_{75} monolayer on the pure water surface slowly increases as the liquid-expanded (LE) phase when the surface density is higher than 0.9 nm^2 per molecule. After a flat plateau (LE-LC phase) around 15 mN/m, the liquid-condensed phase (LC) appears, showing an area of 0.46 nm^2 per DPPC. The DPPC-d_{75} monolayer collapses around 56 mN/m. In contrast, only the LE phase is observed for the DOPC monolayer on the water surface. The highly condensed structure of the DPPC-d_{75} monolayer can be attributed to the *all-trans* conformation in its alkyl chains with strong van der Waals interactions. The DOPC monolayer shows a more expanded structure. This is associated with the presence of kink structures induced by the C=C bonds in the *cis*-conformation of the DOPC alkyl chains.

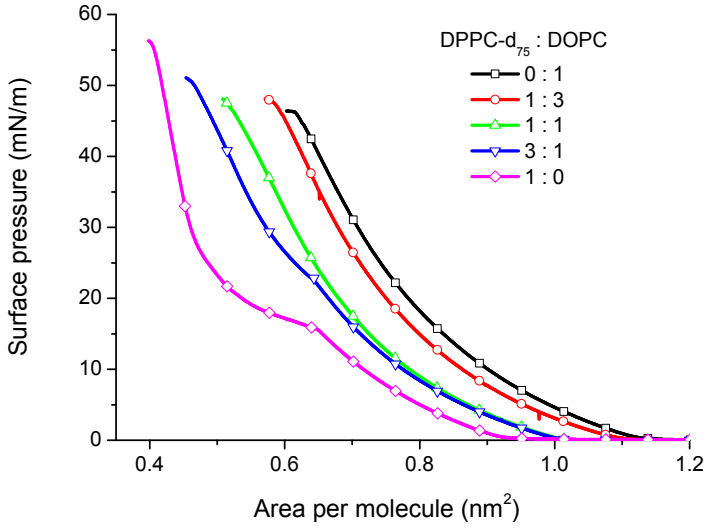

Figure 4.2 π-A isotherms of DPPC-d_{75}/DOPC mixed monolayers. The π-A isotherms is

probed on a pure water surface (22℃) mixed monolayer is in the DPPC-DOPC molar ratio of 0:1, 1:3, 1:1, 3:1, and 1:0. All the isotherms were measured in a nitrogen atmosphere and dark.

The π-A isotherms of the binary DPPC-d_{75}/DOPC mixed monolayers locate between those of the two pure components (Figure 4.2), similar to that of the DPPC/DOPC mixtures previously reported.[13] With the increase of the DOPC component in the mixed monolayer, the π-A isotherm gradually moves to the right, indicating that the molecular density of the monolayer decreases. The LE-LC phase appears as a shoulder around 22 mN/m for the DPPC-d_{75}/DOPC of 3:1, but vanishes for the DPPC-d_{75}/DOPC of 1:1 and 1:3. The ratio of the saturated and unsaturated components in the mixed monolayer significantly affects its structure.

4.3.2 Monolayer Stability in Different Environments

It was found that the reproducibility of the above π-A isotherms above became worse if the LB chamber was opened to our lab air. Thus, we investigated the stability of the surface area of these monolayers at a constant surface pressure of 30 mN/m. The stability of the monolayers under different environments can be sensitively monitored in comparison to the π-A isotherm. The stability was also evaluated by measuring the changes in the surface pressure over a constant surface area.[14-16] Figure 4.3 shows the changes in the surface area as a function of exposure time to nitrogen (0~60 min) and low-level ozone (20 ± 10 ppb) (60~200 min).

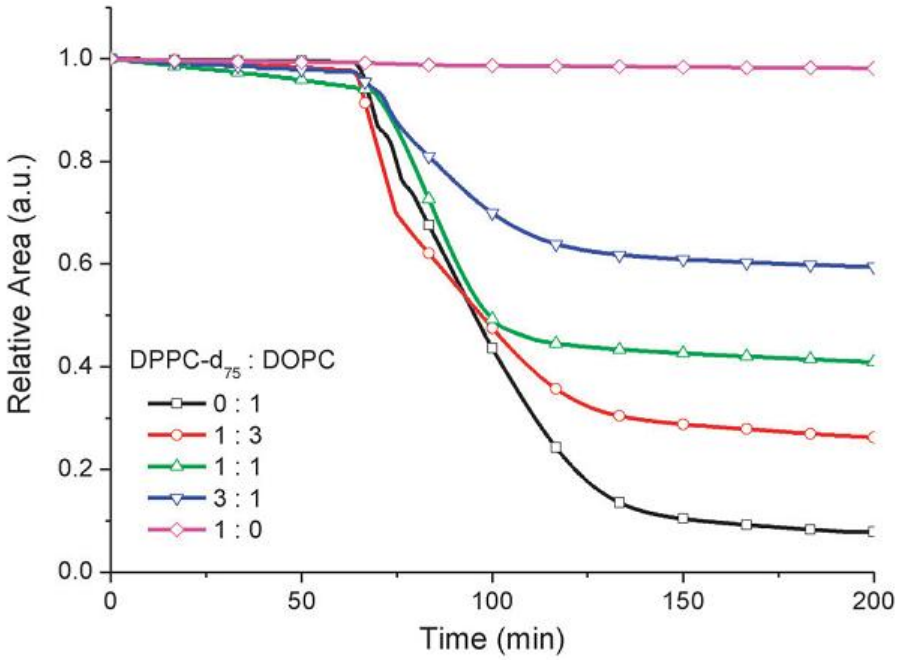

Figure 4.3 Stability of surface area for the DPPC-d_{75}/DOPC mixed monolayers at 30 mN/m as a function of time. The monolayers are exposed to nitrogen in the first 60 min and then switched to an ozone environment (20 ± 10 ppb). All the surface areas are normalized to the initial area. See text for details.

All the monolayers are stable in the nitrogen environment and show only very small decreases in the initial 60 min (Figure. 4.3). The same experiments were also carried out in a pure oxygen environment (results are not shown here), and similar behaviors were observed in nitrogen. On the other hand, when a small amount of ozone is introduced into the chamber (20 ± 10 ppb), all the monolayers, except for the pure DPPC-d_{75}, show fast decreases in the surface area after a short delay (typically 3 min or more) and become almost constant after a certain period (ca. 1 hr.). The decrease in the surface area for the monolayer at a constant surface pressure (30 mN/m) indicates the loss of molecules from the water surface or the area of partially degraded lipid become smaller and implies that the DOPC monolayer and DOPC-contained mixed monolayers are partially decomposed by the ozone exposure. This is in agreement with previously reported results that 100% oxidized DOPC shows a fast

area per lipid decrease in long-timescale by means of molecular dynamics, because the orientation of oxidized lipid molecules was reversed and a micelle-like structure was formed in the aqueous subphase.[17-19] Generally, it was found that the higher the ratio of DOPC in the monolayer, the greater the area loss. For example, the pure DOPC monolayer lost 88.0% of its original area, while the DPPC-d_{75}/DOPC mixed monolayer (3:1) lost 35.7% in the quick decay process after exposure to ozone. The instability of the mixed monolayer seems to be associated with the amount of the unsaturated DOPC in the monolayer. Assuming that the unsaturated DOPC molecules lose their surface area and only saturated DPPC-d_{75} molecules stay on the surface after exposure to ozone, the expected area losses for each mixed monolayer were calculated (Table 4.1). However, a certain area always remained after the fast decay process for the pure DOPC monolayer (Figure. 4.3). Part of the DOPC or its oxidized products may still stay on the water surface and therefore, a small difference was always found between the area loss and the expected loss based on the above assumption for each monolayer. We will discuss the origin for this later based on other AFM and SFG observations.

Table 4.1 The observed and expected area losses for the single and binary mixed monolayers after the ozone exposure.

Monolayer (DPPC-d_{75}:DOPC)	Mole Ratio of DOPC	Mean Area per Molecule (nm^2)	Mean Density ($/nm^2$)	Surface Loss (%)	Expected Loss (%)	Difference D (%)
1:0	0	0.46	2.71	0.8	0	-0.8
3:1	0.25	0.57	1.75	35.7	39.8	4.1
1:1	0.5	0.61	1.63	52.3	62.5	10.2
1:3	0.75	0.68	1.47	68.8	83.1	14.3
0:1	1.0	0.71	1.41	88.0	100	12.0

On the other hand, although a good reproducibility has been obtained on the area loss for different monolayer systems (Figure. 4.2), it is hard to reproduce the time

necessary for the complete the decay process. This may be attributed to the fluctuation of the ozone concentration in the LB chamber as mentioned in the Experimental section. We could not control the ozone concentration at exactly the same value but in a region of 20 ± 10 ppb. It was found that the ozone concentration could significantly affect the reaction rate, which directly influences the time for the decay process of the monolayers in the LB chamber. Due to the technical reason, a quantitative discussion on the reaction kinetics was not carried out in the present study. Fortunately, the fluctuation in the ozone concentration does not affect the equilibrium process for determining the area losses induced by ozone.

It is noteworthy that if the LB trough chamber was opened to our laboratory atmosphere, a similar surface area decreases was also observed. The ozone detector showed that the ozone level in our laboratory changes from 10 to 50 ppb depending on the day. Once the chamber switched back to pure nitrogen (or oxygen), such an influence disappeared. Previously, Stottrup *et al.*[14] and Liljeblad *et al.* reported the instability of unsaturated phospholipids in air but did not clearly reveal its origin[20]. Based on the present experiment, we believe that the changes observed in their experiments should be induced by the ozone present in the ambient air.

Thompson *et al.* found that both surface pressures of the POPC monolayer and POPC/DPPC mixed monolayers at a fixed surface area increase soon after exposure to ozone and then decreases.[15-16] They attributed this change to a fast reorientation of the oxidized tail of the POPC molecule at the interface. In the present study, we did not find any increase in the surface area for the DOPC monolayer, but for the POPC monolayer (See Figure 5.4 in Chapter 5 and discussion there) at the constant surface pressure (30 mN/m). As two hydrocarbon chains in the DOPC contain the *cis*-C=C bond, a smaller reorientation influence is expected in comparison with POPC under

the present conditions.

As discussed above, although the ozone concentration is very low (20 ± 10 ppb), it is readily high enough to oxidize the unsaturated phospholipids on the water surface. However, it is difficult to get further information only from these surface pressure measurements. In the following sections, AFM and SFG characterizations were employed to explore the structure and the morphology changes in these monolayers exposed ozone.

4.3.3 AFM Evaluation of DPPC-d_{75} and DOPC Lipid Monolayers

Figure 4.4 shows a typical AFM image (4 × 4 μm^2) of the mixed monolayer of DPPC-d_{75}/DOPC (1:1) on the mica surface transferred at 30mN/m (a) before and (b) after exposure to low level ozone on the water surface. Figure 4.4a demonstrates the existence of two phases with different heights in the mixed monolayer. Such phase separation features were not observed in the DPPC-d_{75} or DOPC monolayers. A number of parallel stripes are observed on the mixed monolayer surface. The direction of the stripe is perpendicular to the dipping direction of the monolayer (dipping directions are shown by arrows in the images). Vie *et al.*[13] found a similar feature of the DPPC-DOPC mixed monolayer on a mica surface deposited at 37 mN/m. Moraille and Badia[21-22] reported the formation of stripe pattern structures of DPPC and 1,2-dilauroyl-*sn*-glycero- 3-phosphocholine (DLPC) mixed monolayers and bilayers on a mica surface under different conditions. The height difference between the two domains in Figure. 4.4a is 0.8 ± 0.2 nm, close to that reported by Vie *et al.* (0.9 ± 0.1nm).[13] The higher and lower domains can be related to the DPPC-d_{75}-rich domain (in LC-condensed phase) and the DOPC-rich domain (in LC-LE phase), respectively. The fraction analysis of the domains (Figure. 4.4c) shows that the lower domains of

DOPC occupy ca. 78 % (± 5 %) of the surface. This value is higher than that estimated from the π-A isotherm for the 1:1 mixed monolayer (62%, Figure. 4.2). Due to the phase separation, DOPC and DPPC-d_{75} locate in their own domains on the surface. The DOPC molecules in the disordered LE phase occupy the majority of the surface even mixed with saturated DPPC molecules (1:1). DOPC and DPPC-d_{75} can directly interact with each other in the domain boundary region.

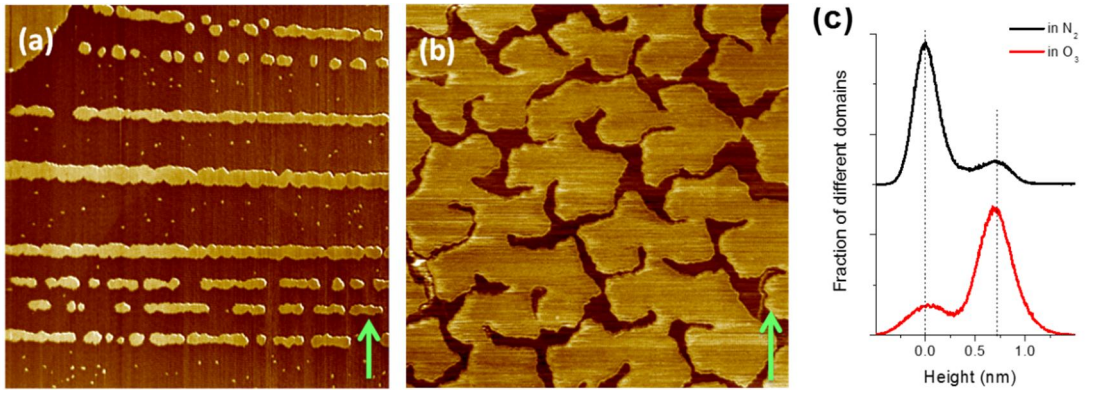

Figure 4.4 AFM images of DPPC-d_{75}/DOPC (1:1) mixed monolayer and height-distribution histogram. AFM images (4 × 4 μm^2) of the DPPC-d_{75}/DOPC (1:1) mixed monolayer transferred from the water surface at 30 mN/m (a) before and (b) after exposure to low-level ozone. (c) The height-distribution histogram for the two AFM images. The arrows in the AFM images show the direction of the monolayer transfer.

If the mixed monolayer on the water was exposed to ozone for 140 min before transfer to the mica substrate, the morphology of the mixed monolayer is typically changed (Figure. 4.4b). Although the phase separation is still visible in the AFM image with a similar height difference (0.8 ± 0.2nm), the stripe features almost disappear and the majority of the surface is now occupied by the higher domain (i.e., DPPC-d_{75}-rich domain). The ratio for the DOPC-rich domain is less than 20 %, significantly lower from that before the ozone exposure (78 %). The narrow DOPC domains are surrounded by wide DPPC-d_{75} domains. The present AFM observation

indicates that the DOPC-rich domains decrease, but the DPPC-d_{75}-rich domains increase induced by the ozone exposure and imply that the DOPC molecules are removed from the monolayer on the water surface by the ozone, while DPPC-d_{75} is very stable under this condition. Since a small portion of DOPC-rich domains is still present on the surface after a long exposure to ozone, the DOPC molecules near the domain boundary may show different properties from the original DOPC domain due to the interaction with the saturated DPPC-d_{75} molecules.

It should be noting that only the DPPC-d_{75}/DOPC (1:1) mixed monolayer is measured here as a representative sample of mixed monolayer. The other ratio of the DPPC-d_{75} to DOPC mixed monolayer is prospected to have similar results and still under further studying now. In addition, we did the AFM observation for the pure DPPC-d_{75} or DOPC monolayers transferred before and after ozone exposure. The surface morphologies are quite homogenous and no clear difference could be observed within our AFM spatial resolution. (Figure is not shown here.) No large difference in the surface morphology was observed after transferring the monolayer to the mica surface and exposing it to laboratory air during the period of the AFM measurement,.

4.3.4 SFG measurement of DPPC-d_{75} and DOPC lipid monolayer

4.3.4.1 Pure DPPC-d_{75} and DOPC lipid monolayer

(1) DPPC-d_{75} Monolayer

Figure 4.5a shows the *ssp*-polarized SFG spectra of the DPPC-d_{75} monolayer prepared in nitrogen (black) and ozone (red) in the C-D stretching region (2000-2300 cm^{-1}). As mentioned in the Experimental section, in order to distinguish the SFG vibrational signals from the DOPC and DPPC molecules in the mixed monolayers deuterated DPPC molecules (DPPC-d_{75}) and hydrogenated DOPC are used in this study. The SFG signals (black open blocks) and fitting results (black trace) based on Eq. (2-23) of the DPPC-d_{75} monolayer in nitrogen exhibit three strong peaks around 2080, 2135, and 2220 cm^{-1}. These peaks are assigned to the C-D symmetric stretching mode (CD_3,ss), Fermi resonance ($CD_{3,FR}$), and asymmetric stretching mode (CD_3,as) of the terminal CD_3 moieties, respectively, in the long alkyl chain of DPPC-d_{75}.[23-24]

The *sps*-polarized SFG spectrum shows only one peak attributed to the CD_3 asymmetric stretching mode (Figure 4.5b). SFG peaks from the CD_2 groups at 2110 cm^{-1} (CD_2,ss) and 2226 cm^{-1} (CD_2,as) are too weak to observe in the SFG spectra. The fitting results show the amplitude ratio between CD_2,ss and CD_3,ss ($A_{CD2,ss}/A_{CD3,ss}$) is quite low (~ 0, Table 4.2). These results revealed that the hydrocarbon chains of DPPC-d_{75} maintained an ordered structure with the *all-trans* conformation in which only the terminal methyl groups are SFG active, but the methylene groups do not contribute to the SFG signals due to the local symmetry restriction.[25] This is consistent with the π-A isotherm (Figure. 4.2) in which the DPPC-d_{75} monolayer at 30 mN/m maintains the LC phase with a high density (0.46 nm^2). The tilt angle (α) of the alkyl chains in the DPPC-d_{75} monolayer was estimated

from the *ssp*- and *sps*-polarized SFG spectra to be 1.6°± 0.5°revealing that the alkyl chains of the DPPC molecules are almost perpendicular to the surface.[26]

The DPPC-d_{75} monolayer prepared in the ozone environment (20 ± 10 ppb) exhibits a similar SFG spectrum (Figure. 4.5a, red). Three intense SFG peaks due to the methyl group are observed with a significant contribution from the methylene group. The tilt angle (α) of the alkyl chain was estimated to be 2.3°± 0.5°. This indicates that the DPPC-d_{75} monolayer on the water surface is stable and keeps the identical structure in the *all-trans* conformation under the low-level ozone exposure.

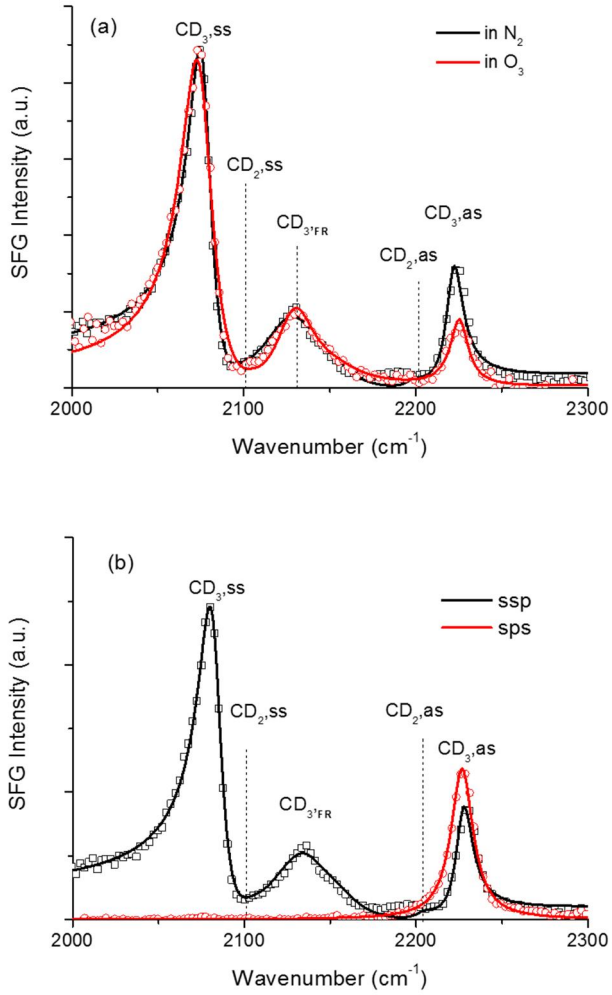

Figure 4.5 SFG spectra of pure DPPC-d_{75} in nitrogen and ozone and the spectra in nitrogen with *ssp*- and *sps*-polarization. (a) The *ssp*-polarized SFG spectra of DPPC-d_{75} monolayer prepared on water surface at 30 mN/m after exposure to nitrogen (black) and ozone (20 ± 10

ppb) for 140 min (red). (b) DPPC-d_{75} in nitrogen with *ssp*- and *sps*-polarization combinations. Open symbols are SFG data and solid traces are fitting results. The intensity is normalized by the peak of the CD_3,ss for clarity. See text for details.

(2) DOPC Monolayer

Figure 4.6a shows the *ssp*-polarized spectra of the DOPC monolayer prepared in nitrogen (black) and ozone (red) in the C-H stretching region (2800-3050 cm^{-1}). Since the SFG peaks of the hydrogenated methyl and methylene from DOPC in the C-H stretching region are different from those of the deuterated ones from DPPC-d_{75} in the C-D stretching region, the general properties for the SFG peaks of the same moiety, for example, CH_3 and CD_3, CH_2 and CD_2, do not change. First, as a typical sign for the DOPC monolayer prepared in nitrogen, an SFG peak is observed at 3012 cm^{-1}, which can be definitely assigned to the vinyl CH stretching mode of DOPC.[20] Second, in addition to the SFG peaks from the terminal CH_3 groups, at 2882 cm^{-1} (CH_3,ss) and 2945 cm^{-1} (Fermi resonance, $CH_{3,FR}$), the SFG spectrum displays two strong SFG peaks attributed to the methylene groups at 2854 cm^{-1} (CH_2,ss) and 2929 cm^{-1} (CH_2,as), very different from the DPPC-d_{75} monolayer which only shows a slight intensity in the CD_2 moieties (Figure. 4.5a).

The *sps*-polarized SFG spectrum of the DOPC monolayer (Figure. 4.6b) also shows two intense peaks from the methylene group in addition to the CH_3,as peak. As also shown in Table 4.2, the amplitude ratio, $A_{CH2,ss}/A_{CH3,ss}$, of the pure DOPC monolayer is estimated to be 1.25 from fitting results, much higher than that corresponding to $A_{CD2,ss}/A_{CD3,ss}$ for pure DPPC-d_{75} monolayer (~0). This indicates that *all-trans* conformation is not available for the alkyl chains in DOPC molecule. Instead, one expects that DOPC takes a more disordered structure with many *gauche* defects which break down the local symmetry, and the methylene groups become SFG-active. The

presence of *gauche* defects should be attributed to the *cis*-C=C bonds of DOPC which significantly disturbs the conformation of the alkyl chains in the DOPC monolayer as also confirmed from its expanded π-A isotherm in comparison to DPPC-d_{75} (Figure. 4.2). Due to the large disordering with the *gauche* defects, the tilt angle, α, was not estimated for DOPC in this study.

The SFG spectrum of the DOPC monolayer prepared in low-concentration ozone (red, Figure. 4.6a) exhibits a totally different SFG spectrum from that in nitrogen (black, Figure. 4.4b): (1) The vinyl C-H stretching mode from the *cis*-C=C bond at 3017 cm^{-1} completely disappears after the ozone exposure. This is clear evidence that the C=C bond is attacked and oxidized by the ozone. (2) All the SFG peaks from the CH_3 group significantly decrease, while those of the CH_2 group are still clearly observed. The large decrease in the CH_3 peaks is mainly attributed to the decomposition reaction of DOPC induced by the ozone. The C=C bonds of the DOPC are cleaved and part of the oxidation products containing the CH_3 group readily leave the monolayer due to their high solubility and/or high vapor pressure.

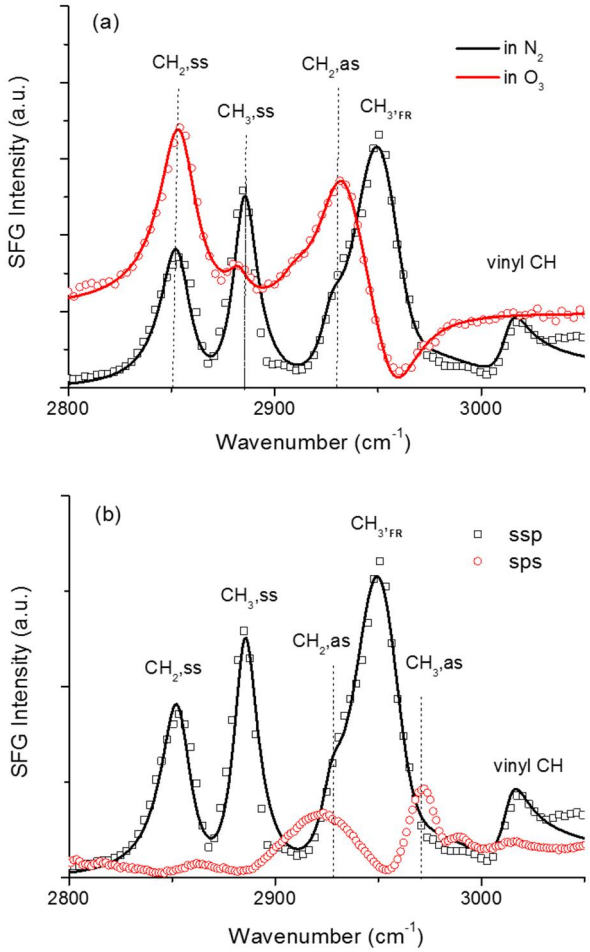

Figure 4.6 SFG spectra of pure DOPC in nitrogen and ozone and the spectra in nitrogen with *ssp*- and *sps*-polarization. (a) The *ssp*-polarized SFG spectra of DOPC monolayer prepared on water surface at 30 mN/m after exposure to nitrogen (black) and ozone (20 ± 10 ppb) for 140 min (red). (b) DOPC in nitrogen with *ssp*- and *sps*-polarization combinations. Open symbols are SFG data and solid traces are fitting results. The fitting result is only provided for ssp-polarization combination. See text for details.

(3) Possible Reaction Mechanism of DOPC Monolayer in Low-concentration Ozone

The C=C bond is known to be oxidized by ozone and Criegee[27] proposed a well-known three-step reaction mechanism for the ozone oxidation. Mass spectroscopic analyses confirmed a number of products expected from the mechanism.[28-29] Thompson *et al.*[15-16] investigated ozone-induced structural changes in the POPC monolayer on a water surface by neutron reflection and found that ozone attacks the C=C bond of the oleoyl strand of POPC, and leads to a rapid loss of the terminal C_9 portion. Scheme 4.1 shows a possible reaction mechanism for DOPC on the water surface based on these previous studies. [7-8, 10-12, 27] The primary ozonide (POZ) intermediate, is formed by ozone attaching to the C=C bond in the first step. POZ on the water surface is expected to be further decomposed as a residual oxidized phospholipid (oxPL), nonanal ($CH_3(CH_2)_7CHO$) and nonanoic acid ($CH_3(CH_2)_7COOH$). The oxPL keeps the phosphocholine head group and has two azelaoyl or 9'-oxo-nonanoyl alkyl chains which depending on its pair product, nonanal or nonanoic acid. [15-16, 28-30]

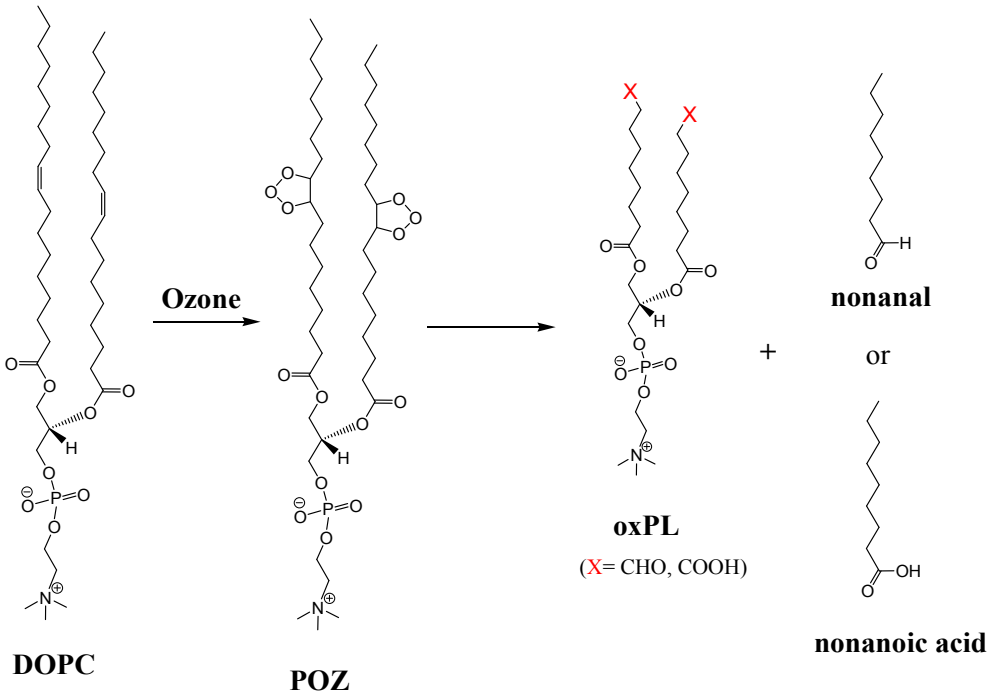

Scheme 4.1. Possible reaction mechanism of ozone oxidation on the unsaturated DOPC on the water surface.

The solubility of nonanal and nonanoic acid in pure water is 0.096 g/L and 0.28 g/L,[31-32] respectively, much higher than DOPC and DPPC. To check whether these two products can stay on the water surface, we first checked their π-A isotherms. Assuming one DOPC generates two nonanal or nonanoic acid in the full decomposition reaction by ozone, the amount for the full monolayer equivalent of nonanal or nonanoic acid can be estimated based on the π-A isotherm of DOPC (Figure. 4.1). However, no surface pressure could be obtained when the monolayer equivalent of nonanal or nonanoic acid was spread on the water surface even when the barrier was compressed to the trough end. This indicates that nonanal and nonanoic acid are difficult to stay on the water surface to reduce the surface tension of the water surface. Wadia *et al.*[29] previously reported that nonanal was detected as a major gas-phase oxidation product of OPPC after exposure to ozone (0.5~1.0 ppm).[29] Allen and her coworkers[31-32] investigated that the oxidation of oleic acid on an air/water

interface by ozone (20 ppm) and reported that nonanal or nonanoic acid, one of the possible oxidation products of oleic acid, did not contribute to the SFG spectra for the oleic acid oxidation by ozone due to their high solubility. Khabiri et al. found nonanal showed very limited water solubility and was expected to be evaporated into gas phase. [17] Thus, as possible oxidized products of DOPC by ozone, nonanal and nonanoic acid are expected to diffuse into the aqueous phase or gas phase soon after the oxidation by ozone, and will not significantly contribute to the observed SFG signals. At the present stage, the residual oxidized phospholipid (oxPL) is expected to partially stay on the water surface and mainly provide a spectral contribution for the SFG spectra after a sufficient exposure to ozone.

If one checks the SFG spectrum of DOPC after the ozone exposure, one still can find a very small peak close to the CH_3,ss mode. This should not be due to the methyl groups in the hydrophilic head group of DOPC or oxPL residues since which give totally different positions and a very low intensity.[33] In addition to oxPL, a very small amount of un-oxidized DOPC and other reaction products may were transferred to the substrate surface.

4.3.4.2 DPPC-d_{75}/DOPC Mixed Monolayers

(1) DPPC-d_{75} Component in DPPC-d_{75}/DOPC Mixed Monolayers

Figure 4.7a shows the *ssp*-polarized SFG spectra (open symbol) and fitting results (solid trace) in the C-D stretching region for the DPPC-d_{75} component in the DPPC-d_{75}/DOPC mixed monolayer prepared in nitrogen. According to Eq. (2-11 and 2-12), the SFG intensity is proportional to the square of the molecule density, thus, the SFG intensities in Figure. 4.6a are normalized by the square of the densities of DPPC-d_{75} in each monolayer (i.e., the amplitude A in Eq. (2-23) is linearly proportional to N). Similar to the pure DPPC-d_{75} spectrum (Figure. 4.4a), the mixed monolayers also exhibit three major peaks attributed to the terminal methyl group of the hydrocarbon chains, i.e., CD_3,ss, $CD_{3,FR}$, and CD_3,as. The normalized peak intensities for the methyl group are quite similar (Figure. 4.7a and Table 4.2), indicating that all of the DPPC-d_{75} in the mixed monolayers behave in a similar way. On the other hand, the SFG peaks around 2110 cm^{-1} (CD_2,ss) and 2203 cm^{-1} (CD_2,as) for the methylene group are weak when the molar ratio of DPPC-d_{75} is high (Table 4.2). The relative peak intensities of the methylene group significantly increase with an increase in the DOPC component in the mixed monolayer. As shown in Figure. 4.7a, CD_2,ss is almost comparable to $CD_{3,FR}$ in the DPPC-d_{75}/DOPC (1:1) mixed monolayer and becomes higher than $CD_{3,FR}$ in the 1:3 mixed monolayer. As shown in the AFM image for the mixed monolayer (Figure. 4.4a), the two components are separated into their individual domains. However, with an increase in the DOPC in the mixed monolayer, the DPPC-d_{75} domains are embedded in the larger DOPC domains and more DPPC-d_{75} molecules on the domain boundaries are affected by the unsaturated DOPC molecules and thus become slightly disordered. As a confirmation, the pure DOPC monolayer did not give any SFG signals in the C-D stretching region (Figure. 4.6a,

open square in black)

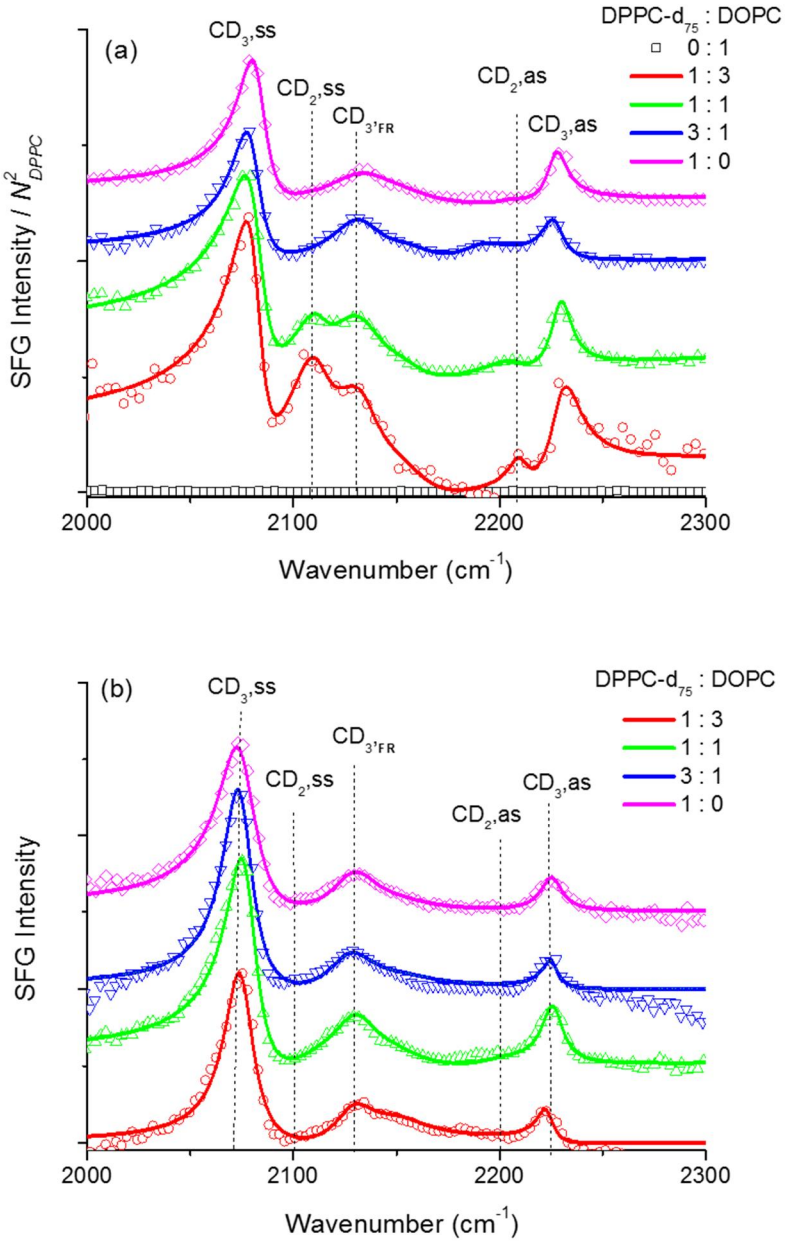

Figure 4.7 The *ssp*-polarized SFG spectra of DPPC-d_{75}/DOPC mixed monolayers for different molar ratios in nitrogen and ozone. The *ssp*-polarized SFG spectra of DPPC-d_{75}/DOPC mixed monolayers for different molar ratios observed in the C-D stretching region for DPPC-d_{75} component (a) before and (b) after exposure to ozone (20 ± 10 ppb). Open symbols are SFG data, and solid traces are fitting results. In order to compare the SFG intensities of DPPC-d_{75} in Figure. 4.7a, it is normalized by the square of their relative molecular density of DPPC-d_{75}, $(N)^2$, where N is the molecular density of DPPC-d_{75} on the water surface at 30 mN/m determined from each π-A isotherm in Figure. 4.2. All the spectra

are offset for clarity. See text for details.

Table 4.2 Fitted amplitudes for symmetric modes of the methylene and methyl groups in C-D stretching region.

DPPC-d_{75}:DOPC		CD_2,ss	CD_3,ss	CD_2,ss/CD_3,ss	CD_3,ss/N_{DPPC}
N_2	0 : 1	--	--	--	--
	1 : 3	0.05	0.12	0.42	0.33
	1 : 1	0.07	0.29	0.24	0.35
	3 : 1	0	0.45	0	0.34
	1 : 0	0	0.83	0	0.38
O_3	0 : 1	--	--	--	--
	1 : 3	0	0.39	0	0.18
	1 : 1	0	0.42	0	0.19
	3 : 1	0	0.43	0	0.20
	1 : 0	0	0.39	0	0.18

Fitted amplitudes for symmetric modes of the methylene and methyl groups in DPPC-d_{75} ($CD_{2,ss}$ and $CD_{3,ss}$) for each monolayers under different conditions. The ratios and normalized amplitudes are also given. See texts for details. The peak amplitudes are fitted with <10% error.

Figure 4.7b shows the same SFG spectra in the C-D stretching region for the DPPC-d_{75}/DOPC mixed monolayer after a 140-min exposure to ozone on the water surface. No intensity normalization by the molecular density was performed in the Figure. 6b. All of the mixed monolayers show three strong peaks from the CD_3 group with negligible peaks from the CD_2 group. The three SFG spectra for the DPPC-d_{75}/DOPC mixed monolayers (1:3, 1:1, 3:1) show almost the identical spectral shape and intensity as the pure DPPC-d_{75} monolayer (Table 4.2). In other words, the four monolayers are almost identical regarding the DPPC-d_{75} component after exposure to a low level of ozone. It is quite different with the reported results of DPPC/POPC mixed monolayer system. In DPPC/POPC mixed monolayers DPPC component is affected largely by the presence of oxidized-POPC (PoxnoPC and PazePC). [18] Because POPC molecule has one oleic acid chain and one palmitic acid chain, and the oxidized POPC (PoxnoPC and PazePC) is mainly on the water surface due to the presence of saturated palmitic acid chain, while most of oxidized DOPC products are

dissolved and formed micelle-structure in the water. Comparing the SFG spectra of the mixed monolayers before the ozone exposure (Figure. 6a), the molecular density for DPPC-d_{75} increases as high as that for the pure DPPC-d_{75} monolayer. Furthermore, the *gauche* defects of DPPC-d_{75} molecules mixed monolayers completely disappear after exposure to ozone from the amplitude ratio $A_{CD2,ss}/A_{CD3,ss}$ (Table 4.2).

(2) DOPC Component in DPPC-d_{75}/DOPC Mixed Monolayers

As the counterparts to Figures 4.7a and b, Figures 4.8a and b show the *ssp*-polarized SFG spectra (open symbol) and fitting results (solid line) for the DOPC components in the DPPC-d_{75}/DOPC mixed monolayers, prepared in nitrogen and ozone (140 min), in the C-H stretching region (2800-3050 cm^{-1}), respectively. The SFG intensities in Figure. 4.8a are also normalized by square of the DOPC density in the monolayers. This is different from that for the DPPC-d_{75} component (Figure. 4.7a), and the spectral shape and peak intensity depend on the composition of the mixed monolayer. The strong methylene peaks observed in the pure DOPC monolayer become weaker with an increase in the DPPC-d_{75} component in the monolayer and almost disappear in the DPPC-d_{75}/DOPC (3:1) mixed monolayer (Figure. 4.8a). According to the fitting results, the ratio of $A_{CH2,ss}/A_{CH3,ss}$ decreases with the increase in the mole fraction of the DPPC-d_{75} (Table 4.3), indicating that the DOPC becomes more ordered by DPPC-d_{75} in the monolayer. The deviation from the square relationship of the DOPC molecular density should be associated with the greater changes in the orientation and conformation of hydrocarbon chains of the DOPC molecules in the mixed monolayer. The conformational ordering of DOPC significantly increases with the increase in DPPC-d_{75} in the mixed monolayer. Similar

condensing effects were reported for the stearyl alcohol on dioctadecyldimethyl-ammonium chloride (DOAC) monolayers,[34] and palmitic acid on DPPC monolayers.[35] Furthermore, no SFG signals from the DPPC-d_{75} monolayer are observed in the C-H stretching region, as expected.

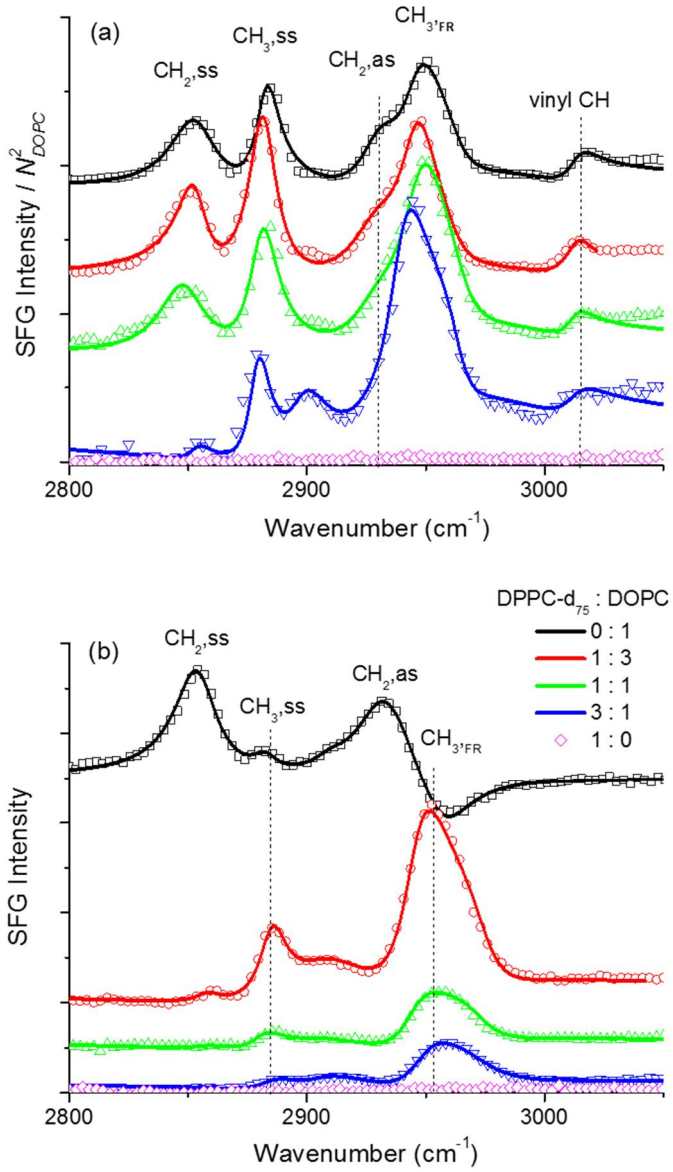

Figure 4.8 SFG spectra of DPPC-d_{75}/DOPC mixed monolayers. The ssp-polarized SFG spectra of DPPC-d_{75}/DOPC mixed monolayers for different molar ratios observed in the C-H stretching region for DOPC component (a) before and (b) after exposed to ozone (20 ± 10 ppb). Open symbols are SFG data, and solid traces are fitting results. In order to compare the SFG intensities of DOPC in Figure. 8a, it is normalized by the square of their relative molecular

density of DOPC, $(N)^2$ where N is the molecular density of DOPC on the water surface at 30 mN/m determined from each π-A isotherm in Figure. 2. All the spectra are offset for clarity. See text for details.

Table 4.3 Fitted amplitudes for symmetric modes of the methylene and methyl groups in C-H stretching region.

DPPC-d_{75}:DOPC		CH_2,ss	CH_3,ss	CH_2,ss/CH_3,ss	CH_3,ss/N_{DOPC}
N_2	0 : 1	0.4	0.32	1.25	0.23
	1 : 3	0.30	0.32	0.94	0.29
	1 : 1	0.15	0.19	0.79	0.23
	3 : 1	0.03	0.09	0.33	0.20
	1 : 0	--	--	--	--
O_3	0 : 1	0.27	0.03	9.00	0.02
	1 : 3	0.05	0.21	0.24	0.19
	1 : 1	0.04	0.13	0.31	0.16
	3 : 1	0.03	0.11	0.27	0.25
	1 : 0	--	--	--	--

Fitted amplitudes for symmetric modes of the methylene and methyl groups in DOPC ($CH_{2,ss}$ and $CH_{3,ss}$) for each monolayers under different conditions. The ratios and normalized amplitudes are also given. See texts for details. The peak amplitudes are fitted with <10% error.

The SFG spectra for DOPC components in the mixed monolayers on the water surface significantly change after exposure to ozone, quite different from that observed in the pure DOPC monolayer (Figure. 4.6). As also shown in Figure. 4.6, the pure DOPC monolayer exhibits strong CH_2,ss and CH_2,as peaks and a very weak CH_3,ss peak after the ozone exposure. However, the SFG peaks for the CH_2 groups of the DOPC component in the mixed monolayers are very weak and the SFG peaks attributed to CH_3,ss and $CH_{3,FR}$ become obvious after exposure to ozone (Figure. 4.8b and Table 4.3). The CH_3,ss and $CH_{3,FR}$ should be attributed by the terminal methyl group of the hydrocarbon chains of DOPC since the oxidation products of oxPL, nornanal and nonanoic acid will not contribute to these peaks as discussed in a previous section. In fact, it is interesting to note that the SFG spectrum for DPPC-d_{75}/DOPC (3:1) in nitrogen (Figure. 4.8a) is very similar to the SFG spectra of the

mixed monolayers except for the pure monolayer of DOPC after exposure to ozone (Figure. 4.8b). In other words, part of the DOPC molecules remain on the surface. It is expected that the DPPC-d_{75} components in the mixed monolayer can partially protect the DOPC molecules from the ozone oxidation. The *all-trans* hydrocarbon chains of DPPC-d_{75} with a strong van der Waals interaction with each other can form a well-packed monolayer. The DPPC-d_{75} can significantly condensate DOPC in a more ordered structure and reduce the *gauche* defects,-The packing density and orientation ordering of DOPC are significantly improved by the presence of DPPC-d_{75} molecules in the mixed monolayer, and this can partially protect DOPC from ozone attack on the defect sites.

4.4 Conclusions

Based on all the observations from the π-A isotherm, AFM and SFG observations, a possible reaction mechanism for (a) DPPC monolayer, (b) DOPC monolayer and (c) DPPC/DOPC mixed monolayers on a water surface induced by ozone is illustrated in Scheme 2. The models schematically exhibit molecular structures per unit area at a constant surface pressure of 30 mN/m. The DPPC-d_{75} molecules construct a well-defined monolayer on the water surface and are very stable in the low-level ozone (Scheme 2a). The pure DOPC monolayer can only form a disordered LE phase with *gauche* defects due to the low packing density of DOPC from its *cis*-C=C bonds. The DOPC monolayer on the water surface can be oxidized by extremely low concentration ozone in gas phase. The C=C bonds are attacked by ozone and decomposed to oxPL, nonanal and nonanoic acid. The latter two species dissolve in the aqueous phase or go into gas phase soon after the reaction. OxPL is mainly dissolved and form micelle in the water phase, and a very small amount of oxPL species may stay on the water surface after the ozone oxidation (Scheme 2b). The conformational ordering of DOPC is largely improved by mixing with saturated DPPC-d_{75} molecules although a phase separation is still present in the mixed monolayers. After exposure to ozone, it was found that the DPPC-d_{75} molecules are stable but the DOPC molecules are selectively oxidized. Some DOPC molecules in the mixed monolayer remain on the water surface after the ozone oxidation (Scheme 2c), different from the pure DOPC monolayer (Scheme 2b).

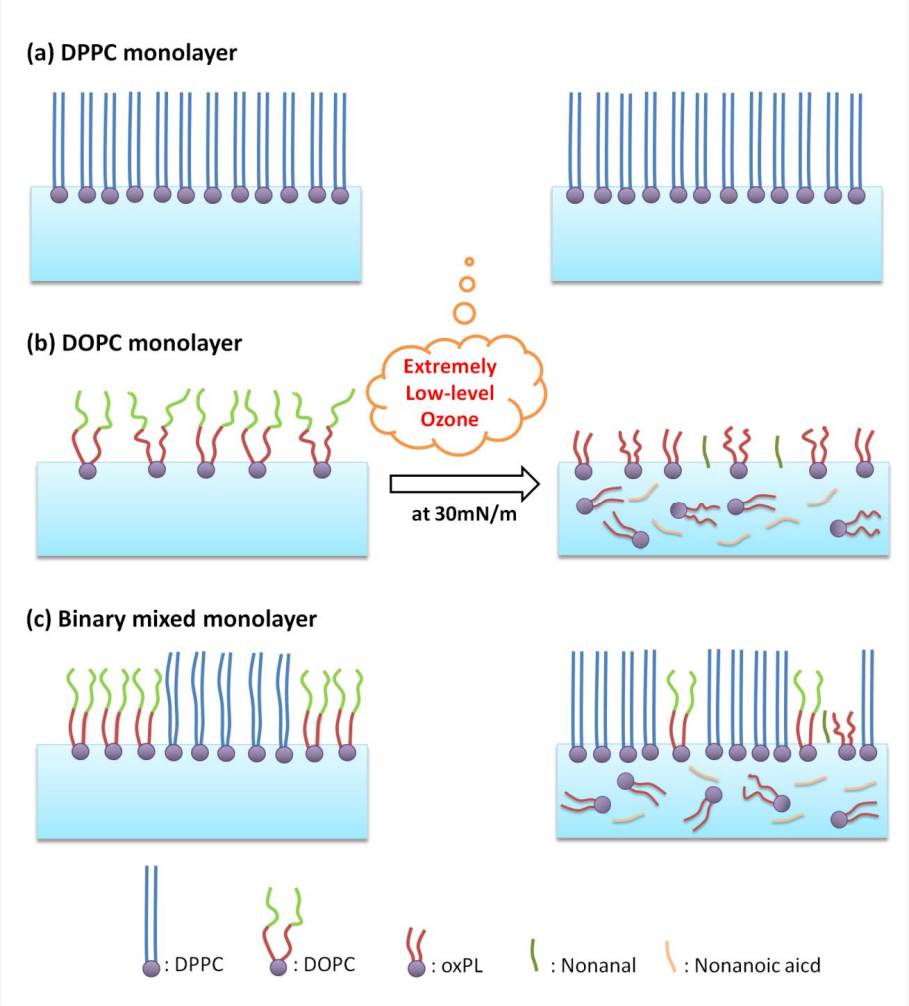

Scheme 4.2 The schematic models for DPPC-DOPC pure and mixed monolayer in nitrogen and low-level ozone. (a) DPPC monolayer, (b) DOPC monolayer and (c) DPPC-DOPC mixed monolayer on a water surface before (left) and after (right) exposure to an extremely low-level ozone. All the models schematically exhibit molecular structures per unit area at a constant surface potential of 30 mN/m. See text for details.

The present study shows that in daily life, ozone in the air cannot be ignored. A low concentration of ozone has significant negative effects on the unsaturated components in a cell membrane, especially for the lung and skin cells. The saturated lipid can affect the oxidation process of the unsaturated lipids. This is a warning that the harmful effects of ozone must be controlled. It is a new insight that the saturated lipid can affect the oxidation process of the unsaturated lipids

REFERENCES

1. Sadava, D.; Heller, C.; Orians, G.; Purves, W.; Hillis, D., *Life*. 8th ed.; Sinauer Associates, Inc.: Sunderland, MA, 2008.

2. Roberts, R. A.; Laskin, D. L.; Smith, C. V.; Robertson, F. M.; Allen, E. M. G.; Doorn, J. A.; Slikkerk, W., Nitrative and Oxidative Stress in Toxicology and Disease. *Toxicol. Sci.* **2009,** *112* (1), 4-16.

3. Reis, A.; Spickett, C. M., Chemistry of phospholipid oxidation. *Biochim. Biophys. Acta-Biomembr.* **2012,** *1818*, 2374-2387.

4. Shen, Y. R., *The Principles of Nonlinear Optics*. John Wiley & Sons, Inc.: New York, 1984.

5. Bain, C. D., Sum-frequency vibrational spectroscopy of the solid/liquid interface. *J. Chem. Soc. Faraday Trans.* **1995,** *91*, 1281-1296.

6. Miranda, P.; Shen, Y. R., Liquid interfaces: a study by sum frequency vibrational spectroscopy. *J. Phys. Chem. B* **1999,** *103*, 3292-3307.

7. Richmond, G. L., Molecular Bonding and Interactions at Aqueous Surfaces as Probed by Vibrational Sum Frequency Spectroscopy. *Chem. Rev.* **2002,** *102*, 2693-2724.

8. Holman, J.; Davies, P. B.; Nishida, T.; Ye, S.; Neivandt, D. J., Sum frequency generation from Langmuir-Blodgett multilayer films on metal and dielectric substrates. *J. Phys. Chem. B (Feature Article)* **2005,** *109*, 18723 -18732.

9. Bonn, M.; Campen, R. K., Optical methods for the study of dynamics in biological membrane models. *Surf. Sci.* **2009,** *603*, 1945-1952.

10. Zhang, C.; Myers, J. N.; Chen, Z., Elucidation of molecular structures at buried polymer interfaces and biological interfaces using sum frequency generation vibrational spectroscopy. *Soft Matter* **2013,** *9*, 4738-4761.

11. Nihonyanagi, S.; Mondal, J. A.; Yamaguchi, S.; Tahara, T., Structure and Dynamics of Interfacial Water Studied by Heterodyne-Detected Vibrational Sum-Frequency Generation. *Annu. Rev. Phys. Chem.* **2013,** *64*, 579-603.

12. Ye, S.; Osawa, M., Molecular structures on solid substrates probed by sum frequency generation (SFG) vibration spectroscopy. *Chem. Lett.* **2009,** *38*, 386-391.

13. Vie, V.; Van Mau, N.; Lesniewska, E.; Goudonnet, J. P.; Heitz, F.; Le Grimellec, C., Distribution of ganglioside G(M1) between two-component, two-phase phosphatidylcholine monolayers. *Langmuir* **1998,** *14*, 4574-4583.

14. Stottrup, B. L.; Stevens, D. S.; Keller, S. L., Miscibility of Ternary Mixtures of Phospholipids and Cholesterol in Monolayers, and Application to Bilayer Systems. *Biophys. J.* **2005,** *88*, 269-276.

15. Thompson, K. C.; Rennie, A. R.; King, M. D.; Hardman, S. J. O.; Lucas, C. O. M.; Pfrang, C.; Hughes, B. R.; Hughes, A. V., Reaction of a Phospholipid Monolayer with Gas-Phase Ozone at the Air-Water Interface: Measurement of Surface Excess and Surface Pressure in Real Time. *Langmuir* **2010,** *26*, 17295-17303.

16. Thompson, K. C.; Jones, S. H.; Rennie, A. R.; King, M. D.; Ward, A. D.; Hughes, B. R.; Lucas, C. O. M.; Campbell, R. A.; Hughes, A. V., Degradation and Rearrangement of a Lung Surfactant Lipid at the Air–Water Interface during Exposure to the Pollutant Gas Ozone. *Langmuir* **2013,** *29*, 4594-4602.

17. Khabiri, M.; Roeselova, M.; Cwiklik, L., Properties of oxidized phospholipid monolayers: An atomistic molecular dynamics study. *Chem Phys Lett* **2012,** *519–520* (0), 93-99.

18. Sabatini, K.; Mattila, J. P.; Megli, F. M.; Kinnunen, P. K. J., Characterization of two oxidatively modified phospholipids in mixed monolayers with DPPC. *Biophys J* **2006,** *90* (12), 4488-4499.

19. Cwiklik, L.; Jungwirth, P., Massive oxidation of phospholipid membranes leads to pore creation and bilayer disintegration. *Chem Phys Lett* **2010,** *486* (4), 99-103.

20. Liljeblad, J. F. D.; Bulone, V.; Tyrode, E.; Rutland, M. W.; Johnson, C. M., Phospholipid Monolayers Probed by Vibrational Sum Frequency Spectroscopy: Instability of Unsaturated Phospholipids. *Biophys. J.* **2010,** *98*, L50-L52.

21. Moraille, P.; Badia, A., Nanoscale stripe patterns in phospholipid bilayers formed by the Langmuir-Blodgett technique *Langmuir* **2003,** *19*, 8041-8049.

22. Badia, A.; Moraille, P.; Tang, N. Y. W.; Randlett, M.-E., Nanostructured phospholipid membranes. *Int. J. Nanotechnol.* **2008,** *5*, 1371-1395.

23. Yang, C. S.-C.; Richter, L.; Stephenson, J.; Briggman, K., In Situ, Vibrationally Resonant Sum Frequency Spectroscopy Study of the Self-Assembly of Dioctadecyl Disulfide on Gold. *Langmuir* **2002,** *18*, 7549-7556.

24. Tong, Y.; Li, N.; Liu, H.; Ge, A.; Osawa, M.; Ye, S., Mechanistic studies by sum-frequency generation spectroscopy: Hydrolysis of a supported phospholipid bilayer by phospholipase A_2. *Angew. Chem. Int. Ed.* **2010,** *49*, 2319-2323.

25. Guyot-Sionnest, P.; Hunt, J. H.; Shen, Y. R., Sum-frequency vibrational spectroscopy of a Langmuir film: Study of molecular orientation of a two-dimensional system. *Phys. Rev. Lett.* **1987,** *59*, 1597-1600.

26. Ye, S.; Noda, H.; Nishida, T.; Morita, S.; Osawa, M., Cd^{2+}-induced interfacial structural changes of Langmuir-Blodgett films of stearic acid on solid substrates: A sum frequency generation study. *Langmuir* **2004,** *20*, 357-365.

27. Criegee, R., Mechanism of Ozonolysis. *Angew. Chem. Int. Ed.* **1975,** *14*, 745-752.

28. Lai, C. C.; Yang, S. H.; Finlayson-Pitts, B. J., Interactions of monolayers of unsaturated phosphocholines with ozone at the air-water interface. *Langmuir* **1994,** *10*, 4637-4644.

29. Wadia, Y.; Tobias, D. J.; Stafford, R.; Finlayson-Pitts, B. J., Real-time monitoring of the kinetics and gas-phase products of the reaction of ozone with an unsaturated phospholipid at the air-water interface. *Langmuir* **2000,** *16*, 9321-9330.

30. Reis, A.; Spickett, C. M., Chemistry of phospholipid oxidation. *Bba-Biomembranes* **2012,** *1818* (10), 2374-2387.

31. Voss, L. F.; Hadad, C. M.; Allen, H. C., Competition between atmospherically relevant fatty acid monolayers at the air/water interface. *J. Phys. Chem. B* **2006,** *110*, 19487-19490.

32. Voss, L. F.; Bazerbashi, M. F.; Beekman, C. P.; Hadad, C. M.; Allen, H. C., Oxidation of oleic acid at air/liquid interfaces. *J. Geophys. Res.* **2007,** *112*, D06209.

33. Liu, J.; Conboy, J., Structure of a Gel Phase Lipid Bilayer Prepared by the Langmuir-Blodgett/Langmuir-Schaefer Method Characterized by Sum-Frequency Vibrational Spectroscopy *Langmuir* **2005,** *21*, 9091-9097.

34. Ge, A.; Wu, H.; Darwish, T. A.; James, M.; Osawa, M.; Ye, S., Structure and Lateral Interaction in Mixed Monolayers of Dioctadecyldimethylammonium Chloride (DOAC) and Stearyl Alcohol. *Langmuir* **2013,** *29*, 5407-5417.

35. Ma, G.; Allen, H. C., Condensing effect of palmitic acid on DPPC in mixed Langmuir monolayers. *Langmuir* **2007,** *23*, 589-597

Chapter 5

Structure and Stability Studies of POPC Monolayer and DPPC-POPC Mixed Monolayers in Low-level Ozone

5.1 Introduction

The lipid oxidation processes of saturated DPPC, unsaturated DOPC, and their mixtures have been discussed in detail by employing different surface-specific approaches in Chapter 4. The results have revealed unique structural changes for these molecules at the interface after exposed to low-level ozone. As shown in Figure 3.1, DPPC and DOPC consist of two identical alkyl chains. In natural cell membrane, however, many phospholipid molecules contain both saturated chain and unsaturated chain esterified to a glycerol moiety. For instance, as a common component (ca. 25%) of pulmonary surfactants that constitute the surface of the terminal respiratory units (alveoli) in human lungs, l-palmitoyl-2-oleoyl-*sn*-glycero-3-phosphocholine (POPC) has the same choline head group as DPPC and DOPC. Whereas, in the alkyl chain portion, POPC has one saturated chain at *sn*-1 position similar to that in DPPC, and one unsaturated chain at the *sn*-2 position similar to that in DOPC (Fig. 3.1).[1] Thus, one may regard POPC as a natural intramolecular mixture of DPPC and DOPC. POPC efficiently reduces surface tension at the air–liquid interface of the alveoli during expiration, and plays a crucial role in preventing alveolar collapse and pulmonary edema.[2,3]

Since the lung exposes its surface to ambient environment during respiration, the structure and stability of the lipids in the pulmonary surfactants is very important.[2, 4-7] Hence, POPC, with the unique structure and crucial biological functions, is a good choice for modeling natural cell membrane. Many researches have been carried out to investigate the oxidation process of POPC in environment containing with ozone.[8-14] However, most of these studies were done in a concentration (0.3–10 ppm), much higher than the ambient environment (few tens of ppb).[8-14] Moreover, these previous researches were rarely performed at the interface or explored at a molecular level.

Therefore, in this chapter, we aim to study the oxidation of POPC in a very low-concentration of ozone at gas/water interface with the combination of different surface science techniques, such as π-A isotherms, AFM, and SFG spectroscopy. Since DPPC is the most abundant component (ca. 50%) in the pulmonary surfactants,

not only reaction of the single component of POPC monolayer, but also the mixed monolayers of DPPC-POPC have been studied in an environment containing a trace amount of ozone (ca. 20±10 ppb).

5.2 Experimental

In this chapter, one unsaturated lipid POPC were mainly used to mimic the cell membrane, and the mixed monolayer of saturated DPPC and unsaturated POPC was also studied. The molecular structures of DPPC, POPC, as well as their deuterated forms which are used in SFG measurement, are shown as followed. More details about the chemicals can be found in Chapter 3.

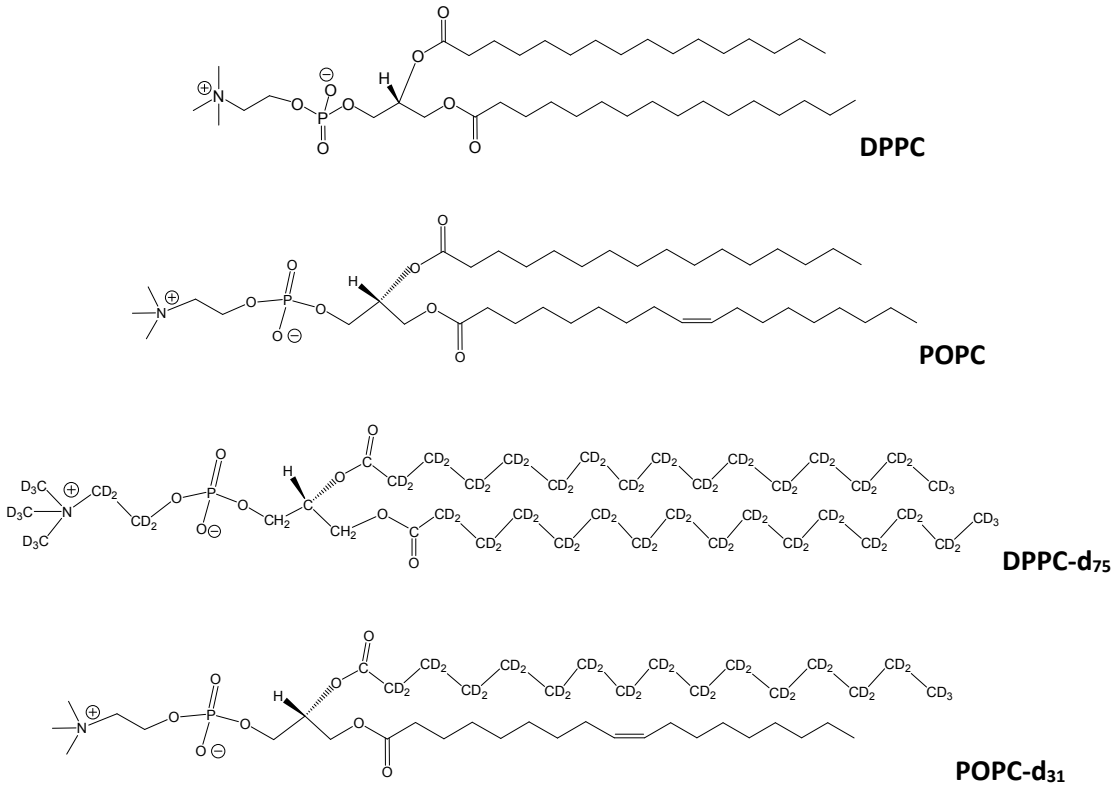

Figure 5.1 Molecular structures of DPPC, POPC, DPPC-d_{75}, and POPC-d_{31}.

In addition, as prospective oxidized products for POPC, a number of oxidized phospholipids, 1-palmitoyl-2-azelaoyl-*sn*-glycero-3-phosphocholine (PAzPC), 1-

palmitoyl-2-(9'-oxo-nonanoyl)-*sn*-glycero-3-phospho-choline (POnPC), have also been investigated (Figure 5.2).Details about the chemicals can be found in Chapter 3.

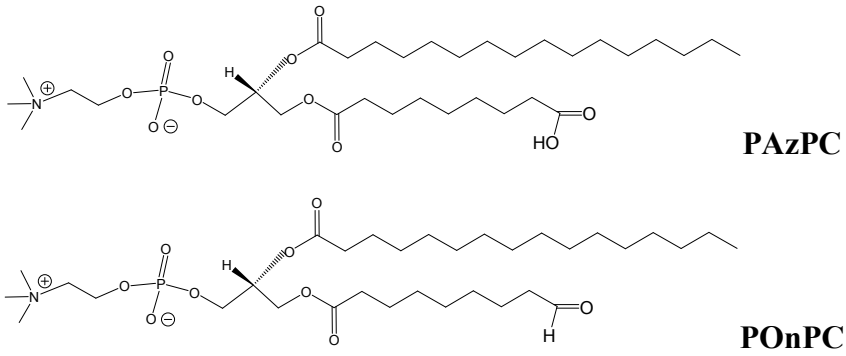

Figure 5.2 Molecular structures of oxidized phospholipids PAzPC and POnPC, and their counterpart residues 1-nonanal and nonanoic acid.

Langmuir-Blodgett (LB) trough (100 mm×366 mm, FSD-500, USI) was used to measure the π-A isotherms, the stability of the monolayer in different atmosphere, and transfer the monolayer to mica or CaF_2 prism surface to further study on the morphology or molecule structure by AFM and SFG, respectively. Another small LB trough with a dimension of 140mm×70mm (KSV NIMA-102M) was employed, especially for the in-situ SFG measurement on the water surface. Except π-A isotherms experiments, all others were performed under the constant surface pressure of 30 mN/m or 15 mN/m. The temperature of the water subphase is 22℃. Details for the π-A isotherms, AFM and SFG experiments have been given in Chapter 3.

5.3 Results and Discussion

5.3.1 π-A Isotherms

Figure 5.3 shows the π-A isotherms of the DPPC, POPC and DPPC/POPC mixtures with molar ratios of 3:1, 1:1, and 1:3 in a nitrogen environment. All the liquid expanded (LE), liquid expanded-liquid condensed (LE-LC) coexist, and LC phases are observed in the π-A isotherm of DPPC (black line, Figure 5.3). The initial LE phase appears when the area per molecule is smaller than 0.82 nm^2, then the flat plateau for the phase transition (LE-LC coexist phase) is found around 7 mN/m. After that, the monolayer is compressed to the LC at an area of 0.46 nm^2 per DPPC, and finally collapses around 58 mN/m. The highly condensed structure is consistent with the results of DPPC-d_{75} in Figure 4.2. This structure should be attributed to the strong hydrophobic force and van der Waals interaction between the alkyl chains of the DPPC molecules with *all-trans* conformation. Noting that DPPC has some slight deviations from DPPC-d_{75}, including the smaller initial area per molecule where surface pressure starts to increase (0.82 nm^2 for DPPC while 0.9 nm^2 for DPPC-d_{75}) and the lower phase transition pressure (7mN/m for DPPC while 15mN/m for DPPC-d_{75}), which due to the effect of isotopic substitution (also see Figures 4.2 and 5.3). [15]

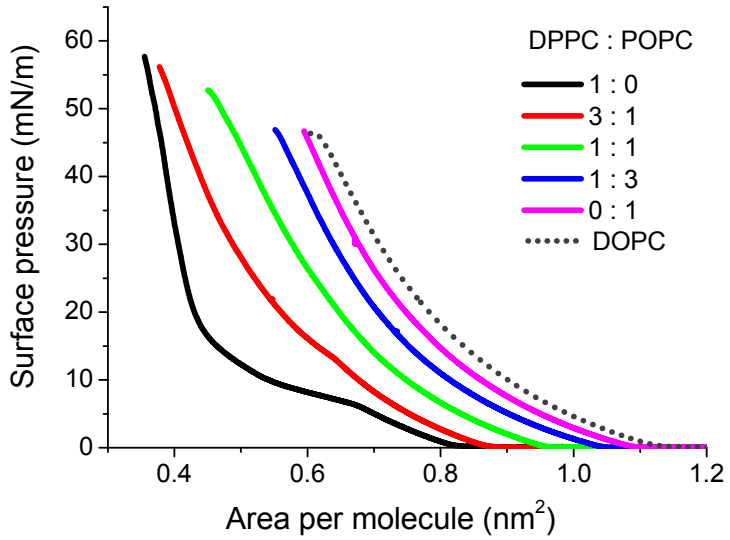

Figure 5.3 π-A isotherms of DPPC-POPC mixed monolayers. Pure water was used as subphase. DPPC-POPC molar ratios of 0:1, 1:3, 1:1, 3:1, and 1:0 were used. The π-A

isotherm of DOPC monolayer is also shown in dot line for comparison. All the isotherms were measured in dark and a nitrogen atmosphere (22℃).

In contrast, POPC monolayer only shows a more expanded structure with a LE phase on the water surface (pink line, Figure 5.3). This results are consistent with the results reported previously.[16] The expanded structure of POPC monolayer on the water surface is due to the kink on the oleoyl chain induced by the *cis*-C=C bonds. In Figure 5.3 (dot line in black), the π-A isotherm of DOPC is also shown for comparison. The small deviation of density between POPC and DOPC is due to the saturated palmitoyl chain enhanced the hydrophobic force and van der Waals interactions between the alkyl chains.

The π-A isotherms of the binary DPPC/POPC mixed monolayers locate between those of the two pure components of DPPC and POPC (Figure 5.3). With the increase of the POPC component in the mixed monolayer, the π-A isotherm gradually moves to the right, indicating the monolayer become more expanded. A shoulder around 15 mN/m is attributed to the LE-LC coexist phase for the DPPC/POPC with molar ratio of 3:1. This feature is not observed in the DPPC/POPC mixed monolayers with molar ratios of 1:1 and 1:3. This verifies that the ratio of saturated and unsaturated components in the mixed monolayer do affect its structure significantly, similar to those of DPPC/DOPC mixed monolayers (Figure 4.2).

In summary, the lipid monolayers with different saturation degree, such as DPPC, POPC, and DOPC, exhibit large differences in the π-A isotherms, especially between the saturated one and unsaturated ones. The different alkyl chains of POPC show a comprehensive effect on the monolayer structure. The unsaturated portion of the lipid expands the monolayer dramatically, whereas the saturated portion of the lipid condenses the monolayer as well.

5.3.2 Time Dependence of Monolayer Area

As studied in Chapter 4, the saturated DPPC and unsaturated DOPC molecules show totally different responses to oxidation in extremely low-level ozone. In the following part, POPC, which has both saturated and unsaturated alkyl chains in one molecule, will be investigated by the similar methods exposed to a similar low-level ozone environment.

(1) Comparison of Pure DPPC, POPC, DOPC Monolayers

As shown in Figure 5.4, three monolayers of DPPC, DOPC and POPC with a surface pressure of 30 mN/m, are stable in the nitrogen (0-60 min). However, in the low-level of ozone environment, these monolayers show totally different behaviors. The surface area of POPC monolayer first increases quickly to a maximum and then decays slowly. Similar behaviors have also been reported previously that the surface pressure of POPC monolayer at a fixed surface area increased after exposing to ozone (Figure 1.4).[8-9] There is approximately 11% increase in surface area on the maximum point normalized surface area of the POPC monolayer, after exposure to ozone. The surface area for the POPC monolayer decays all the way and no stable state was observed even after 6 hours exposure in the ozone environment.

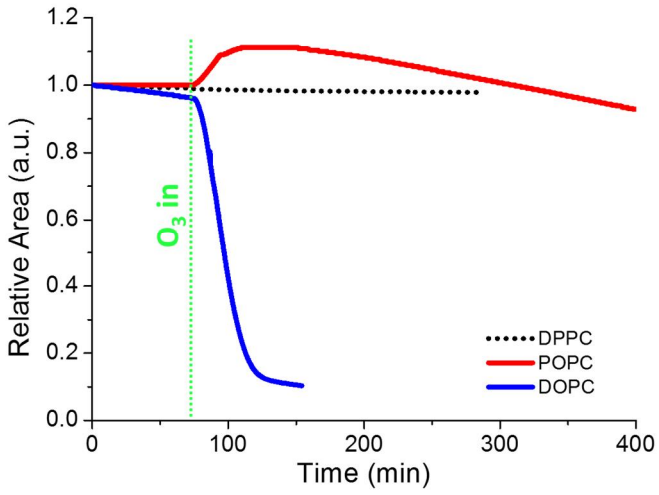

Figure 5.4 Stability of surface area for the DPPC, POPC, and DOPC monolayers at 30 mN/m

as a function of time. The monolayers are exposed to nitrogen in the first 60 min and then switched to an ozone environment (20 ± 10 ppb). All the surface areas are normalized to the initial area.

The reason for initial increase of the surface area at a constant surface pressure of 30 mN/m is still under debates. There are several hypotheses proposed to explain the phenomenon which are summarized as following,

a) The numbers of species at the surface increase because the cleavage of the alkyl chain can create more oxidation fragments that squeeze into the residual unreacted monolayer and expand the area.[17]

b) The interaction between the oxidized products is enhanced, such as the polar oxidized fragment and head group. As a result, the surface area increases.[17]

c) After oxidation, the residual group on the alkyl chain becomes more hydrophilic, and tends to change its direction to the water, which leads to an increase of surface area. [12, 18]

However, most of these arguments were discussed based on the speculations with less reliable experimental evidences. Understanding such increase of surface area at a molecular level is one of the purposes of the present study. The reason for these phenomena will be discussed in the later sections by a combination of different measurements.

On the other hand, the decrease in the monolayer area also implies that the POPC monolayer is decomposed by the ozone while its decomposition mechanism should be different from that of DOPC. As discussed in Chapter 4, most of the oxidative products of DOPC are water-dissolvable and thus induce the decreases of the monolayer area with exposure. One may expect the similar reason for the POPC monolayer. To further understand this, the dependence of mixing ratio with saturated DPPC monolayers have been investigated in details. As shown in Figure 4.3, the more DPPC, the less decrease of surface area and higher the decay rate (i.e., slopes of the decay curves) in the mixed DOPC-DPPC monolayers after exposure to the low-level ozone. We investigated the similar cases for POPC-DPPC monolayer for comparison (Figure 5.5).

(2) Mixed Monolayers at High Surface Pressure

Figure 5.5 shows the stability of DPPC-POPC mixed monolayers exposure to nitrogen and low-concentration ozone. After initial compressing to target pressure (30mN/m) all the monolayers are stable in the nitrogen (0-60 min). However, except DPPC, all the mixed monolayers show similar unstable behavior after exposure to a low-level ozone environment (20 ± 10 ppb) (after 60 min). The surface area of DPPC-POPC mixed monolayers also increase firstly and then decrease slowly, very similar to that of pure POPC monolayer in ozone (Figure 5.4). The maximum points of the monolayer area are 101%, 104%, 106% and 111% for DPPC-POPC with molar ratios of 3:1, 1:1, 1:3 and 0:1, respectively. The maximum values seem to depend on the POPC amount in the mixed monolayer.

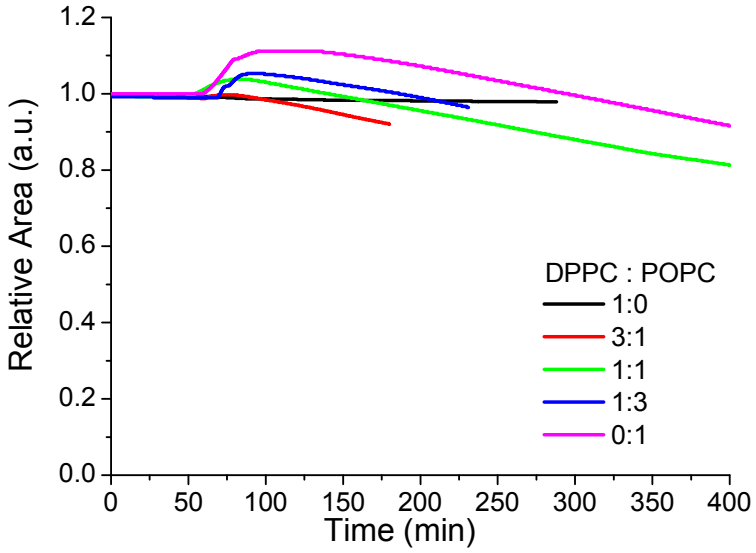

Figure 5.5 Stability of surface area for the DPPC/POPC mixed monolayers at 30 mN/m as a function of time. The monolayers are exposed to nitrogen in the first 60 min and then switched to an ozone environment (20 ± 10 ppb). All the surface areas are normalized to the initial area.

However, the decay rate is quite comparable to each other, independent of the ratio of POPC in the mixed monolayer. This implies that the decrease of surface area for POPC-DPPC mixed monolayers should be related with some other parameters, which is not exist for DOPC-DPPC monolayers (Figure 4.3). Lai *et al.* reported that

during the uptake speed of the reaction products by the subphase become fast under high surface pressure (ca. 30 mN/m) when POPC temporally exposed to ozone (30 ppb) for 30 min.[19] Thompson *et al.* found that the stability of POPC monolayer at a constant monolayer area was related to the initial surface pressure when exposed to ozone. Comparing the high initial surface pressure (ca.30 mN/m), the lower one (ca. 20 mN/m) induced a less increase first and followed by a significantly slower decay in surface pressure.[8] These previous results suggest a strong relationship between the stability of POPC in ozone and the lateral surface pressure (i.e., surface density of POPC). In order to prove this hypothesis, the stability of the surface area of POPC monolayer has been further investigated with lower surface pressure (i.e., lower surface density).

(3) Pure and Mixed Monolayers at Low Surface Pressure

Figure 5.6 shows the surface stability of POPC monolayer in nitrogen (0-40 min) and ozone (40-350 min) at 15 mN/m (0-300 min). The surface pressure is increased to 30 mN/m from 300 min while other conditions are the same (300-350 min). POPC monolayer is also stable in nitrogen at 15 mN/m. After exposure to ozone, the surface area of the POPC monolayer increases to a maximum point of 110%, and then becomes constant with only small decrease for a long exposure time (260 min), quite different from that at 30 mN/m (Figure 5.4). After 300 min, a fast decrease of surface area is observed when the surface pressure is increased to 30 mN/m. That implies that the decrease of the monolayer area at 30mN/m should be affected significantly by the surface pressure or the surface density of POPC molecules.

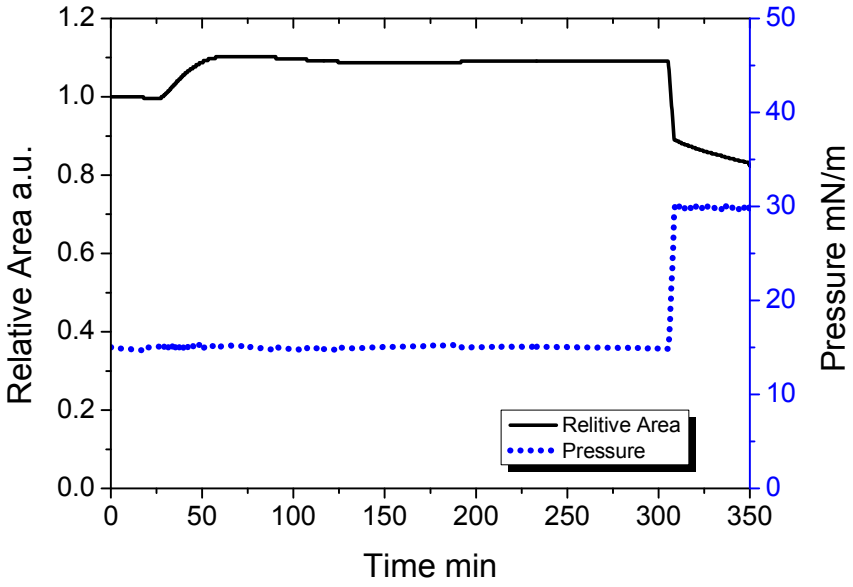

Figure 5.6 Stability of surface area of the POPC monolayer at 15 mN/m exposed to nitrogen (0-40 min), and then introducing ozone into the chamber (40-350 min, 20 ± 10 ppb), and the surface pressure is increased to 30 mN/m at 300 min. All the surface areas are normalized to the initial area. The surface pressure is also shown in the figure.

Similar measurements were also performed for the mixed POPC-DPPC monolayers. Figure 5.7 shows the results of DPPC-POPC 1:1 mixed monolayer in nitrogen (0-40 min) and ozone (40-200 min) at 15 mN/m (0-150 min) and 30 mN/m (150-200 min). The present time-dependency of DPPC-POPC mixed monolayer is similar to that of pure POPC monolayer in Figure. 5.6. The present results demonstrate that the surface stability of the oxidized monolayer is strongly dependent on the lateral pressure and surface molecular density. The increase of lateral pressure may promote the rates of the dissolution of oxidation products into the water subphase.

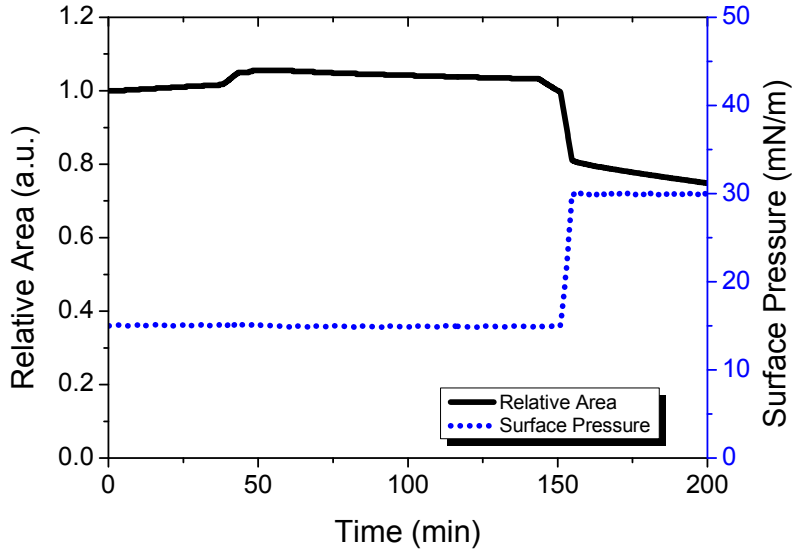

Figure 5.7 Stability of surface area of the DPPC-POPC 1:1 monolayer at 15 mN/m exposed to nitrogen (0-40min), and then introducing ozone into the chamber (40-150min, 20 ± 10 ppb). After 150 min, the surface pressure is increased to 30 mN/m. All the surface areas are normalized to the initial area. The surface pressure is also shown in the figure.

In summary, the stability of the surface area of POPC is totally different with DPPC and DOPC. After exposure to ozone, the area of POPC monolayer exhibits a rapid increase firstly and, then shows slow decrease with exposure time only when the surface pressure is high (30 mN/m).

In the following sections, the SFG and AFM characterizations were further utilized to investigate the molecular structure and morphology information of these monolayers exposed to low-level ozone.

5.3.3 The Molecular Structure of Pure POPC Monolayer

(1) SFG Results of Pure POPC Monolayer

Figure 5.8 shows the *ssp*-polarized *in-situ* SFG spectra of the DPPC (black trace) and fresh POPC (red trace) monolayer prepared in lab air on LB trough at 30 mN/m. DPPC monolayer exhibits two strong peaks at 2880 cm^{-1} and 2945 cm^{-1}, attributed to the C-H symmetric stretching mode (CH_3,ss) and Fermi resonance ($CH_{3,FR}$) of the terminal CH_3 moieties on the long alkyl chains of DPPC, respectively.[20] The peaks from CH_2 symmetric and asymmetric stretching modes at 2854 cm^{-1} (CH_2,ss) and 2920 cm^{-1} (CH_2,as) are almost invisible. It indicates structure of DPPC molecule is ordered with *all-trans* conformation. [21-24] The present results are in agreement with the SFG spectra of the DPPC-d_{75} (Figure 4.5), obtained by *ex-situ* SFG measurement. This indicates that no much difference between the results of in-situ and ex-situ SFG measurements for saturated DPPC monolayer.

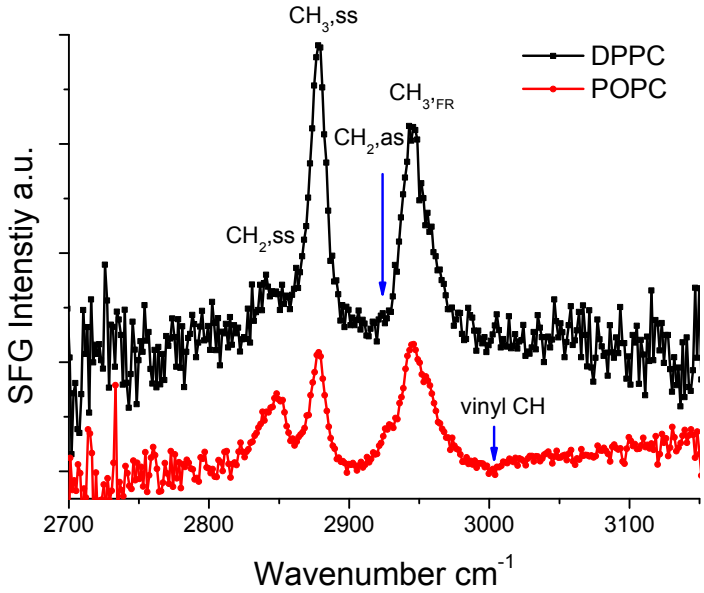

Figure 5.8 The *ssp*-polarized in-situ SFG spectra of DPPC (black trace) and fresh POPC (red trace) in lab air at 30 mN/m. The spectra are offset for clarity.

The SFG spectrum of fresh POPC (red trace, Figure 5.8) is very different from that of DPPC. The spectrum of POPC shows that the intensity of CH_2,ss at 2854 cm^{-1} and CH_2,as at 2920 cm^{-1} are almost comparable with CH_3,ss and $CH_{3,FR}$. It means that the POPC monolayer at 30 mN/m still has much more *gauche*-defects than DPPC. It should be noted that a small dip is appeared at around 3000 cm^{-1}, which is due to the vinyl C-H stretching mode from the C=C bond of the POPC unsaturated chain.[17, 25-27] This negative dip should be due to the interference between vinyl C-H stretching mode and the O-H stretching signal of water molecules adsorbed at the interface. [28] Moreover, the whole SFG intensity of POPC is weaker than that of DPPC, because the larger area per molecule of POPC at 30 mN/m results in the lower molecular density of POPC than DPPC at water surface, since the intensity of the SFG spectra is proportional to the square of the molecule density.

However, since both saturated and unsaturated alkyl chains in POPC molecules give contributions to the SFG spectrum in the C-H stretching region, one is hard to directly distinguish their contributions. In order to figure out individual information from each chain, a partially deuterated POPC-d_{31} with the saturated chain is deuterated (see molecular structure in Figure 5.1) was purchased for detailed characterizations. In such case, the saturated chain and unsaturated chain can be separated at C-D (2000-2300 cm^{-1}) and C-H (2800-3050 cm^{-1}) regions in SFG spectra, respectively.

Figure 5.9 (a) shows the time-dependence curve of the POPC monolayer at 30 mN/m and (b) the corresponding *ssp*-polarized spectra of POPC-d_{31} monolayer in the C-H stretching region (2800-3050 cm^{-1}) as a function of exposure time to the lab air with an ozone concentration about 10 ± 10 ppb. It took 6mins for single SFG spectrum. The corresponding surface area changes were also shown in Figure 5.9a. Since POPC-d_{31} is partially deuterated, these SFG signal in the C-H stretching region should be only contributed from the unsaturated chain. The most remarkable change in Figure 5.9 (b) is the decrease of CH_3,ss (about 2880 cm^{-1}) as a function of exposure time. At the beginning (12 min), the intensity of CH_3,ss peak is about half of CH_2,ss (2850 cm^{-1}), and becomes weaker along with the exposure time, while the intensity of CH_2,ss keeps almost constant. More than 240 min later, the CH_3,ss peak becomes too weak to be distinguished. It means the unsaturated chain was oxidized by ozone and the terminal CH_3 group on the unsaturated chain was lost from the water surface. Furthermore, the vinyl C-H (about 3000 cm^{-1}) has a similar change that is from weak negative peak to be indiscernible. It indicates the ozone in the air attacked the C=C bond in the unsaturated chain of POPC. The present results are in agreement with the recent neutron reflection studies that the terminal 9-carbon portions of the oleoyl strand of POPC was rapidly lost from the interface when the POPC monolayer exposed to gas-phase ozone.[9] During this evolution, no obvious changes of the intensities of CH_2,ss (2850 cm^{-1}) and $CH_{3,FR}$ (2945 cm^{-1}) were observed. But a shoulder around 2930 cm^{-1}, which attributed to CH_2,as, shows a little increase with the exposure time. It suggests that the *gauche*-defect increased the residual oxidized part of the unsaturated chain.

The SFG results suggest that the molecular structure of the POPC is significantly modified during oxidation process. One may suppose that the initial increase and then decrease of the monolayer area shown in Figure 5.9a should be strongly related to the characterization of the oxidation products. Since the C=C double bond is oxidized by ozone, the modified groups at this position may be aldehyde or acid, and both of them are more hydrophilic than their parental oleoyl chain. It may induce the packing orientation of the residual molecule to bend into water and cause the packing density

decrease. The increase of the monolayer area then shown as a result. More discussion about this mechanism will be given later.

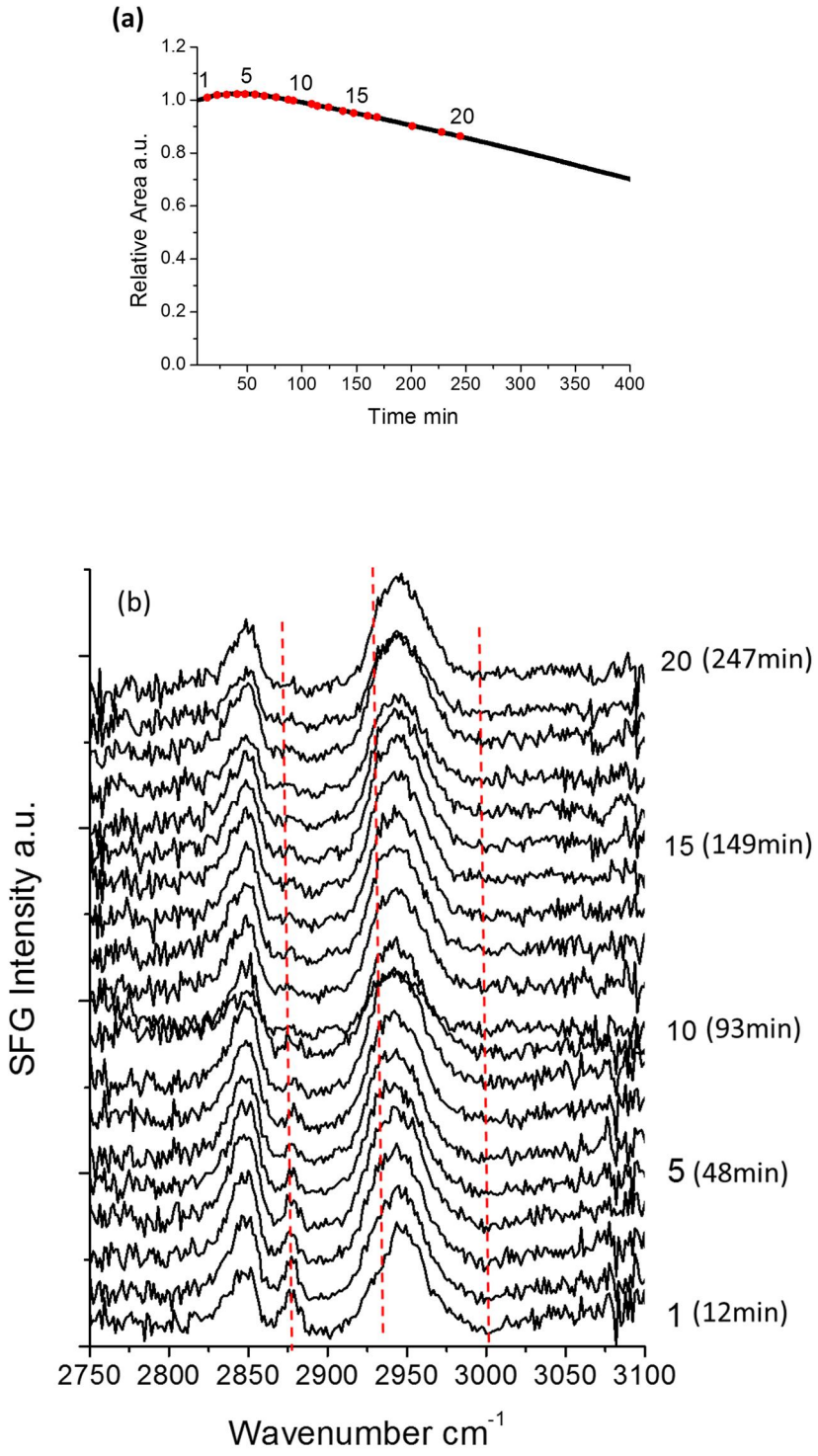

Figure 5.9 (a) The time dependence curve of the POPC monolayer in air at 30 mN/m; (b) In-situ SFG spectra of pure POPC-d_{31} in C-H stretch region as a function of the exposure time in lab air. The red dot in (a) is the mark for the time when probed SFG spectra.

As a counterpart, Figure 5.10 shows the SFG spectra of POPC-d_{31} monolayer in the C-D stretching region in nitrogen (black trace) and ozone (red trace). These spectra are obtained by *ex-situ* SFG measurement after the monolayer was transferred to the CaF_2 surface, since the SFG signal at water surface in C-D stretching region is too weak to be observed under the present experimental condition. For the monolayer prepared in the nitrogen (Figure 5.10, in black), except the strong peak from CD_3,ss (2080 cm^{-1}) and CD_3,as (2226 cm^{-1}), the peaks of CD_2,ss (2100 cm^{-1}) are obviously observed as well. It means that the saturated chain of POPC is very disordered, which is similar to the ordering of DPPC-d_{75} in the DPPC-d_{75}/DOPC mixed monolayer (Figure 4.6a). It should be noted that the spectral shape of POPC-d_{31} in nitrogen is almost identical with the spectra of DPPC-d_{75}/DOPC 3:1 in nitrogen (red trace, Figure 4.7a,). This indicates that the structure of saturated chain in POPC is very similar to that of DPPC in the mixed monolayer of DPPC-d_{75}/DOPC 3:1 in nitrogen. POPC is naturally resemblance to DPPC-d_{75} to DOPC of 1:1 in one molecule. Because the alkyl chains in one molecule are nearer than in different molecule, the close distance can induce greater interaction between the saturated and unsaturated chains. The disordered unsaturated chain may easily induce the conformational disordering of the saturated chain.

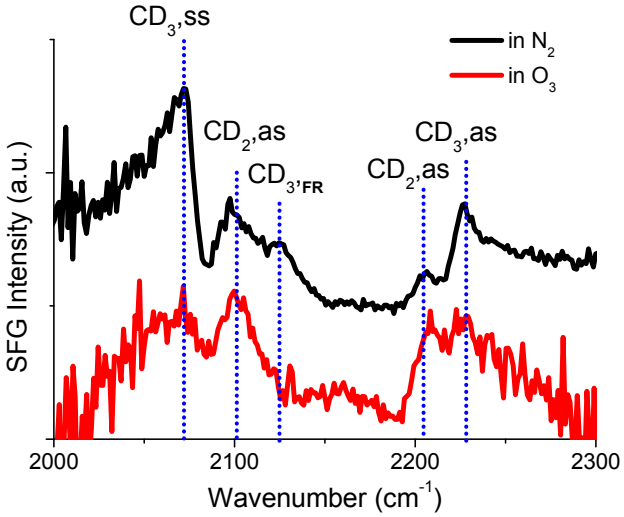

Figure 5.10 Ex-situ SFG spectra of pure POPC-d_{31} monolayer in C-D stretching region in nitrogen and ozone. The spectra are offset for clarity.

After introducing a trace amount of ozone into the chamber (red trace, Figure 5.10), the peaks of the CD_3,ss, $CD_{3,FR}$ (2135 cm^{-1}) and CD_3,as decrease largely, while

the peaks of CD_2,ss (2135 cm^{-1}) and CD_2,as (2203 cm^{-1}) increase. The increase of the methylene peaks indicates that the oxidation process may introduce more *gauche*-defects in the saturated chain in the POPC. It may be contributed to the strong interaction between the saturated chain and the oxidized residuals of the unsaturated chain which is known to be a very disordered structure (Figure 5.9b). This disturbing of the ordering of DPPC alkyl chain may induce the increase of monolayer area in Figure 5.4 and 5.9a. Details will be given in next section. The saturated chain cannot be oxidized since the concentration of ozone is extremely low there. Moreover, neutron reflection studies revealed that the saturated chain does not decompose by ozone even at even higher concentration 0.3-3.2 ppm.[9] The decrease of CD_3 peaks may be due to the decrease of molecular density or the orientation change of methyl groups.

In comparison with the saturated chain in mixed-alkyl lipid POPC, the saturated lipid DPPC in the DPPC-DOPC mixed monolayer shows different behavior. For the DPPC-DOPC mixed monolayer, after ozone exposure, the DPPC molecules recover to the ordered state same as pure DPPC monolayer. This is because the oxidation products of DOPC are almost removed from the water surface, either dissolving in the water or evaporating to the air. The residuals on the water surface are believed to have little interaction with DPPC. On the contrary, the oxidized residuals of POPC are still on the water surface. And the unsaturated chains have strong effect on the saturated portion, since the two chains esterified to the same head group and relatively close to each other.

(2) Possible Oxidation Mechanism of POPC in Low-level Ozone

Up to now, a plenty of the structural information about the POPC oxidation process has obtained from π-A isotherms and SFG observations. Based on these results, a possible mechanism of ozone oxidation on the unsaturated POPC on water surface is proposed in Scheme 5.1. Firstly, the C=C bond is attacked by ozone and followed by the Criegee reaction mechanism to generate a primary ozonide (POZ)

intermediate. [29-30] The POZ is unstable at water surface and tends to further generate 9 carbons portions (C9) and oxidized phospholipid (oxPL). The C9 portions are nonanal ($CH_3(CH_2)_7CHO$) and nonanoic acid ($CH_3(CH_2)_7COOH$), which are easily leave the monolayer due to their high solubility and/or vapor pressure. Details have been already discussed in the section 4.3.4. These C9 portions get away with the terminal methyl group, that is the reason why the CH_3,ss peak sharply disappeared in the SFG spectra of POPC-d_{31} (Figure 5.9b). On the other hand, the residual oxPLs are more complex, since they have both hydrophobic palmitoyl chain and modified the oleoyl chain with hydrophilic group of either aldehyde or acid as the new end. The new terminal group tends to dissolve into the water, but the nearby hydrophobic saturated chain like a float to stay on the water surface. The competition between the two parts conclude oxidized lipid to dissolve into the water or not. As shown in the time-dependency experiment, a lot of products are still kept to stay on the water surface for a long time (Figures 5.4). The results from neutron reflection studies also proved that the palmitoyl moiety was still on the water surface and could keep on water surface at least several hours under their experimental conditions.[9] Recent MD simulation showed the evidence that the alkyl chain of the oxPLs of POPC[12] or DOPC[31] could reverse its orientation to point into the water subphace.

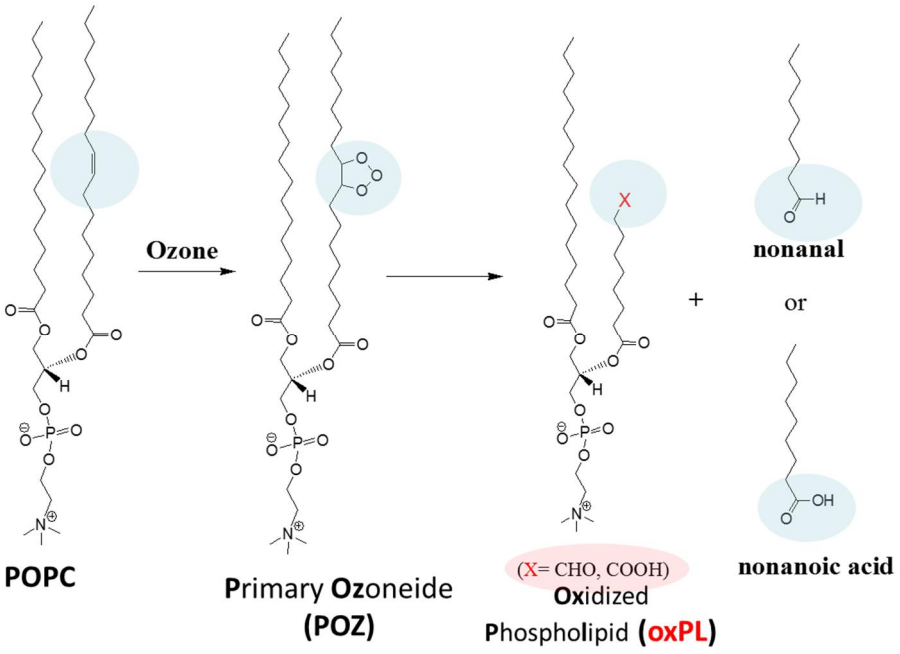

Scheme 5.1 Possible reaction mechanism of ozone oxidation on the unsaturated POPC on water surface.

(3) Verification of the Oxidation Products

In order to further confirm the oxidation mechanism of POPC in ozone, the SFG spectroscopy was employed to investigate the monolayers of oxidation products of the experiments and expected products. As shown in the Scheme 5.1 the oxidized form of POPC in ozone is prospected as POnPC and PAzPC (Figure 5.2), with terminal group of aldehyde or acid in the original oleoyl chain of POPC.

As shown in Figure 5.11, the SFG spectra of products and expected products are almost identical with strong CH_2,ss, CH_3,$_{FR}$ peaks and weak CH_3,ss, CH_2,as peaks. These results strongly support that the oxidation products of POPC should be POnPC and PAzPC. However, it is hard to figure out the ratio of these two oxPLs. It was reported that the proportion of PAzPC increased if the ozone concentration is up to 30ppm or under high compression conditions.[19] The difference of the SFG intensities in Figure 5.11 should be due to the difference of molecular orientation, which is hard to analyze in detail based on the present results.

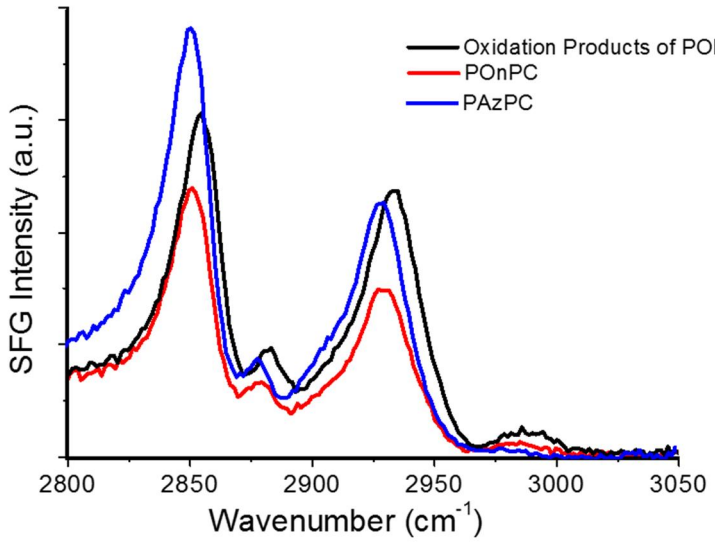

Figure 5.11 *ssp*-SFG spectra of oxidation products of POPC by the experiment and expected products: oxidized lipid with terminal group of aldehyde (POnPC) or acid (PAzPC). All the monolayers were prepared at 30 mN/m on water surface.

In order to further confirm the oxidation reaction of POPC monolayer in ozone, the π-A isotherms of POnPC and PAzPC were measured as shown in Figure 5.12. At certain surface pressure, the area per molecule POnPC is larger than pure DPPC, POPC, and DOPC. And that of PAzPC is even larger than POnPC. That can explain why the area of POPC monolayer or POPC-containing monolayers expended when exposed to ozone in the time dependence experiment (Figures 5.4 and 5.5). Moreover, the collapse pressure of oxPLs is around 38 mN/m, which is very close to the transfer pressure that we used in most of the experiment. One can expect that the oxPLs should be in a very unstable state at 30 mN/m and may be slowly dissolved into water subphase with the oxidation process of POPC. In order to confirm this assumption, we checked the stability of the oxPLs at different surface pressures.

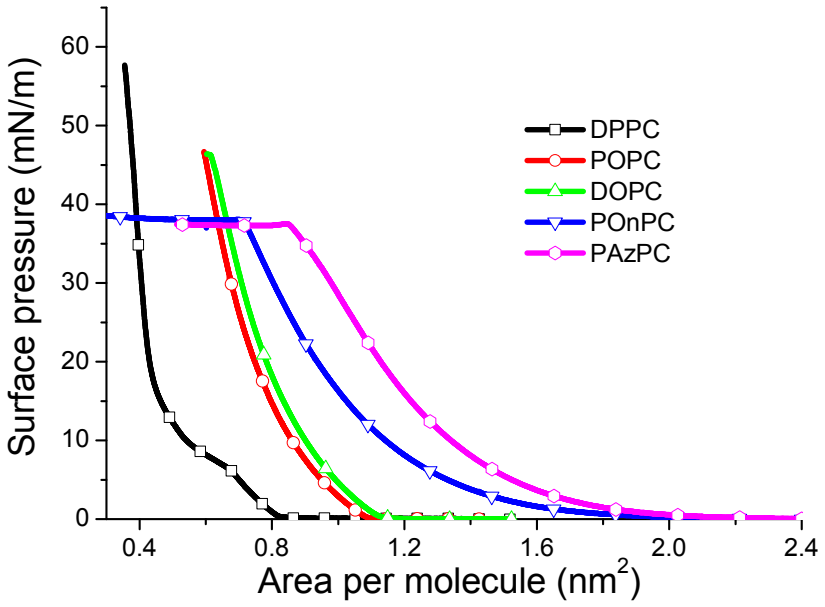

Figure 5.12 π-A isotherms of DPPC, POPC, DOPC, and oxPLs including POnPC and PAzPC. The π-A isotherms were obtained on a pure water surface (22℃) under nitrogen atmosphere and in dark.

As shown in Figure 5.13, from the left to the right the surface pressure increased to 8, 12, 16, 20, 24, 26, 28, and 30 mN/m step by step (blue dot line) with the interval of several tens of minutes. The monolayer area changes accompanied with increase of the surface pressure. When surface pressure is below 15 mN/m, both POnPC and PAzPC are very stable with slightly reduce in the monolayer area. However, when the monolayer compressed to a pressure higher than 15 mN/m, the monolayer area decline obviously. This confirms our speculation that the oxPLs are very unstable at high lateral pressure. That is why the area decreases at high surface pressure but stable at lower one in time dependence experiments. These results also provide the evidence to support the mechanism that POnPC and PAzPC are oxidation products of POPC in the low-concentration ozone.

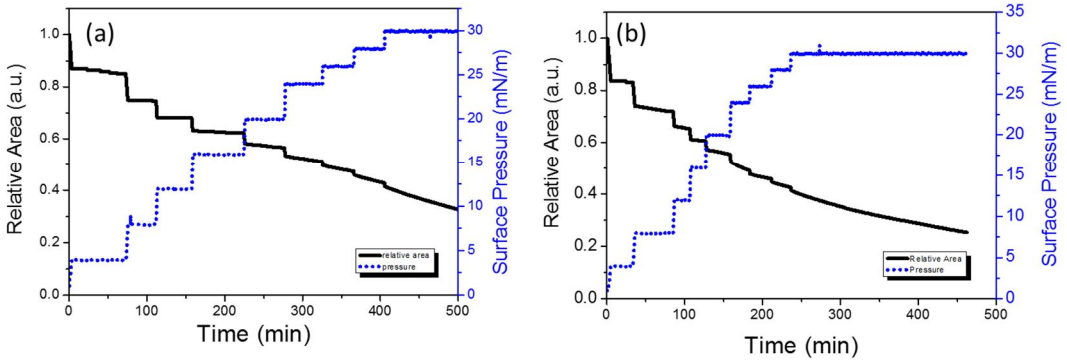

Figure 5.13 The stablilty of oxPLs on water surface at different surface pressures. (a) POnPC, (b) PAzPC. The curve of relative area is shown in black color (left axis). The curve of surface pressure is shown by dot line in blue color (right axis).

Based on the structural information obtained for the POPC oxidation process above, one may be able to get a further detailed picture about the unique time-dependency results of POPC in Figures 5.4 and 5.5. At the present stage, we think the increase of the surface area of the POPC monolayer in ozone, is not due to the number of species at the surface, since the small C9 portion readily remove from the interface. The increase of the monolayer area is mainly come from the hydrophilic modification of POPC to oxPLs, since the oxPLs could change their orientation to bend into water. [12, 18]As shown in the Scheme 5.2a, the hydrophilic aldehyde or acid group induce the modified chain of oxPLs to lie down to the water surface, thus increase the area per

molecule. Since the interaction between the oxidized portion and saturated chain is enhanced, the *gauche* defects on the saturated part increase during the reaction in ozone. That could cause the increase of monolayer area. Moreover, the increase of *gauche*-defects results in larger area per molecule. As shown in the Scheme 5.2b, the *gauche*-defects in the alkyl chain may induce a kink in the chain direction, and cause the chain have to occupy more space than the *all-trans* conformation. With increase of surface pressure, these oxPLs gradually dissolve into water subphase which is one of possible reasons inducing the decrease of surface area at higher surface pressure (for example, 30 mN/m).

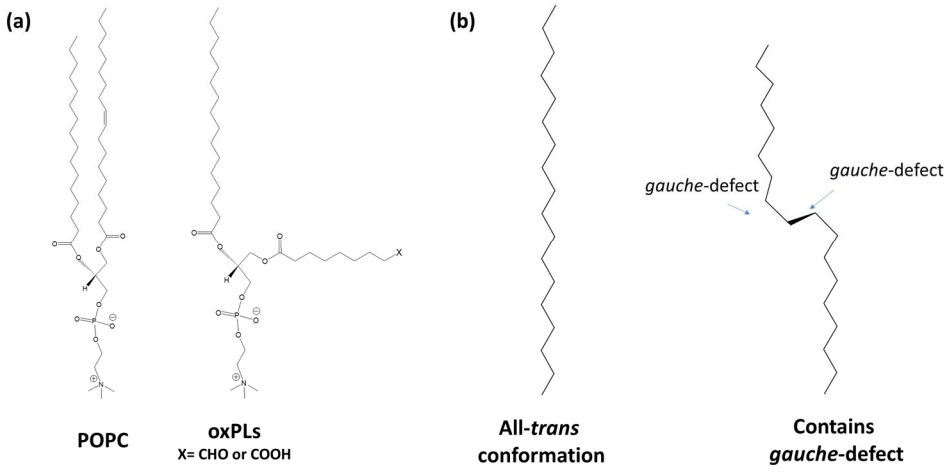

Scheme 5.2 The scheme of reason for the increase of POPC monolayer area after exposed to ozone. (a) reorientation of the oxidation modified alkyl chain. (b) alkyl chains with all-trans conformation and contains two gauche-defects. [14, 32]

In summary, the stability of pure POPC monolayer is studied by SFG spectroscopy. It is found that the *cis*-double bond on the unsaturated lipid was oxidized by the low-level of ozone. The terminal C9 portion is get away from the water surface. The residual oxidized lipids are POnPC and PAzPC. Because they have larger area per molecule and unstable in high lateral pressure, the POPC and POPC contain mixed monolayer shows a unique behaver in time-dependency experiment (Figures 5.4 and 5.5), that is increase first and then decreased slowly in the monolayer area which can be related to the surface reorientation as well as dissolution of these oxidized products at higher surface pressure.

5.3.4 The Molecular Structure of POPC-DPPC Mixed Monolayers

To investigate the molecular structure of lipids in detail, the SFG observations using different combinations of hydrogenated and deuterated lipids have been carefully designed (See Figure 5.1). Since the two alkyl chain of POPC have different unsaturation degree, partially deuterated POPC was used in the present experiment. As a result, the signals from the saturated chain (C-D stretching region) and unsaturated chain (C-H stretching region) can be separately observed in the SFG vibrational spectroscopy. In order to investigate alkyl chain of POPC and DPPC in mixed monolayers individually, the experiment is designed as shown in Table 5.1. In the mixed monolayer of DPPC-d_{75} and POPC, deuterated DPPC can be directly evaluated in C-D regions by SFG spectroscopy. Moreover, by using the combination of DPPC-d_{75} – POPC-d_{31}, the unsaturated chain of POPC in the mixed monolayer can be selectively detected in the C-H stretching region by SFG. On the other hand, the information of saturated chain of POPC is shown in C-D stretching region in mixed monolayer DPPC – POPC-d_{31}.,

Table 5.1 Experiment Design and Corresponding Expected Information.

Mixture	Molecule	Information
dDPPC + POPC	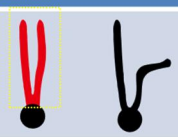	Chains of DPPC @ C-D region
dDPPC + dPOPC	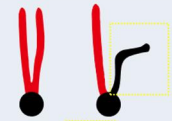	Unsaturated chain of POPC @ C-H region
DPPC + dPOPC	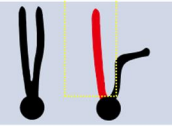	Saturated chain of POPC @ C-D region

Left column: the constitution of mixed monolayer. Middle column: the scheme of the molecule and the deuterated portion is in red color. The right column: the target information and available region.

It should be noted that all the monolayers were transferred to CaF_2 prism at 30 mN/m in the protection nitrogen.

(1) DPPC-d_{75} / POPC Mixed Monolayers

Figure 5.14 shows the *ssp*-polarized SFG spectra in the C-D stretching region for the DPPC-d_{75} component in the DPPC-d_{75}/POPC mixed monolayer prepared in nitrogen (a) and ozone (b). All the information is come from the DPPC component in the mixed monolayer. In the nitrogen, with the increase of POPC in the mixed monolayer, the CD_2,ss and CD_2,as peaks increased. It means the DPPC molecules in the monolayer become more disordered after mixing with POPC. After exposure to ozone, the DPPC molecules in the monolayer become more disordered since the intensity of the CD_2,ss and CD_2,as peaks significantly increase.

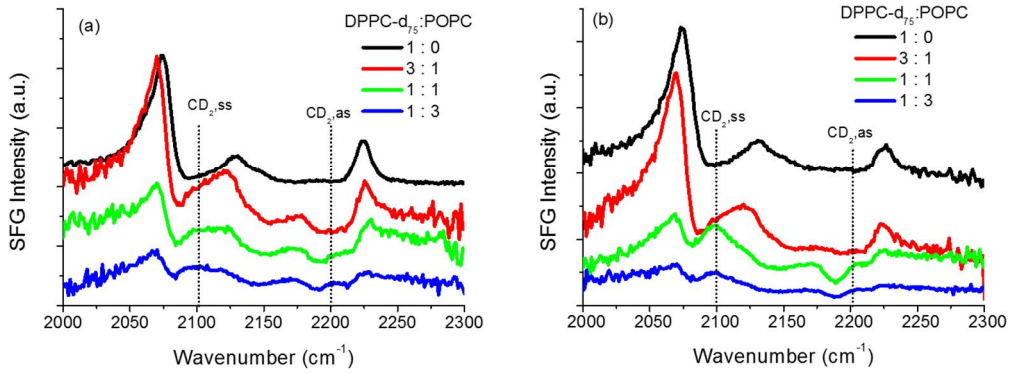

Figure 5.14 The *ssp*-polarized SFG spectra of DPPC-d_{75}/POPC mixed monolayers for different molar ratios observed in the C-D stretching region for DPPC-d_{75} component (a) before and (b) after exposure to ozone (20 ± 10 ppb).

(2) DPPC-d_{75} / POPC-d_{31} Mixed Monolayers

Figure 5.15 shows the *ssp*-polarized SFG spectra in the C-H stretching region for the DPPC/POPC-d_{31} mixed monolayer prepared in nitrogen (a) and ozone (b). All the information is come from the unsaturated chain of POPC-d_{31} in the mixed monolayer. The strong CH_3,ss peaks are shown in the nitrogen for all the mixed monolayer, while they are largely decreased after exposure to ozone. Comparing to the pure POPC monolayer, the unsaturated chain maintained a weak CH_3,ss in the mixed monolayer, that may due to oxidation process is inhibited or slowed down.

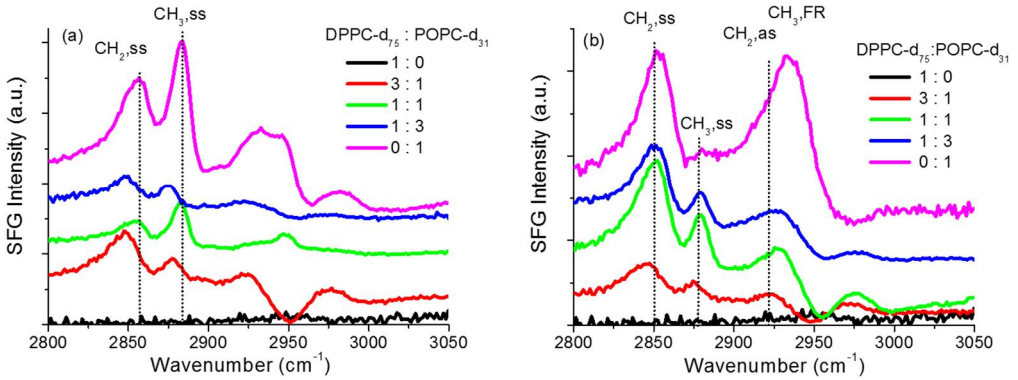

Figure 5.15 The *ssp*-polarized SFG spectra of DPPC-d_{75}/POPC-d_{31} mixed monolayers for different molar ratios observed in the C-H stretching region for unsaturated chain of POPC-d_{31} component (a) before and (b) after exposure to ozone (20 ± 10 ppb).

(3) DPPC / POPC-d_{31} Mixed Monolayers

Figure 5.16 shows the *ssp*-polarized SFG spectra in the C-D stretching region for the DPPC/POPC-d_{31} mixed monolayer prepared in (a) nitrogen and (b) ozone. All the signals come from the saturated chain of POPC. In both nitrogen and ozone the intensity of the SFG signal diminished fast with the increase of DPPC mole ratio, which due to the density of the saturated chain of POPC is diluted largely by mixing with DPPC. In the nitrogen, the intensity of the peaks from CD_2 group is about half of CD_3 group, while they become comparable after ozone exposure. The increase of DPPC in the monolayer seems to less helpful for the ordering of the saturated chain of POPC, different from that of DOPC (Figure 4.8).

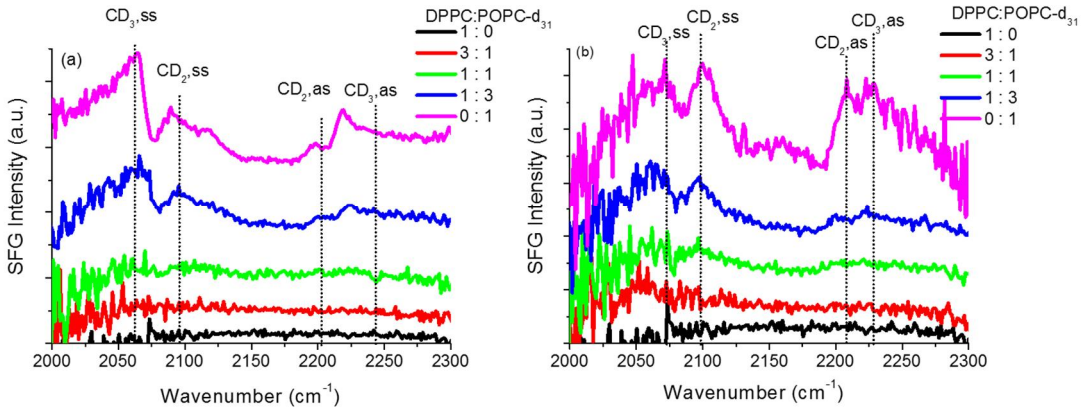

Figure 5.16 The *ssp*-polarized SFG spectra of DPPC/POPC-d_{31} mixed monolayers for different molar ratios observed in the C-D stretching region for saturated chain of POPC-d_{31} component (a) before and (b) after exposure to ozone (20 ± 10 ppb).

In summary, in this section the mixed monolayers composed by the different combination of POPC, DPPC, POPC-d_{31} and DPPC-d_{75}, have been characterized by SFG in detail It is found that DPPC molecules in the monolayers are largely influenced by presence of both POPC and oxidized POPC residuals. The oxidation process of unsaturated portion of POPC is partially inhibited due to the presence of DPPC, and the saturated portion becomes slightly ordered by mixing with DPPC.

5.3.5 Morphology of DPPC-POPC Mixed Monolayers

(1) Mixed Monolayers at High Surface Pressure

In order to understand the organization of the different components at the interface, it is essential to observe the surface morphology of the mixed monolayers under nitrogen or ozone. Figure 5.17 shows the AFM images of DPPC/POPC mixed monolayers with a surface pressure at 30 mN/m. Phase separation features were observed for all DPPC-POPC mixed monolayers in both nitrogen and ozone, except homogeneous DPPC-POPC 1:3 mixed monolayer in ozone.

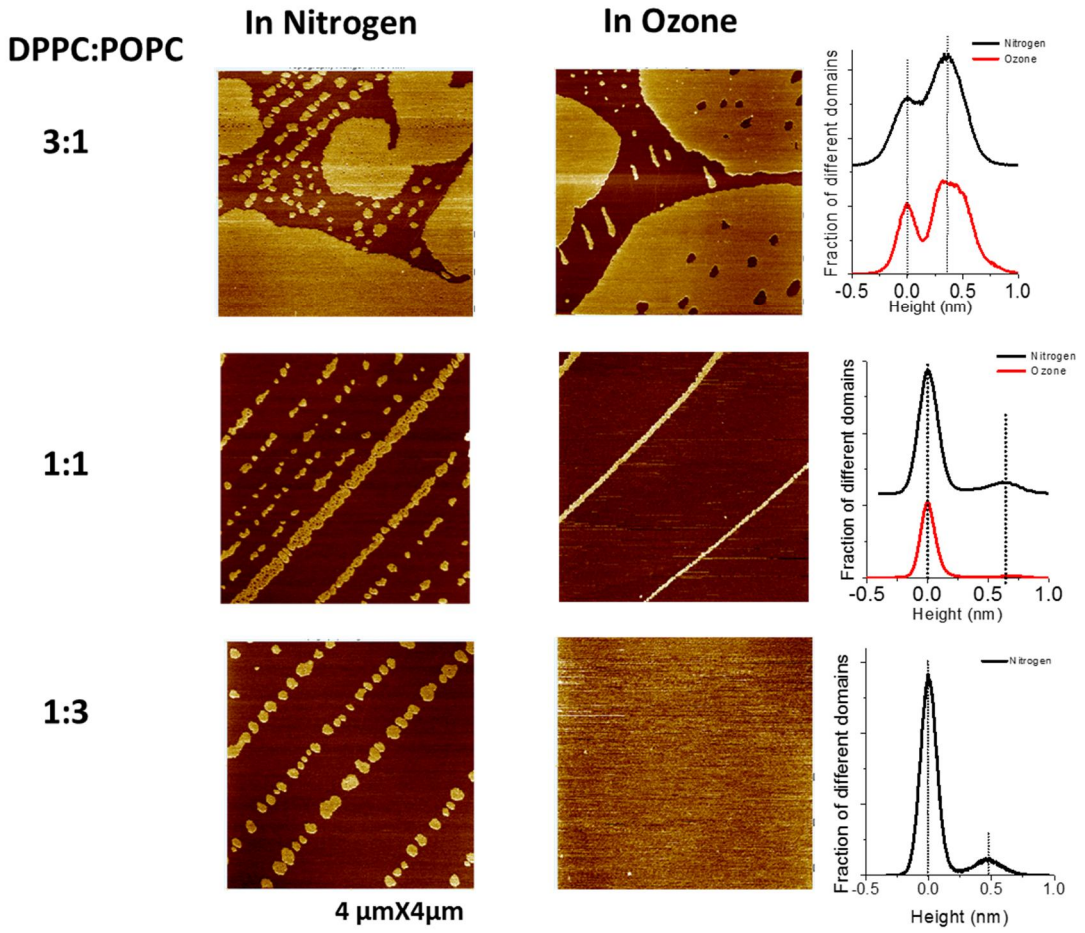

Figure 5.17 AFM images (4 × 4 μm^2) of DPPC-POPC mixed monolayers on the mica surface transferred at 30mN/m (left column) before and (middle column) after exposure to low-level ozone for more than 100 min on the water surface, and the height-distribution histogram (right column) of each domain of these mixed monolayers. (Dipping directions of the monolayer transfer are shown by arrow in the images)

In the nitrogen (Left column, Figure 5.17), the parallel stripe pattern is appeared in all DPPC-POPC mixed monolayers, similar to the observation of DPPC-DOPC 1:1 mixed monolayer in nitrogen (Figure 4.4a).[33] The direction of the stripe is perpendicular to the dipping direction of the monolayer (dipping directions are shown by arrow in the images). It is believed that this kind of surface pattern is similar to DPPC-DOPC mixed monolayer which is possibly caused by the combined effects of hydrodynamic shear, the surface pressure and film viscoelastic properties.[34]

The height difference between the two domains in Figure 5.17 is generally around 0.5 nm, but with a slight difference depending on the molar ratio of POPC component. The DPPC-POPC mixtures with molar ratios of 3:1 and 1:3 have a little lower height

differences of 0.4 nm and 0.5 nm, respectively, than the 1:1 mixed monolayer of 0.6 nm. Moreover, the proportion of lower domain is 20±10%, 80±10% and 85±5% for DPPC-DOPC 3:1, 1:1, and 1:3, respectively. The area of lower domain increases significantly with the increase of POPC portion in mixed monolayer. This indicates the lower domain is the POPC-rich domain and the higher domain is the DPPC-rich domain.

All the values of height-difference of DPPC-POPC mixed monolayers are little smaller than those of DPPC-DOPC mixed monolayers (around 0.8±0.2nm). This tiny distinction should be due to the difference of the molecule structures. DOPC has two unsaturated chains, while POPC has one saturated chain and one unsaturated chain. The saturated chain is generally longer than unsaturated chain which has a kink due to the *cis*-C=C bond. Therefore, the absolute height of lipid is related with the unsaturation degree. The height sequence of these lipid monolayers is DOPC < POPC< DPPC at the same surface pressure and temperature. That is why the height-difference between DOPC-rich and DPPC-rich domain is larger than that between POPC-rich and DPPC-rich domain.

For the fraction analysis, the lower domain of DPPC-POPC 1:1 mixed monolayer occupy a similar area (80±10%) with that of DPPC-DOPC mixed monolayer (78±5%). It indicates there is little difference between the area ratio of unsaturated lipid and saturated lipid in DPPC-POPC and DPPC-POPC mixed monolayers. However, according to the π-A isotherms, the mean area per molecule of DOPC-POPC 1:1 mixed monolayer is 0.58 nm^2 at the surface pressure of 30 mN/m, which is a little smaller than 0.61 nm^2 for DPPC-DOPC monolayer. This suggests that not only POPC has a smaller area per molecule than DOPC, but also DPPC is more ordered when mixing with POPC than with DOPC.

AFM images of DPPC-POPC mixed monolayers after exposure to ozone for more than 100 min at gas/water interface have been given in middle column of Figure 5.17. In comparison with the monolayer prepared under nitrogen, the morphologies of all mixed monolayers under ozone are significantly changed. The phase separation is still

visible in the AFM image of DPPC to POPC 3:1 and 1:1 mixed monolayer, but absent for 1:3 mixed monolayer.

Unlike the common parallel stripes pattern in nitrogen, the morphology of the domain in ozone becomes more complex with the parallel stripes only shown in DPPC-POPC 1:1 mixed monolayer. For the DPPC-POPC 3:1 monolayer, the higher domain is no longer homogenous, but with several holes in it. The height difference between the higher domain and the hole is same as that between the higher domain and the lower ocean. It indicates the molecules in the hole are similar to the molecules in the lower ocean.

In addition, the difference of the domain height did not change after exposure to ozone for each mixed monolayer. Similar to the results in nitrogen, the higher and lower domains should correspond to the DPPC domain and POPC (or some oxidized lipid) domain, respectively. Moreover, the fraction of the lower domain increase largely with the growth of the POPC portion in the mixed monolayer, from 30±5% to 90±5%, 100% for 3:1, 1:1, and 1:3 mixed monolayers (DPPC:POPC), respectively. These values are larger than those in nitrogen (20±10%, 80±10% and 85±10%). Because the saturated DPPC has less possibility to be oxidized in ozone, the fraction changes are probably due to the oxidation of POPC. It indicates that POPC tends to occupy a larger domain after exposure to ozone, which is in accordance with the increase of the monolayer area in the stability study (Figures 5.4 and 5.5). However, this is totally different from the results of DOPC in the DPPC-DOPC mixed monolayers, in which DOPC-rich domain greatly declined after the ozone exposure (Figure 4.3). It implies that part of POPC is still present on the surface after a long period exposure in ozone.

(2) Time Dependence of Morphology

The morphology of the DPPC-POPC mixed monolayers are further investigated as a function of exposure time in ozone. In this study, the DPPC-POPC 1:1 mixed monolayer was taken as an example to study the time dependence effect.

Figure 5.18a shows the stability curve of the DPPC-POPC 1:1 mixed monolayer in nitrogen and ozone as a function of time at 30 mN/m. Figure 5.18b shows the AFM images of the mixed monolayer transferred at the time point of A, B and C, respectively. Monolayer A is transferred to mica surface before ozone exposure. Monolayer B is transferred to mica surface when the surface area decreased to the initial value, and C is transferred to mica surface after exposure to ozone for about 10 hours. The percentage of the lower domain area firstly increased from 80±10% (Figure 5.18b-A) to 90±5% (Figure 5.18b-B), then decreased to 57±30% (Figure 5.18b-C), and to 10±5% (Figure 5.18b-D) after long time exposure.

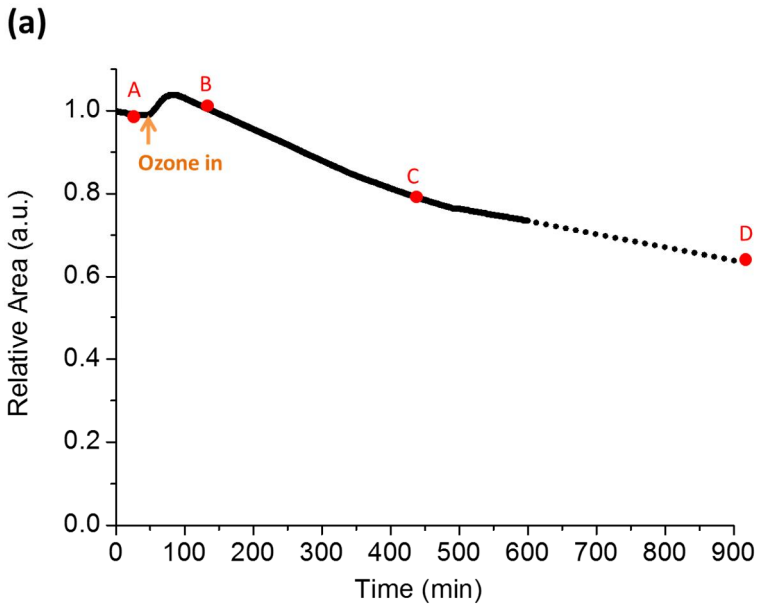

(b)

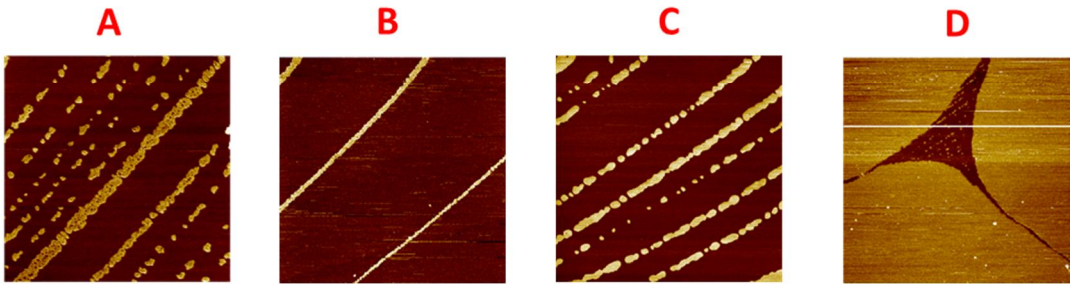

Figure 5.18 Morphology changes of DPPC-POPC 1:1 mixed monolayers under ozone exposure at 30 mN/m. (a) Surface area changes as a function of exposure time in ozone; (b) AFM images of the mixed monolayers with different time of ozone exposure. The time for monolayer transfer is shown in the figure (a) by red dot. Noting that 600min reached the maximum record number of the LB trough, thus the curve after 600min is just a predict curve shown in dot line.

The explanation and a possible mechanism is given in the Scheme 5.3. As already discussed in the previous sections, when the surface area changes from A to B, the unsaturated POPC is oxidized by ozone and the domain area increase since the oxPLs has a larger area per molecule which is induced by the reorientation of the residual part of the oleoyl chain. Furthermore, the surface area changes from B to C is due to the oxPLs dissolve into water since they are hard to keep on the water surface under the high compressed lateral pressure (30 mN/m) , although it takes extremely long time (more than 10 hours) to fully dissolve into the water. In addition, with the decrease of the ratio of oxPLs in the monolayer, the DPPC can help the residual molecule on the surface to become more ordered and results in the height difference decrease.

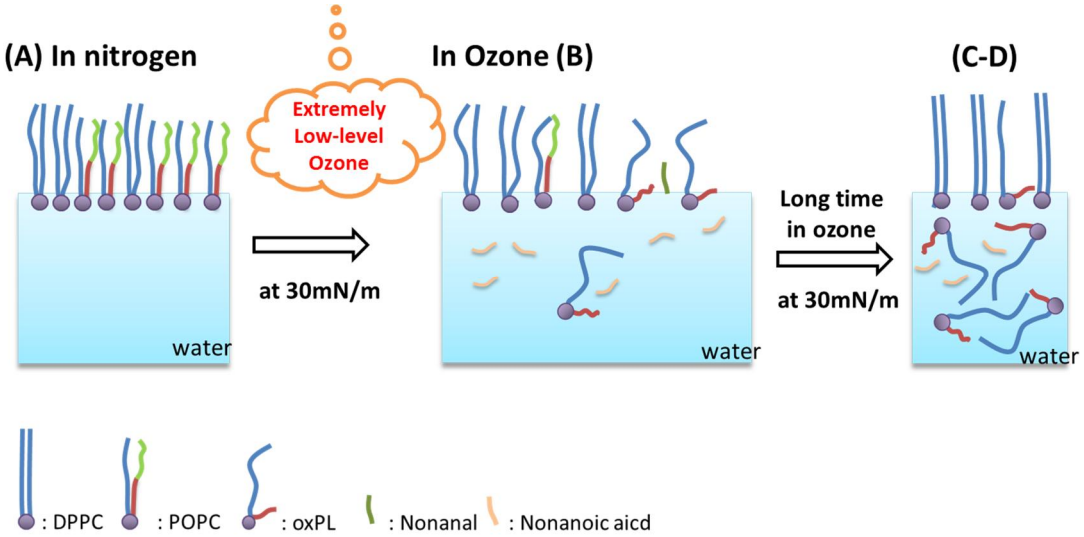

Scheme 5.3 Schematic representations of DPPC-POPC mixed monolayer after exposure to ozone for different time scale. (A) before ozone exposure (B) exposure for 100min (C-D) exposure more than 400 min and 10hours.

In summary, the present AFM observation indicates that the surface organization of mixed monolayer is strongly affected by the molar ratio of the saturated to unsaturated lipids. The results also suggest that the molecular structure of the unsaturated lipid play an important role in the organization of mixed monolayer under ozone exposure.

5.4 Conclusions

In this chapter, the oxidation reaction of POPC-containing monolayers in low-level ozone has been extensively discussed on the basis of experimental results of π-A isotherm, SFG and AFM. A possible reaction mechanism for DPPC-POPC mixed monolayers on a water surface in nitrogen and in low-level ozone for short time is illustrated in Scheme 5.4.

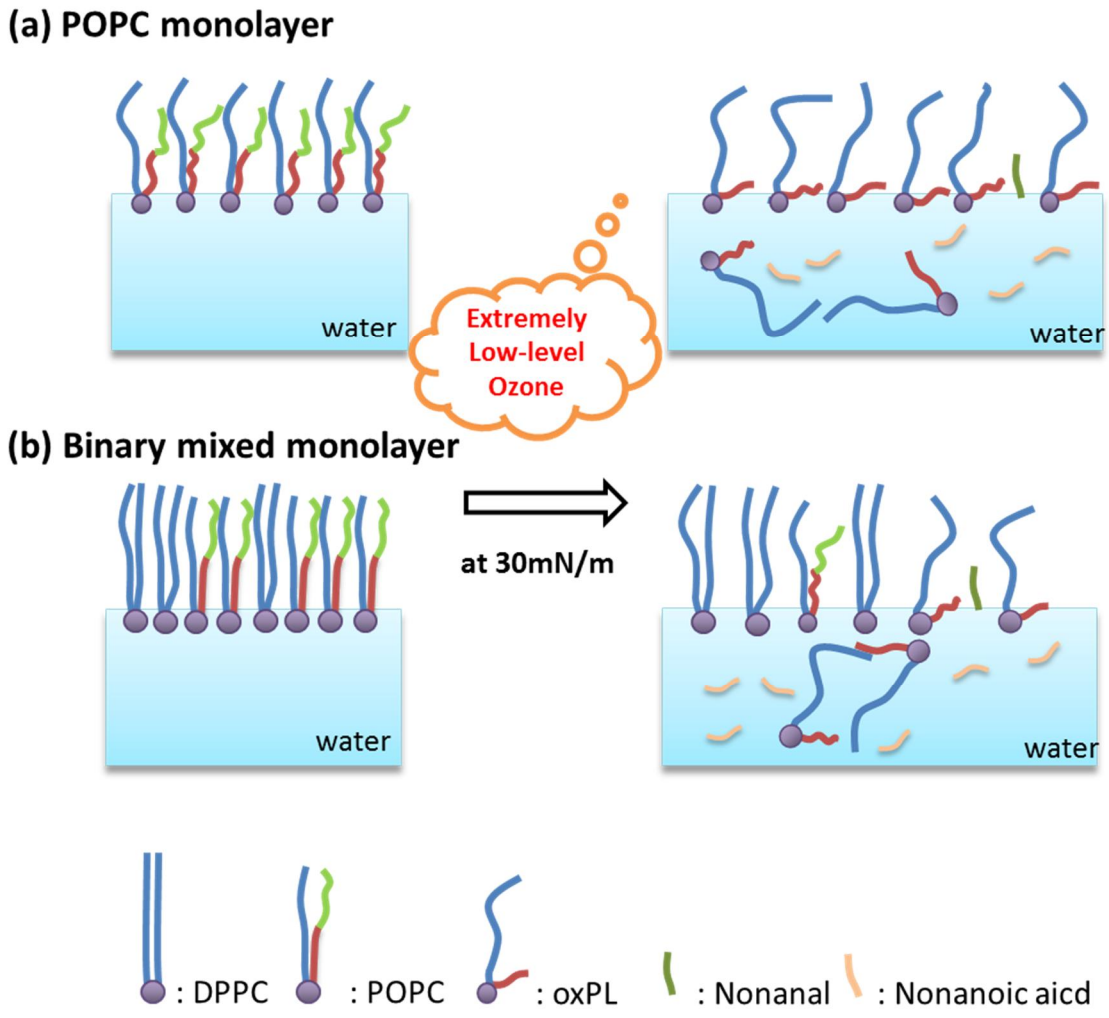

Scheme 5.4 The schematic models for (a) the POPC monolayer and (b) mixed monolayer on a water surface before (left) and after (right) exposure to a low-level ozone. All the models schematically exhibit molecular structures per unit area at a constant surface potential of 30 mN/m.

The pure POPC monolayer is found to form a disordered LE phase with *gauche*-defects due to the low packing density (Scheme 5.4a). The *cis*-double bond of POPC can be oxidized by extremely low-concentration ozone. The C=C bonds are attacked by ozone molecules and decomposed to oxPLs, nonanal and nonanoic acid, which is supported by our SFG spectra. The surface stability of the oxidized monolayers, which shows very different behavior in comparison with DOPC monolayer, is found to be dependent on the surface pressure. Moreover, it is found that the conformation of the saturated alkyl chain of POPC can be strongly influenced by another unsaturated chain, resulting in more *gauche*-defects.

For the DPPC-POPC mixed monolayer (Scheme 5.4b) in nitrogen environment, the phase separation is observed by AFM observation. However, the phase separation of the mixed monolayer experienced a complicated process when exposed to ozone. The increase of surface area and POPC-rich domain is due to the larger area per molecule of oxPLs than POPC, in which C9 part is believed to easily dissolve into water subphase or evaporate into gas phase after oxidation. Furthermore, the decrease in surface area and POPC-rich domain in next stage is attributed to a very slow dissolution of oxPLs into water under a high lateral pressure (while some reorientation of remained POPC and oxPLs may be also included in the process). It is also confirmed DPPC has strong interaction with POPC or its oxidation products. In both cases, the conformation ordering of the DPPC molecules are reduced.

The results of POPC-containing monolayers verify that the low-concentration ozone in air can induce significant influence on the unsaturated lipids. Furthermore, such oxidation induced effects on the membrane structure and stability at the interface are found to strongly depend on the unsaturation degree of the lipid.

REFERENCES

1. Van Meer, G.; Voelker, D. R.; Feigenson, G. W., Membrane lipids: where they are and how they behave. *Nature reviews molecular cell biology* **2008,** *9* (2), 112-124.
2. King, R., Pulmonary surfactant. *Journal of Applied Physiology* **1982,** *53* (1), 1-8.
3. Perez-Gil, J.; Weaver, T. E., Pulmonary surfactant pathophysiology: current models and open questions. *Physiology* **2010,** *25* (3), 132-141.
4. Mustafa, M. G., Biochemical basis of ozone toxicity. *Free Radical Biology and Medicine* **1990,** *9* (3), 245-265.
5. Ciencewicki, J.; Trivedi, S.; Kleeberger, S. R., Oxidants and the pathogenesis of lung diseases. *Journal of Allergy and Clinical Immunology* **2008,** *122* (3), 456-468.
6. Pérez-Gil, J., Structure of pulmonary surfactant membranes and films: The role of proteins and lipid–protein interactions. *Biochimica et Biophysica Acta (BBA) - Biomembranes* **2008,** *1778* (7–8), 1676-1695.
7. Bargagli, E.; Olivieri, C.; Bennett, D.; Prasse, A.; Muller-Quernheim, J.; Rottoli, P., Oxidative stress in the pathogenesis of diffuse lung diseases: A review. *Respir. Med.* **2009,** *103* (9), 1245-1256.
8. Thompson, K. C.; Rennie, A. R.; King, M. D.; Hardman, S. J. O.; Lucas, C. O. M.; Pfrang, C.; Hughes, B. R.; Hughes, A. V., Reaction of a Phospholipid Monolayer with Gas-Phase Ozone at the Air− Water Interface: Measurement of Surface Excess and Surface Pressure in Real Time. *Langmuir* **2010,** *26*, 17295-17303.
9. Thompson, K. C.; Jones, S. H.; Rennie, A. R.; King, M. D.; Ward, A. D.; Hughes, B. R.; Lucas, C. O. M.; Campbell, R. A.; Hughes, A. V., Degradation and Rearrangement of a Lung Surfactant Lipid at the Air–Water Interface during Exposure to the Pollutant Gas Ozone. *Langmuir* **2013,** *29* (14), 4594-4602.
10. Finlayson-Pitts, B.; Mautz, W.; Lai, C.; Bufalino, C.; Messer, K.; Mestas, J.; Koch, H.; Lucio, L., Are changes in breathing pattern on exposure to ozone related to changes in pulmonary surfactant? *Inhalation toxicology* **1994,** *6* (3), 267-287.
11. Dilbeck, C. W.; Finlayson-Pitts, B. J., Heterogeneous oxidation of a phosphocholine on synthetic sea salt by ozone at room temperature. *Phys Chem Chem Phys* **2013,** *15* (6), 1990-2002.
12. Khandelia, H.; Mouritsen, O. G., Lipid gymnastics: evidence of complete acyl chain reversal in oxidized phospholipids from molecular simulations. *Biophys J* **2009,** *96* (7), 2734-2743.
13. Smith, H. L.; Howland, M. C.; Szmodis, A. W.; Li, Q.; Daemen, L. L.; Parikh, A. N.; Majewski, J., Early Stages of Oxidative Stress-Induced Membrane Permeabilization: A Neutron Reflectometry Study. *J Am Chem Soc* **2009,** *131* (10), 3631-3638.
14. Wallgren, M.; Beranova, L.; Pham, Q. D.; Linh, K.; Lidman, M.; Procek, J.; Cyprych, K.; Kinnunen, P. K. J.; Hof, M.; Grobner, G., Impact of oxidized phospholipids on the structural and dynamic organization of phospholipid membranes: a combined DSC and solid state NMR study. *Faraday Discuss* **2013,** *161* (0), 499-513.
15. Brumm, T.; Naumann, C.; Sackmann, E.; Rennie, A.; Thomas, R.; Kanellas, D.; Penfold, J.; Bayerl, T., Conformational changes of the lecithin headgroup in monolayers at the air/water interface. *European biophysics journal* **1994,** *23* (4), 289-295.

16. Volinsky, R.; Paananen, R.; Kinnunen, P. K. J., Oxidized Phosphatidylcholines Promote Phase Separation of Cholesterol-Sphingomyelin Domains. *Biophys J* **2012,** *103* (2), 247-254.
17. Liljeblad, J. F. D.; Bulone, V.; Tyrode, E.; Rutland, M. W.; Johnson, C. M., Phospholipid monolayers probed by vibrational sum frequency spectroscopy: instability of unsaturated phospholipids. *Biophys J* **2010,** *98* (10), L50-L52.
18. Volinsky, R.; Kinnunen, P. K. J., Oxidized phosphatidylcholines in membrane-level cellular signaling: from biophysics to physiology and molecular pathology. *Febs J.* **2013,** *280* (12), 2806-2816.
19. Lai, C.; Yang, S.; Finlayson-Pitts, B., Interactions of monolayers of unsaturated phosphocholines with ozone at the air-water interface. *Langmuir* **1994,** *10* (12), 4637-4644.
20. Ma, G.; Allen, H. C., DPPC Langmuir Monolayer at the Air−Water Interface: Probing the Tail and Head Groups by Vibrational Sum Frequency Generation Spectroscopy. *Langmuir* **2006,** *22* (12), 5341-5349.
21. Ye, S.; Noda, H.; Morita, S.; Uosaki, K.; Osawa, M., Surface Molecular Structures of Langmuir−Blodgett Films of Stearic Acid on Solid Substrates Studied by Sum Frequency Generation Spectroscopy. *Langmuir* **2003,** *19* (6), 2238-2242.
22. Ge, A.; Wu, H.; Darwish, T. A.; James, M.; Osawa, M.; Ye, S., Structure and Lateral Interaction in Mixed Monolayers of Dioctadecyldimethylammonium Chloride (DOAC) and Stearyl Alcohol. *Langmuir* **2013**.
23. Yang, C. S. C.; Richter, L. J.; Stephenson, J. C.; Briggman, K. A., In Situ, Vibrationally Resonant Sum Frequency Spectroscopy Study of the Self-Assembly of Dioctadecyl Disulfide on Gold. *Langmuir* **2002,** *18* (20), 7549-7556.
24. Tong, Y.; Li, N.; Liu, H.; Ge, A.; Osawa, M.; Ye, S., Mechanistic Studies by Sum-Frequency Generation Spectroscopy: Hydrolysis of a Supported Phospholipid Bilayer by Phospholipase A2. *Angewandte Chemie International Edition* **2010,** *49* (13), 2319-2323.
25. Stokes, G. Y.; Buchbinder, A. M.; Gibbs-Davis, J. M.; Scheidt, K. A.; Geiger, F. M., Chemically diverse environmental interfaces and their reactions with ozone studied by sum frequency generation. *Vib Spectrosc* **2009,** *50* (1), 86-98.
26. Tyrode, E.; Niga, P.; Johnson, M.; Rutland, M. W., Molecular Structure upon Compression and Stability toward Oxidation of Langmuir Films of Unsaturated Fatty Acids: A Vibrational Sum Frequency Spectroscopy Study. *Langmuir* **2010,** *26* (17), 14024-14031.
27. Voss, L. F.; Bazerbashi, M. F.; Beekman, C. P.; Hadad, C. M.; Allen, H. C., Oxidation of oleic acid at air/liquid interfaces. *J. Geophys. Res* **2007,** *112*, D06209.
28. Allen, H., VSFS Environment. *Annu Rev Phys Chem* **2012,** *63* (1).
29. Criegee, R., Mechanism of ozonolysis. *Angewandte Chemie International Edition in English* **1975,** *14* (11), 745-752.
30. Wadia, Y.; Tobias, D. J.; Stafford, R.; Finlayson-Pitts, B. J., Real-Time Monitoring of the Kinetics and Gas-Phase Products of the Reaction of Ozone with an Unsaturated Phospholipid at the Air−Water Interface. *Langmuir* **2000,** *16* (24), 9321-9330.
31. Khabiri, M.; Roeselova, M.; Cwiklik, L., Properties of oxidized phospholipid monolayers: An atomistic molecular dynamics study. *Chem Phys Lett* **2012,** *519–520* (0), 93-99.
32. Gennis, R. B., Biomembranes: Molecular Structure and Function. In *Biomembranes*, Springer: New York, 1989.

33. Qiao, L.; Ge, A.; Osawa, M.; Ye, S., Structure and stability studies of mixed monolayers of saturated and unsaturated phospholipids under low-level ozone. *Phys Chem Chem Phys* **2013,** *15* (41), 17775-17785.
34. Badia, A.; Moraille, P.; Tang, N. Y. W.; Randlett, M.-E., Nanostructured phospholipid membranes. *International Journal of Nanotechnology* **2008,** *5* (9), 1371-1395.

Chapter 6

General Conclusion

In present thesis, the structure and stability of single and binary mixed monolayers of saturated phospholipid, DPPC, and unsaturated phospholipids, POPC and DOPC, have been investigated in ozone of extremely low concentration (20±10 ppb), which is very close to our ambient environment, by π-A isotherm, AFM and SFG vibrational spectroscopy at a molecular level.

Firstly, the saturated lipid shows high stability in both nitrogen and the low-level ozone environments. The unsaturated lipids are stable in nitrogen but unstable in the low-level ozone environment. Although the oxidization behaviors significantly depend on the structures of the unsaturated lipids, the oxidation reaction starts from the oxidation of the *cis*-C=C bond in the extremely low-concentration ozone.

Secondly, unsaturated lipids in the mixed monolayer will be selectively oxidized by the low-level ozone although the presence of saturated lipids in the mixed monolayer can partially inhibit the oxidation of unsaturated lipids. Furthermore, the presence of the saturated alkyl chain the molecule can also slow down improve the oxidation process by the ozone.

Thirdly, the structure of the unsaturated lipid molecules significantly affects the oxidation behaviors by the low-level ozone. This behavior is expected to strongly associate with the dissolubility of the oxidized products from these unsaturated lipids on the water surface, which can be also largely affected by the surface pressure. The high surface pressure can induce the instability of monolayer by accelerating the dissolution of the oxidized products.

The present study provides important information for understanding of the physicochemical properties and stability of the cell membranes in ambient environment. A low concentration of ozone has significant negative effects on the unsaturated components in a cell membrane, thus can show its worse influence to our health, especially for those exposed to air, such as lung and skin cell.

Based on the work of present thesis, there are plenty of issues about the lipid oxidation should be probed in the near future. First, the effect of the different head groups of the phospholipid on the oxidation process is still unclear yet, since they have large influence on the molecular packing in the cell membrane. Secondly, the position of the double bond in the alkyl chain may also influence the oxidation process as reported by the mass spectroscopy measurement recently, but the knowledge about the mechanism is still rather limited. Furthermore, the effect of low-concentration of ozone on the lipid bilayer is rarely studied yet. Since the lipid bilayer is the basic structure of the cell membrane, it is of great importance to explore the oxidation process in this kind of mimic cell membrane system. It is anticipated that more details will be mastered about the lipid oxidation in the low-concentration ozone. That is not only a hazard warning but also provided method to avoid the harmful effects of ozone in the ambient.